sEEnergies

QUANTIFICATION OF SYNERGIES BETWEEN ENERGY EFFICIENCY FIRST PRINCIPLE AND RENEWABLE ENERGY SYSTEMS

D4.4

Cost and capacity analysis for representative EU energy grids depending on decarbonisation scenarios

This project has received funding from the European Union's Horizon 2020 Research and Innovation Programme under Grant Agreement No 846463.

Project

Acronym	**sEEnergies**
Title	Quantification of Synergies between Energy Efficiency First Principle and Renewable Energy Systems
Coordinator	Brian Vad Mathiesen, Aalborg University
Reference	846463
Type	Research and Innovation Action (RIA)
Programme	HORIZON 2020
Topic	LC-SC3-EE-14-2018-2019-2020 - Socio-economic research conceptualising and modelling energy efficiency and energy demand
Start	01 September 2019
Duration	30 months
Website	https://seenergies.eu/

Consortium	**Aalborg Universitet (AAU)**, Denmark **Hogskolan i Halmstad (HU),** Sweden **TEP Energy GmbH (TEP),** Switzerland **Universiteit Utrecht (UU),** Netherlands **Europa-Universität Flensburg (EUF),** Germany **Katholieke Universiteit Leuven (KULeuven),** Belgium **Norges Miljø- og Biovitenskapelige Universitet (NMBU),** Norway **SYNYO GmbH (SYNYO)**, Austria **Fraunhofer-Gesellschaft zur Förderung der angewandten Forschung e.V. (Fraunhofer),** Germany

Deliverable

Number	**D4.4**
Title	**Cost and capacity analysis for representative EU energy grids depending on decarbonisation scenarios**
Lead beneficiary	KULeuven
Work package	WP4
Dissemination level	Public (PU)
Nature	Report (RE)
Copyright license	CC BY 4.0
Due date	15.03.2021
Submission date	15.03.2021

Authors	**Simon Meunier (KULeuven)** **Christina Protopapadaki (KULeuven)** **Urban Persson (HU)** **Luis Sánchez-García (HU)** **Bernd Möller (EUF)** **Eva Wiechers (EUF)** **Noémi Cécile Adèle Schneider (AAU)** **Dirk Saelens (KULeuven)**
Reviewers	**Martin Jakob (TEP)** **Katerina Kermeli (UU)**

Document history

Version	Date	Comments
1	24.02.2021	Internal draft to reviewers
1.1	10.03.2021	Reviewed version
2	15.03.2021	Submitted version

Acknowledgement: This project has received funding from the European Union's Horizon 2020 Research and Innovation Programme under Grant Agreement No 846463.

Executive Summary

Cite as: Meunier, S., Protopapadaki, C., Persson, U., Sánchez-García, L., Möller, B., Wiechers, E., Schneider, N.C.A, Saelens, D. (2021). *Cost and capacity analysis for representative EU energy grids depending on decarbonisation scenarios.* Report in the frame of the H2020 EU project sEEnergies.

Keywords: energy grids, low-voltage distribution grid, district heating, gas grids, low-carbon technologies, energy transition.

This work studies the transformation of energy grids of the European Union (EU) in the frame of the energy transition. Three energy grid types are considered namely the **electricity**, **thermal** and **gas** grids.

Regarding **electricity** grids, we investigate the required reinforcements of the low-voltage networks (e.g. replacing the distribution transformer by one of higher nominal power, replacing cables by cables of larger cross-section) in order to integrate residential low-carbon technologies such as heat pumps, photovoltaic systems and electric vehicles. To do so, we develop a methodology for the quantification of EU low-voltage grid reinforcement costs following residential low-carbon technologies integration. This methodology uses urbanisation data to determine the share of dwellings in rural and urban areas in EU28 countries (EU27 + United Kingdom). It is also based on a model that quantifies the grid reinforcement cost as a function of the low-carbon technologies integration scenario for representative rural and urban grids. This model is composed of three sub-models, namely the dwelling, grid and economic models. We also collected data from 24 open access grids (i.e. grids of which the specifications are freely accessible online) and 23 scientific articles and reports to determine the parameter values of the grid and economic models for EU28 countries. Finally, we provide example applications that illustrate the methodology by computing the grid reinforcement costs from heat pumps and photovoltaic systems integration in Belgium and Italy. Results indicate that, in the largest majority of cases, both for Belgian and Italian grids, the reinforcement cost per dwelling remains below 350 € per dwelling (total cost for the whole lifespan of 33 years). The only case where more significant reinforcement costs occurred (> 350 €/dwelling and up to 1150 €/dwelling) is for the Belgian rural grid with heat pump integration rates larger than 40%.

When it comes to **thermal** grids, we investigate the deployment of district heating, a heat supply technology that by its fundamental idea incorporates energy efficiency and thus can trigger important greenhouse gas emissions reduction. For this purpose, we proposed an approach to map the cost of thermal grids deployment per heat demand unit in the EU. This approach is based on the concept of representative thermal grids which corresponds to a principal equation that defines the distribution capital costs as the ratio of empirically derived specific investments costs and the linear heat density. In the sEEnergies project, this concept is expanded to comprise better cost models based on actual district heating network layouts at the spatial resolution of 1 hectare. While in the Heat Roadmap Europe project, the variables were generated only for the 14 EU Member States with largest annual volumes of building heat demands, the present approach covers all EU27 Member States plus United Kingdom. In this deliverable, we focus on the current year, while the deliverable 4.5 focuses on the future years.

Regarding **gas** grids, we present the key technical and economic characteristics of the existing gas grids and storages in the EU28 countries. We focus not only on infrastructure for natural gas but also for biogas, biomethane, syngas and hydrogen, which could play an important role in the decrease of greenhouse gas emissions. This techno-economic review provides important information to assess the cost of retrofitting and developing gas grids depending on the decarbonisation scenarios.

Contents

Figures

Tables

Abbreviations

We here present the abbreviations that are used throughout the whole report

D	deliverable
DH	district heating
DSO	distribution system operator
EU	european union
HP	heat pump
LCT	low-carbon technology
LNG	liquified natural gas
LV	low-voltage
MS	member state
MV	medium-voltage
OH	overhead
PV	photovoltaic
UG	underground
VAT	value-added tax
WP	work package

Nomenclature for electricity grids

We here present the notations that are used throughout the Section 2 on electricity grids.

Indices

area	area: urban or rural
γ	country
d	dwelling
dc	dwelling connection
dl	dwelling link
fs	feeder segment
j	phase index
k	position in the feeder
n	node
t	time
τ	transformer

Variables

b_f	feeder replacement variable (binary)
b_τ	transformer replacement variable (binary)
$b_{3\phi}(d)$	3-phase connection variable (binary)
$E_l(\tau)$	yearly energy losses in the transformer (kWh)
$E_l(f)$	yearly energy losses in the detailed feeder (kWh)
$fl(fs)$	feeder segment overloading
$FL(fs)$	feeder segment overloading indicator
FL	overloading indicator for the whole feeder
$i(dl)$	current in dwelling link (A)
$i(fs)$	current in feeder segment (A)
$i(\tau^j)$	current in phase j of the transformer (A)
IC	investment costs corresponding to a reinforcement option (€)
LCC_d	life-cycle cost per dwelling corresponding to a reinforcement option (€)
LCC_d^*	cost of the cheapest technically viable reinforcement option (€)
LCT_σ	low-carbon technology integration scenario
OC	operating costs corresponding to a reinforcement option (€)
$S(\tau)$	apparent power through the transformer (kVA)
$tl(\tau)$	transformer overloading
TL	transformer overloading indicator
$v(dc_k^j)$	line-to-neutral voltage at the dwelling connection in position k and for phase j (V)
$v(n_k^{j,j'})$	line-to-line voltage at the node in position k between phases j and j' (V)

$VD(d_k)$	voltage deviation indicator for the dwelling in position k
VD	voltage deviation indicator for the whole feeder
$vu(n_k)$	voltage unbalance at the node in position k
$VU(n_k)$	voltage unbalance indicator at the node in position k
VU	voltage unbalance indicator for the whole feeder

Parameters

$cr(f)$	feeder cables cross-section (mm^2)
$C(E_l)$	cost per kWh of energy losses for the DSO (€/kWh)
$C(\tau)$	transformer investment cost, i.e. cost of the newly installed transformer (€)
$C_l(dl)$	linear cost of replacing the current one-phase dwelling link by a three-phase cable (€/m)
$C_l(f)$	linear cost of installing the new feeder cables (€/m)
$C_l(\mathrm{UG}, area)$	linear cost of underground cable replacement in the area (€/m)
$C_l(\mathrm{OH}, area)$	linear cost of overhead cable replacement in the area (€/m)
C_r	cost of reconnecting a dwelling link to the feeder (€)
$C_{3\phi,m}$	cost of a three-phase meter (€)
$D_r(\gamma)$	number of dwellings in rural areas of the country
$D_u(\gamma)$	number of dwellings in urban areas of the country
D_f	number of dwellings in the detailed feeder
D_i	number of dwellings in the island
δ	discount rate
$i_{nom}(fs)$	feeder segment ampacity (A)
$l(dl)$	dwelling link length (m)
$l(fs)$	feeder segment length (m)
$l_t(f)$	feeder length (m)
L	lifetime, i.e. planning horizon for grid reinforcements (years)
$P_0(\tau)$	transformer no-load losses (kW)
$R(\tau^j)$	transformer phase resistance (Ω)
$R_l(dl)$	dwelling link linear resistance (Ω/m)
$R_l(fs)$	feeder segment linear resistance (Ω/m)
$S_{nom}(\tau)$	transformer nominal power (kVA)
$X(\tau^l)$	Transformer phase reactance (Ω)
$X_l(dl)$	dwelling link linear reactance (Ω/m)
$X_l(fs)$	feeder segment linear reactance (Ω/m)
$\%\mathrm{OH}(area)$	percentage of the LV cable length which is overhead in the area
$\%\mathrm{UG}(area)$	percentage of the LV cable length which is underground in the area

1 General introduction

An adaptation and/or a further deployment of EU energy (electricity, thermal and gas) grids is essential to successfully carry out the energy transition. First, regarding the electricity grid, distribution networks have to be reinforced in order to integrate residential low-carbon technologies such as heat pumps, photovoltaic systems and electric vehicles. Second, when it comes to thermal grids, the development of district heating, a technology that incorporates energy efficiency and resource synergy principles, can trigger important greenhouse gas emissions reduction. Third, the well-developed natural gas grid infrastructure can be used to distribute renewable gas (e.g. biogas, biomethane and hydrogen) and offer storage capacity.

This deliverable investigates the potential transformation of the electricity, thermal and gas grids in the EU28 (EU27 + United Kingdom). It is composed of three main sections:

- **Section 2 (pages 13 to 64) focuses on electricity grids**. This section develops a method to evaluate the required low-voltage grid reinforcement cost as a function of the residential low-carbon technologies integration scenario for the different EU28 countries.
- **Section 3 (pages 65 to 76) deals with thermal grids**. This section presents a methodology to map the cost of thermal grids deployment per heat demand unit in the EU.
- **Section 4 (pages 77 to 88) focuses on gas grids.** This section presents key technical and economic data on current infrastructures for natural and renewable gases.

Each of these three sections is structured as following: summary of the section, introduction, main content (which can contain several sub-sections), conclusion.

Several European universities have contributed to this deliverable. KU Leuven (KUL, Belgium) carried out the work on electricity grids and coordinated the deliverable. Halmstad University (HU, Sweden) and Europa-Universität Flensburg (EUF, Germany) performed the work on thermal grids. Aalborg University (AAU, Denmark) focused on gas grids.

2 Electricity grids

2.1 Summary of the section

The deployment of low-carbon technologies (LCTs) in buildings, such as photovoltaic (PV) systems, heat pumps (HPs) and electric vehicles, can significantly contribute to the reduction of greenhouse gas emissions. However, the integration of these LCTs has a strong impact on the stability of the electricity distribution grids, which therefore often need to be reinforced (e.g. transformers and/or cables may have to be replaced by ones of higher capacity).

We propose a methodology to evaluate the reinforcement costs of EU low-voltage (LV) grids depending on LCT integration. This methodology uses the share of dwellings in rural and urban areas in EU28 countries as well as a model that evaluates the grid reinforcement cost as a function of the LCT integration scenario for representative rural and urban grids. This model is composed of three sub-models, namely the dwelling, grid and economic models. In addition to presenting each of the developed sub-models, we identified their key parameters. In order to determine the parameter values of the grid and economic models for EU28 countries, we also collected data from 24 open access grids (i.e. grids of which the specifications are freely accessible online) and 23 scientific articles and reports.

The dwelling model, based on occupant behaviour and building properties, produces realistic dwelling load and generation profiles depending on the integrated LCTs. The grid model, based on unbalanced power flow simulations, evaluates the influence of the dwellings' load/generation profiles and of the reinforcement options on the grid stability. Using the data from open access grids and scientific articles and reports, we were able to define six sets of grid parameter values. These sets represent rural and urban grids of Belgium, Germany and the EU in general. The EU sets can be used for the remaining EU countries, for which sufficient data could not be retrieved. The economic model computes the life-cycle cost associated to a grid reinforcement option. It includes both investment and operating costs of the LV grid. The literature review was used to define one set of economic parameter values that is common to all EU28 countries.

Finally, we provide example applications that illustrate the methodology by computing the grid reinforcement costs from HPs and PV systems integration in Belgium and Italy.

2.2 Introduction

In electricity distribution grids, deploying low-carbon technologies (LCTs), such as photovoltaic (PV) systems and heat pumps (HPs), can significantly contribute to the reduction of greenhouse gas emissions (Good, Ceseña, Zhang, & Mancarella, 2016). Nonetheless, the integration of these new generation sources and loads significantly affects the distribution grid stability, which therefore often requires to be reinforced (Andoni, Robu, Früh, & Flynn, 2017). In order to guide the LCT deployment strategy in the European Union (EU), it is thus required to quantify the cost of LCT integration into the distribution grids for the different EU28 countries.

More specifically, we focus on low-voltage (LV) grids and we propose a methodology that allows determining the LV grid reinforcement cost as a function of the LCT integration scenario and the considered EU country. We consider three types of possible reinforcements: (1) replacing the distribution transformer by one of higher nominal power, (2) replacing cables by cables of larger cross-section and (3) connecting LCTs to three phases instead of one. We also examine all the combinations between these three reinforcement types.

The first objective of this part on electricity grids is to present the overall methodology developed for the quantification of LV grids reinforcement costs for EU28 countries. This methodology is based on urbanisation data for the different EU28 countries, provided by work package 5 (WP5), and a model that allows determining the grid reinforcement cost as a function of the integration scenario for representative LV grids.

The second objective is to present the above-mentioned model. This model is built on three sub-models namely the dwelling, grid and economic models. The dwelling model, based on occupants and building properties, derives temporal electricity demand and generation profiles depending on the integrated LCTs. The grid model, based on unbalanced power flow simulations, evaluates the influence of the dwellings' load/generation profiles and of the reinforcement options on the grid stability. The economic model computes the cost associated to the reinforcement options.

The third objective is to identify the parameters required in the three sub-models and to determine values of these parameters for the different EU28 countries. While the parameters of the dwelling model are mostly obtained from work package 1 (WP1), which is notably focusing on buildings, we performed a literature review to determine the values of the parameters of the grid and economic models. These parameters will be used when applying the developed methodology to estimate grid reinforcement costs in the EU.

The fourth objective is to illustrate the methodology on case studies. We thus present the application of the methodology to compute the grid reinforcement costs from HPs and PV systems integration in Belgium and Italy, representative for a moderate and warm climate.

In Section 2.3, we present the framework considered. In Section 2.4, we provide the urbanisation data and give an overview of the model used to determine the grid reinforcement cost as a function of the LCT integration scenario for representative LV grids. In Sections 2.5, 2.6 and 2.7 we present the three sub-models, the associated parameters and the values encountered for these parameters through literature review. In Section 2.8, we present the application of the methodology to Belgium and Italy. Finally, in Section 2.9, we discuss the methodology.

2.3 Framework

The distribution grid is composed of the medium voltage (MV) and low voltage (LV) levels as shown in Figure 1. A large share of the facilities of the industry and service sectors is connected to the MV network. The residential sector and some buildings of the service sector (e.g. small offices) are connected to the LV network.

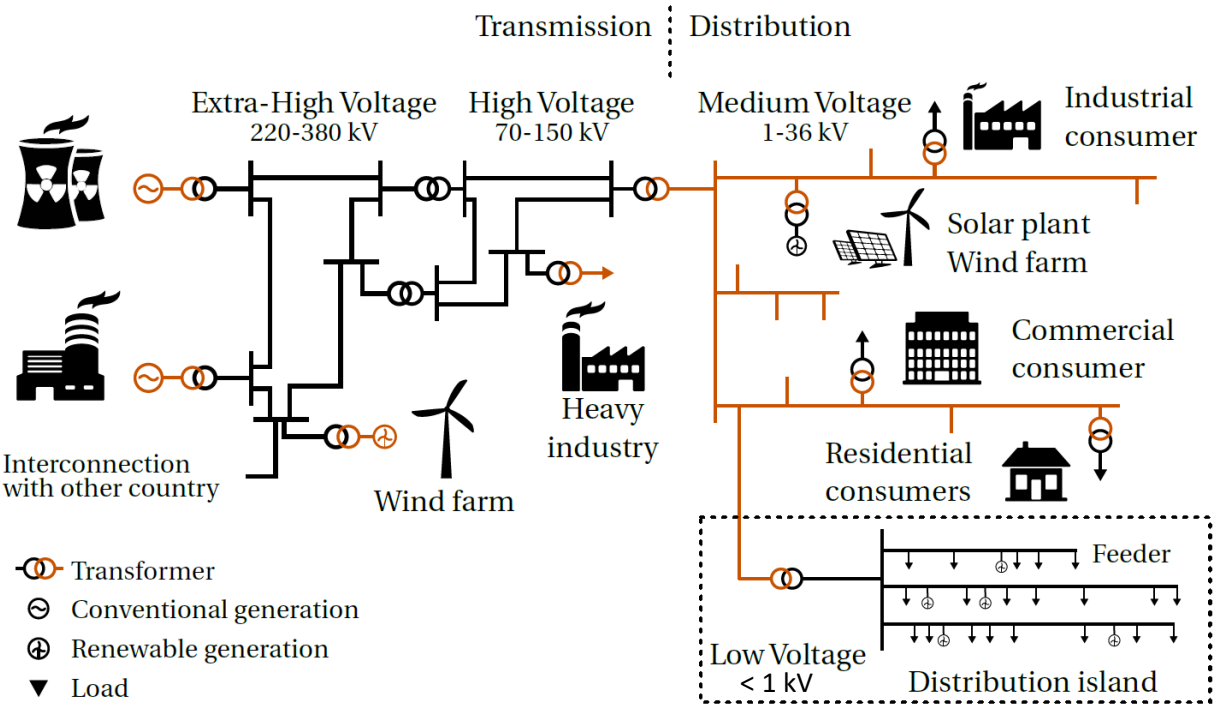

Figure 1 – Overview of electricity grids (Protopapadaki, 2018)

The integration of LCTs (e.g. photovoltaic systems, heat pumps) impacts the stability of the MV and LV grids (e.g. transformer overloading). The grids thus often need to be reinforced, which comes at an added cost for the distribution system operator (DSO) (Andoni et al., 2017).

In this report, we focus and develop a methodology to study the influence of LCTs integration on low-voltage (LV) grids. In addition, for LV grids, we focus on LCT integration in the residential sector. Even though the integration in the service sector would also have been interesting to study, we decided to focus on the residential sector for the following reasons:

- The generation of electricity demand profiles of the service sector is different from the generation of electricity load profiles for the residential sector and would thus require significant research time.
- In the EU, the electricity consumption for the service and the residential sectors represents 30% and 29% of the total consumption respectively (Tsemekidi-Tzeiranaki et al., 2018). However, we can expect that a significant share of the electricity consumption for the service sector takes place in large buildings (e.g. shopping malls, office centres, hospitals, universities) which are usually directly connected to the MV grid with their own transformer (F2 Energy, 2018). For instance, in the United States, buildings with more than 25 000 m^2 accounted for 68% of the total energy consumption of the service sector (eia, 2018).

- The buildings of the service sector that are connected to the LV level (e.g. small offices) are mostly located in urban areas. Additionally, the reinforcement costs may be expected to be low in urban areas as shown in (McKenna, Djapic, Weinand, Fichtner, & Strbac, 2018).
- In general, residential buildings have their consumption peak in the evening when significant grid stability problems may thus be expected. On the opposite, service sector buildings connected to the LV grid are expected to have a consumption peak during working hours. Consequently, the service sector may not strongly increase the simultaneity in the evening and is expected not be responsible for significant additional reinforcements.

Figure 2 presents an example of Belgian rural and urban low-voltage grids. In each grid, there is one transformer and several feeders (4 for the rural grid and 5 for the urban one). The LV grid, which is constituted of the transformer and the feeders, is also called a 'distribution island'. The average length of feeder cable per dwelling is higher in the rural grid than in the urban one. In Figure 2, different rates of integration of LCTs in the households of the island are also shown (20, 40 and 60% integration of heat pumps in this case). The households that receive a LCT are determined randomly.

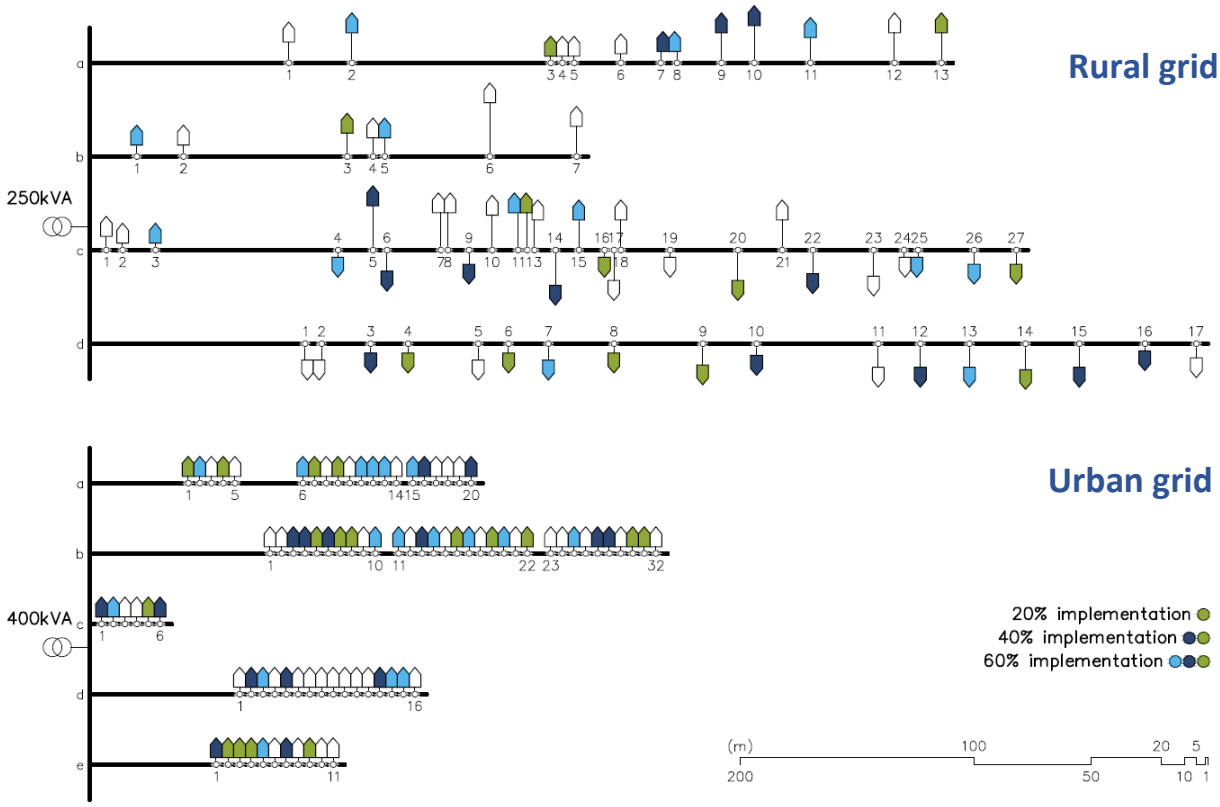

Figure 2 – Example of Belgian urban and rural grids with varying rates of heat pumps integration. Adapted from (Baetens, 2015).

2.4 Methodology overview

The objective of the methodology is to estimate the LV grid reinforcement cost for a country γ as a function of the LCT integration scenario[1] LCT_σ in residential areas of this country. We propose the following formula for the LV grid reinforcement cost, $LCC^*(\gamma, LCT_\sigma)$:

$$LCC^*(\gamma, LCT_\sigma) = D_r(\gamma) \cdot LCC^*_{d,r}(\gamma, LCT_\sigma) + D_u(\gamma) \cdot LCC^*_{d,u}(\gamma, LCT_\sigma) \quad (1)$$

where:

- $D_r(\gamma)$ and $D_u(\gamma)$ are the number of dwellings in rural and urban areas of the country γ respectively. They are computed from households density maps (see section 2.4.1).
- $LCC^*_{d,r}(\gamma, LCT_\sigma)$ and $LCC^*_{d,u}(\gamma, LCT_\sigma)$ are the reinforcement costs per dwelling following LCT integration in rural and urban areas of the country respectively. They are computed from representative rural and urban grids (see section 2.4.2 and sections 2.5 to 2.7).

2.4.1 Number of dwellings in rural and urban areas of each EU country

In Table 1, we provide the number of households in rural and urban areas of each EU country. This database has been developed by Europa-Universität Flensburg (EUF) and Halmstad University (HU) from the 2011 European Census (Eurostat, 2011) as part of their work on spatial analyses. More specifically, the number of rural and urban households in each country is obtained from the EU household density map by first identifying coherent and connected land use. Then each identified area is categorized as rural if it contains less than 200 people or it is smaller than 5 ha, and as urban otherwise. We observe that the largest majority of dwellings (89%) are located in urban areas of the EU. In this report, we consider that each household is associated to one dwelling.

It is important to note that the definition used for categorizing rural and urban areas may differ from one study on spatial mapping to the other (Jonard, Lambotte, Ramos, Terres, & Bamps, 2009; United Nations Statistics Division, 2017), which may influence the share of urban and rural dwellings in each country. Additionally, LV grids are usually classified as rural or urban in the literature (see Section 2.6.3.3) but authors very rarely specify the definition used for separating rural from urban areas. These two elements may be a source of uncertainty regarding the approach presented in this deliverable.

[1] A detailed definition of 'LCT integration scenario' is given in Section 2.4.2.1

Table 1 – Number of households in urban and rural areas of EU28 countries
Data based on the 2011 European Census (Eurostat, 2011)

Country	Urban		Rural	
	Number of households	% of households	Number of households	% of households
AT (Austria)	3.60×10^{6}	88%	4.83×10^{5}	12%
BE (Belgium)	4.95×10^{6}	96%	1.86×10^{5}	4%
BG (Bulgaria)	3.48×10^{6}	95%	1.86×10^{5}	5%
CY (Cyprus)	3.23×10^{5}	94%	2.21×10^{4}	6%
CZ (Czechia)	5.11×10^{6}	91%	5.03×10^{5}	9%
DE (Germany)	3.80×10^{7}	92%	3.18×10^{6}	8%
DK (Denmark)	2.41×10^{6}	87%	3.55×10^{5}	13%
EE (Estonia)	5.63×10^{5}	86%	8.81×10^{4}	14%
EL (Greece)	4.10×10^{6}	83%	8.36×10^{5}	17%
ES (Spain)	1.83×10^{7}	93%	1.45×10^{6}	7%
FI (Finland)	4.30×10^{6}	81%	1.01×10^{6}	19%
FR (France)	2.64×10^{7}	88%	3.58×10^{6}	12%
HR (Croatia)	1.46×10^{6}	81%	3.33×10^{5}	19%
HU (Hungary)	4.58×10^{6}	95%	2.58×10^{5}	5%
IE (Ireland)	1.29×10^{6}	66%	6.63×10^{5}	34%
IT (Italy)	2.28×10^{7}	84%	4.30×10^{6}	16%
LT (Lithuania)	1.23×10^{6}	87%	1.78×10^{5}	13%
LU (Luxembourg)	2.16×10^{5}	91%	2.14×10^{4}	9%
LV (Latvia)	8.62×10^{5}	85%	1.53×10^{5}	15%
MT (Malta)	1.68×10^{5}	96%	6.84×10^{3}	4%
NL (Netherlands)	7.14×10^{6}	91%	6.80×10^{5}	9%
PL (Poland)	1.37×10^{7}	85%	2.44×10^{6}	15%
PT (Portugal)	3.35×10^{6}	76%	1.04×10^{6}	24%
RO (Romania)	8.93×10^{6}	94%	5.21×10^{5}	6%
SE (Sweden)	4.12×10^{6}	87%	5.99×10^{5}	13%
SI (Slovenia)	5.84×10^{5}	62%	3.59×10^{5}	38%
SK (Slovakia)	2.91×10^{6}	94%	1.73×10^{5}	6%
UK (United Kingdom)	2.85×10^{7}	93%	2.19×10^{6}	7%
Total	**2.13×10^{8}**	**89%**	**2.58×10^{7}**	**11%**

2.4.2 Model for computing the reinforcement cost per dwelling for representative grids

2.4.2.1. Presentation

For each country, we consider one representative grid for the urban area and one representative grid for the rural area, which are defined by a set of parameters, as explained in Section 2.6. The grid is labelled as 'representative' as the values of its parameters (e.g. number of feeders) are representative of the ones in the considered country and area (rural/urban). For each representative grid, we compute the reinforcement cost per dwelling from the model presented in Figure 3.

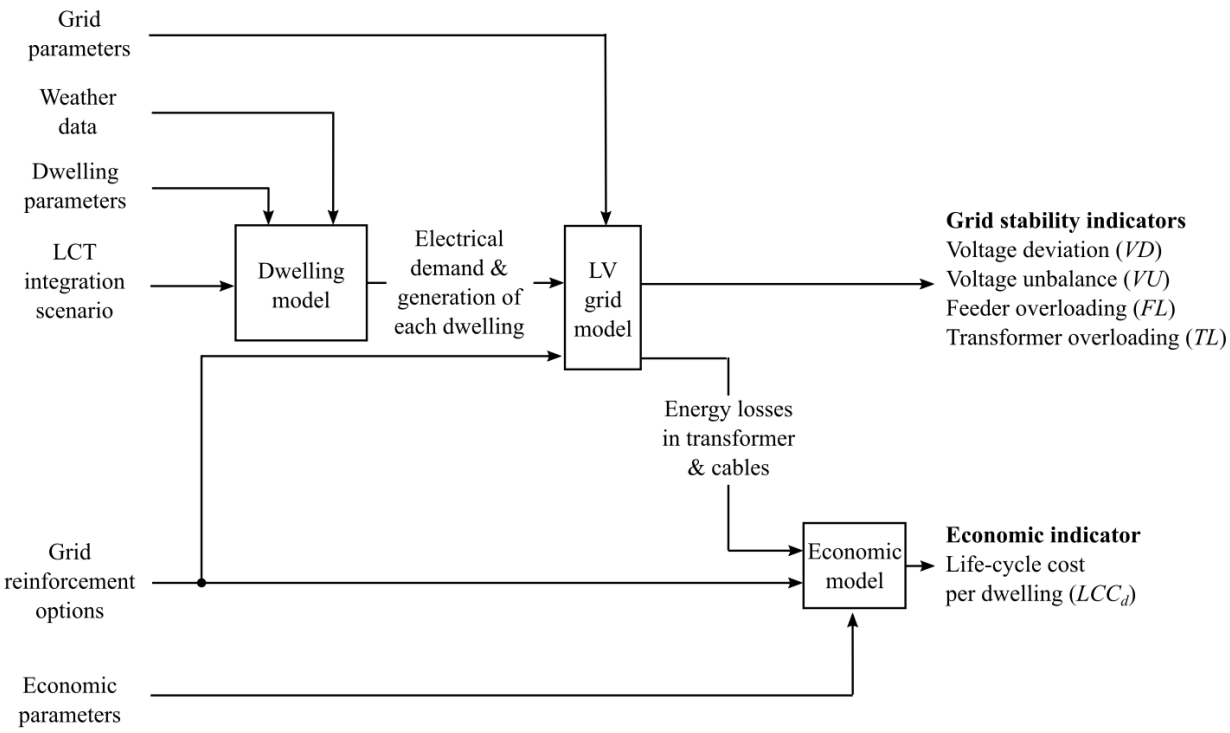

Figure 3 – Model for computing the reinforcement cost per dwelling as a function of the LCT integration scenario for representative grids

The inputs of the model are:

- The **dwelling parameters**, such as the floor area of the dwelling, the window-to-wall ratio and the occupancy profile. These parameters are described in Section 2.5 and their values for EU countries are mostly obtained from WP1 (see Section 2.5.3).

- The **LCT integration scenario**. The main types of LCTs that can be integrated in residential dwellings and that have an impact on the LV grid are heat pumps (HPs), photovoltaic (PV) systems and electric vehicles (EVs). An LCT integration scenario corresponds to the percentage of each LCT, provided by WP6, that is integrated in the dwellings of the grid. A LCT integration scenario would be for instance integration rates of 20% of HPs, 40% of PV systems and 0% of EVs in the dwellings of the grid. This means that 20% of the dwellings have a HP, and 40% have a PV system. The dwellings of the grid that have a LCT are randomly chosen. Some of the dwellings may have several LCTs, for instance both a HP and a PV system. Note that the LCT integration rates in urban and rural grids may differ (a concrete example of that is given in Section 2.8.1.2).

- The **weather data**, such as the irradiance and the outdoor temperature. They are described in Section 2.5.4.

- The **grid parameters**, such as the number of dwellings per distribution island and the percentage of dwellings connected to three phases. These parameters are fully described in Section 2.6.3 and we gathered data on these parameters for the different EU countries and areas (rural/urban).

- The **reinforcement options** are defined relative to the initial grid. The initial grid is designed to have feeder cables and a transformer that satisfy the loads when no LCTs are integrated (see Section 2.4.2.2). This represents an existing grid where no measures have been implemented to enable hosting LCTs. There are no investment costs and the life-cycle cost for this initial grid is composed only of operating costs to cover energy losses. In the following, we present the three considered grid modifications that allow hosting the new LCTs by alleviating potential voltage and loading problems in the distribution island. We also explain the logic behind these modifications:
    - *Replacement of the distribution transformer by one with higher nominal power.* Increasing the nominal power of the transformer decreases transformer loading and contributes to reduce voltage deviation and unbalance, as it reduces voltage variation (Baetens, 2015) (Protopapadaki & Saelens, 2017).
    - *Replacement of the main feeder cables by cables of larger cross-section.* Increasing the cross-section of the main feeder cables reduces feeder loading, by increasing the nominal current of the cable. It also decreases voltage deviation and unbalance, by reducing cable resistance (Protopapadaki, 2018).
    - *Connection of the LCTs of one type in the detailed feeder to three phases instead of one*[2]. For this modification, we suppose that all the LCTs are connected to three phases, limiting the number of reinforcement options[3]. Connecting LCTs to three phases contributes to reduce voltage unbalance, thanks to a better distribution of the power among the three phases (Baetens, 2015).

  A reinforcement option can be composed of one of the three above-mentioned modifications, or any combinations between these modifications (e.g. replacing both the feeder cables and the transformer). We present how the adequate reinforcement option is chosen in Section 2.4.2.2.

- The **economic parameters**, such as the cost of cable replacement and the discount rate. These parameters are fully described in Section 2.7.2 and we gathered data on these parameters for the EU.

The model is composed of three sub-models:

- The **dwelling model** (see Section 2.5), based on dwelling parameters, derives temporal electricity demand and generation profiles for each dwelling depending on the integrated LCTs.

- The **grid model** (see Section 2.6) receives as input the temporal demand and generation profiles of each dwelling (which are applied at the connection point between the dwelling and the feeder), the grid parameters and the considered grid reinforcement option. Thanks to unbalanced power flow simulations, it allows to compute four grid stability indicators which

[2] This modification does not apply to dwellings of the feeder that are already connected to three phases in the initial grid, as the LCTs would be connected by default to three phases in these dwellings.

[3] For instance, let us consider a grid where dwellings are connected to one phase in the initial grid and where HPs and PV systems are integrated. We thus consider the following possibilities: connect (a) all HPs and all PV systems to one phase (no reinforcement), (b) all HPs to three phases and all PV systems to one phase, (c) all HPs to one phase and all PV systems to three phases, (d) all HPs and all PV systems to three phases.

are defined in Section 2.6.2.2. We consider a reinforcement option as technically viable if all four grid stability indicators are within the required limits.

- The **economic model** (see Section 2.7) computes the life-cycle cost per dwelling LCC_d corresponding to the grid reinforcement option.

2.4.2.2. Initialisation and use

In this section, we present four key points about the initialisation and the use of the model. These points are illustrated concretely in Section 2.8.1.

Selecting the cheapest technically viable reinforcement option for a LCT integration scenario

For a given LCT integration scenario (e.g. 20% HP and 40% PV), we apply the model presented in Figure 3 for all the considered reinforcement options. We thus determine the value of grid stability indicators and of the life-cycle cost per dwelling LCC_d for each reinforcement option. The selected grid reinforcement option for the considered LCT integration scenario is the option that fulfils all the grid stability constraints and has the lowest cost. The cost for this option is denoted by LCC_d^* (a 'star' is added in superscript) and it corresponds to the grid reinforcement cost compared to the initial grid for the considered LCT integration scenario.

Model initialisation

In the initial grid (where no LCTs are integrated), all the grid parameters are obtained from the literature except for the cross-section of the feeder cables $cr(f)$ and the nominal power of the transformer $S_{nom}(\tau)$ (see Section 2.6.3). In order to determine these two parameters, we use the model to identify the couple $cr(f)$ & $S_{nom}(\tau)$ that satisfies the grid stability at the lowest cost for 0% integration of all LCTs (Few, Djapic, Strbac, Nelson, & Candelise, 2020).

Capturing uncertainty

In order to capture uncertainties in dwellings' demand and generation, as well as the random distribution of LCTs in a feeder, the methodology allows to perform several repetitions for each LCT integration scenario (Protopapadaki & Saelens, 2019). For each repetition, the dwelling, grid and economic models are evaluated with different occupants and different locations for the LCTs. Within one LCT integration scenario (e.g. 20% HP & 40% PV), the repetition parameters, such as the choice of occupancy profiles and LCT locations, are the same for all reinforcement options, to allow a fair comparison. When repetitions are considered, the grid stability indicators and cost for a given reinforcement option are taken as the average among the different repetitions. The reinforcement option is considered as technically viable if all four grid stability indicators are within the required limits (see Section 2.6.2.2) for all repetitions. The number of repetitions is chosen depending on the available computing time and the desired robustness.

Defining a cost function

To be able to easily use the results of this methodology in WP6, we can develop one cost function per country and type of grid (rural or urban), based on the detailed simulation results. Once the reinforcement cost has been evaluated for a significant number of LCT integration scenarios (e.g. all combinations between [0, 20, 40, 60, 80, 100] %HP and [0, 20, 40, 60, 80, 100] %PV) with the model of Figure 3, it is possible to fit a cost function (typically a polynomial) that relates the LCT integration scenario to the reinforcement cost. We can then use this function to compute the reinforcement cost

for a previously non-considered LCT integration scenario (e.g. 24% HP & 33% PV), without having to go through the whole model and in a reduced computing time.

2.5 Dwelling

The overview of the dwelling model is shown in Figure 4. At the moment, this model integrates photovoltaic systems and heat pumps as LCTs. However, given its customizable components, it is as well possible to integrate EVs. The model is implemented in the IDEAS Modelica library (Baetens et al., 2015)(Jorissen et al., 2018) and it is simulated with the Dymola software. It generates electricity demand and generation profiles of each dwelling with a time step of 10 minutes.

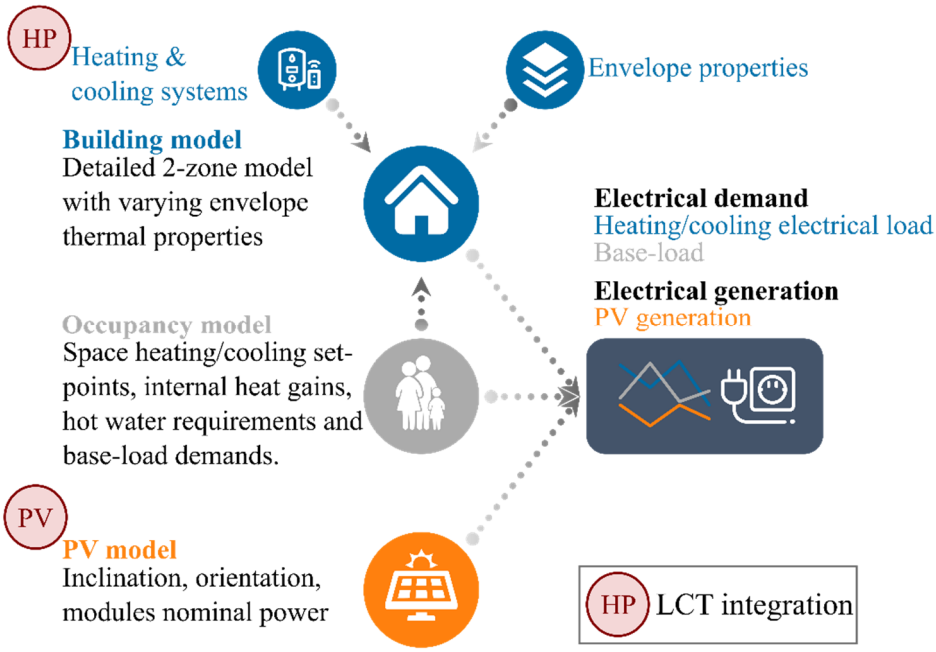

Figure 4 – Main components of the dwelling energy model

The considered building structure and the dwelling model are presented in Section 2.5.1 and Section 2.5.2 respectively. We summarize the dwelling parameters in Section 2.5.3 and we present the weather data in Section 2.5.4.

2.5.1 Structure

We consider the generic structure shown in Figure 5. Each dwelling is considered to be an individual building with the building structure comprising two thermal zones: the day-zone, representing living area and kitchen on the ground floor, and the night-zone including, for instance, bedrooms and corridors on the first floor. The building is assumed to have a pitched roof, and the two zones are connected with a common floor, but no air circulation. Internal heat gains are distributed arbitrarily as 70 % to the day-zone and 30 % to the night-zone. It is expected that more appliances would be located in those rooms, and that occupants would also spend more of their active time in kitchen and living room.

The main parameters of the building's structure are given in Table 2. We consider two building types: detached and terraced. The building type influences the definition of boundary walls, repartition of window area and floor plan dimensions ratio, as illustrated in Figure 5. Walls towards neighbouring houses in case of terraced houses are modelled as adiabatic walls, assuming similar conditions on the other side.

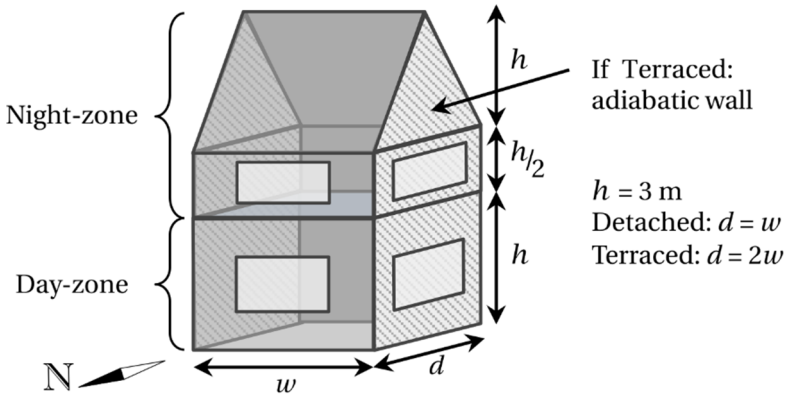

Figure 5 – Generic building structure

2.5.2 Model

Each dwelling is assigned a set of occupant profiles (see Section 2.5.2.1). The thermal building model (see Section 2.5.2.2) then simulates the thermal and electrical demand for the given occupants, envelope properties, heating system (e.g. heat pump), and weather conditions for one year. Furthermore, PV generation is simulated for the same weather and for the considered PV system (see Section 2.5.2.3). All models produce active power profiles. We then implement a power factor for each profile, which depends on the considered electric appliance, in order to obtain the equivalent reactive power profile. We consider power factors of 0.98 for the base-load (Navarro-Espinosa & Ochoa, 2016), 0.98 for HP (Navarro-Espinosa & Ochoa, 2016; Protopapadaki, 2018), 1 for direct electric heating (Energy Sector Management Assistance Program, 2020) and 1 for PV (Synergrid, 2019; Ciric & Markovic, 2017).

2.5.2.1. Occupancy

The stochastic residential occupancy model corresponds to the Python StROBe Package as described in (Baetens & Saelens, 2016). The model produces sets of profiles that include what we refer to as “base load”, corresponding to electricity demand profiles for lighting, domestic appliances and electronics. The occupant model also generates internal heat gains, space heating/cooling set-points and hot-water demand, which are inputs to the building model.

2.5.2.2. Building

The building model allows computing the electrical demand for heating and cooling from the properties of the building envelope, the outputs of the occupancy model, and the chosen heating/cooling system(s).

Firstly, we compute the thermal demand, which comprises the space heating, space cooling and domestic hot water demands. The latter is directly obtained from the occupancy model. The demand for space heating and cooling is simulated with a detailed model of the two thermal zones of the building. The air in each zone is assumed perfectly mixed with uniform temperature, and the envelope components are defined based on typical construction characteristics and specified properties (see Table 2). The building thermal model further makes use of inputs from the occupancy model and weather data (outdoor temperature and solar irradiance).

The thermal demand can be met by electricity (e.g. direct electric heating, heat pumps) or by other energy sources (e.g. gas boiler). When the space heating and cooling demand are fulfilled by electricity

(e.g. direct electric heating, air conditioning), they are supposed to be met directly, i.e. the shape of the electricity demand profile is the same as the one of the thermal demand profile. The final electricity demand profile is obtained through the efficiency of the electric appliance. In the case of the hot water demand, it is considered to be met through a hot water storage tank that is maintained at a constant temperature and heated primarily during the night (i.e. the shapes of the electricity and thermal profiles are different) (Protopapadaki, 2018). This notably allows reducing strong peaks in the electricity consumption.

Regarding the technology of HPs that are integrated in the LCTs integration scenarios, we consider air-source HPs rather than ground-source HPs, as they are the most common ones (U.S. department of energy, 2020) (Vito, 2016) and are also expected to have a higher impact on the grid (Navarro-Espinosa & Mancarella, 2014).

2.5.2.3. **PV**

PV generation is simulated based on the model of De Soto, Klein, and Beckman (2006). This model creates PV production profiles for any rated capacity, inclination and orientation of the PV system as a function of the weather data (notably irradiance on the plane of the PV modules and outdoor temperature). We consider a power density of 164 W_p/m^2 for PV modules and the PV system rated capacity is restricted by the roof's dimensions (no more than 80% of the pitched roof's area on one side can be covered by PV panels) (Protopapadaki, 2018).

In the grid simulation, for each dwelling with a PV system the electricity generated is first used to meet the dwelling's demand, and the remainder is injected to the grid.

2.5.3 **Dwelling parameters**

In Table 2, we summarize the main building parameters. The values of these parameters for the different zones (rural/urban) of each EU country are based on the data from WP1 (see deliverables of WP1 in the sEEnergies website, https://www.seenergies.eu/reports/). We use data corresponding to the building stock in 2020. We apply the following hypotheses to the raw data from WP1 to use them in our analysis on electricity grids:

- For each country, WP1 provides one set of building parameters for dwellings in single-family houses, and one set for dwellings in multi-family houses (buildings where there are several apartments). We model dwellings in single-family houses as detached buildings, using the geometry of Figure 5 and the parameters (e.g. floor area, window-to-wall ratio, U-values) corresponding to single-family houses provided by WP1. In addition, we model dwellings in multi-family houses as individual terraced buildings, using the geometry of Figure 5 and the parameters corresponding to multi-family houses from WP1. This allows us to approximate dwellings in multi-family houses, even though we only use one building structure (see Figure 5). This approach is also conservative. Indeed, by modelling dwellings in multi-family houses as individual terraced buildings we may exaggerate their envelope area exposed to the outdoor environment. This could lead to an overestimation of the heat demand and thus of the grid impacts (when heating is provided by electricity).
- The dwellings are presumed to be oriented North/South. In this case, all the PV modules are oriented towards the South which leads to higher generation compared to other orientations. Second, the fact that all the dwellings have the same orientation increases the simultaneity

between the PV generation profiles. Consequently, orienting all the dwellings North/South is conservative in terms of grid reinforcement cost.

- The U-values provided by WP1 for walls, roof and floors on ground were used to calculate the insulation thickness in predefined typical construction types. This is because the building thermal model uses a detailed representation of the different material layers of each component, such that it can also capture the effects of thermal mass. For the windows, a glazing type with U-value close to the window's U-value is chosen, and the frame's U-value is adjusted to obtain the desired total U-value.
- WP1 provides the share of dwellings which are in a single-family house and the share which are in a multi-family house per EU country in 2020 (these shares are given in Appendix A which is in Section 2.11.1). Let us also remind the reader that all dwellings in single-family houses are modelled as detached buildings and that all dwellings in multi-family houses are modelled as individual terraced buildings. In order to split detached and terraced buildings by rural and urban areas, we proceed in two steps. First, we fill the rural areas with detached buildings. If there are more dwellings in rural areas than there are available detached buildings, we complete the rural areas with terraced buildings. Second, as the remaining dwellings are in urban areas, we obtain from the first step the share of terraced and detached (if any) buildings in urban areas. This procedure to split detached and terraced buildings in urban and rural areas might lead to an overrepresentation of detached buildings in rural areas. However, in the absence of additional data, we chose this procedure as the potential overrepresentation of detached buildings in rural grids, which are the most sensitive to grid stability problems (McKenna et al., 2018), may lead to a potential overestimation of the overall grid reinforcement cost which is thus conservative.

Table 2 – Main building parameters.

Description	Possible values
Building type	Detached, terraced
Floor area (m^2)	Continuous
Window-to-wall ratio	Continuous, between 0 and 1
Orientation	North/South
U-values of building elements (wall, window, roof and basement) (W/m^2K)	Continuous
Air change rate (h^{-1}) (accounts for both hygienic ventilation and infiltration)	Continuous
Type of heating/cooling system(s) (e.g. air-source heat pump, gas boiler)	**Heating systems:** gas boiler (not explicitly modelled), direct electric heater, heat pump **Cooling systems:** split air-conditioners (Heat roadmap europe, 2017)
Efficiency of electrical heating/cooling system(s)	Continuous
PV system rated capacity (W_p)	Continuous (limited by roof size)
PV system inclination (°)	Continuous
PV system orientation	South

Finally, another significant assumptions that we made in the dwelling model is that we considered that, whatever the EU country, we use a pool of 300 stochastic Belgian occupancy profiles, obtained from surveys of 3474 Belgian households through the model StROBe (Baetens & Saelens, 2016). Indeed, it is difficult to find similar surveys for other EU countries and it is extremely time consuming to process these surveys in order to derive occupancy profiles. Nevertheless, even though we consider one set of building parameters for detached buildings and one set for terraced one per EU country, we consider all the 300 different occupancy profiles thus allowing to obtain variation in the resulting electricity profiles.

2.5.4 Weather data

The main weather data considered are the ambient temperature and the irradiance (for the building and PV models). The data for each considered country were retrieved from Meteonorm (Meteotest, 2009). Additionally, we use weather data corresponding to an extreme year (a possibility offered by Meteonorm): high irradiance in summer (and thus high PV electrical generation) and low temperature in winter (and thus high HP electrical demand). Indeed, such an extreme year corresponds to the largest impacts on the LV grid (e.g. voltage deviation, transformer overloading) and may take place during the grid planning horizon. DSOs may thus consider extreme year data for their studies in order to be on the conservative side.

For each EU country, we compute the results using data from one city, preferably around the centre of the country (when available from Meteonorm). Even though this assumption is not without influence, especially for countries where the climate varies from one region to another like France, we had to make it in order to keep a reasonable computing time.

2.6 Low-voltage grid

The grid model receives as input the active and reactive power profiles of each dwelling, which are applied at each connection point in the grid, the grid parameters and the considered grid reinforcement option. Thanks to unbalanced power flow simulations, it allows to compute four grid stability indicators and the energy losses in the transformer and in the cables. In Section 2.6.1, we describe in further detail the grid architecture. In Section 2.6.2, we present the grid model and the definition of the grid stability indicators. In Section 2.6.3, we summarize the grid parameters and present the values for these parameters for EU countries.

2.6.1 Architecture

We consider three-phase four-wire radial grids in star configuration with nominal voltage of 230 V at 50 Hz, which are common in residential EU low-voltage grids (Lampe, Tonello, & Swart, 2016; Protopapadaki, 2018; Van Roy, 2015). The grid architecture considered is presented in Figure 6 (Protopapadaki & Saelens, 2017; Protopapadaki, 2018). In this architecture, the feeder of interest is modelled in detail, while the remainder low-voltage distribution island is represented by an aggregated balanced load (Protopapadaki, 2018; Protopapadaki & Saelens, 2017). This *dummy island* approach allows focusing on the details of a given feeder, while also taking into account loads and distributed generation (DG) sources in the rest of the island and notably assessing the transformer loading and the voltage drop at the transformer due to the remainder of the island. This approach was shown to produce small deviations in simulation results in comparison to full island simulations (simulating all feeders of the island in detail) with important reductions in computing time (Protopapadaki, 2018; Protopapadaki & Saelens, 2017). The dwellings are connected to one or three phases depending of the cases. When single-phase connections are considered, the dwelling connections alternate between the 3 phases (e.g. 1st dwelling on phase 1, 2nd dwelling on phase 2, 3rd dwelling on phase 3, 4th dwelling on phase 1 ….), as shown in Figure 6. Finally, when LCTs are integrated, we consider that the integration rate is the same in the rest of the island as in the detailed feeder.

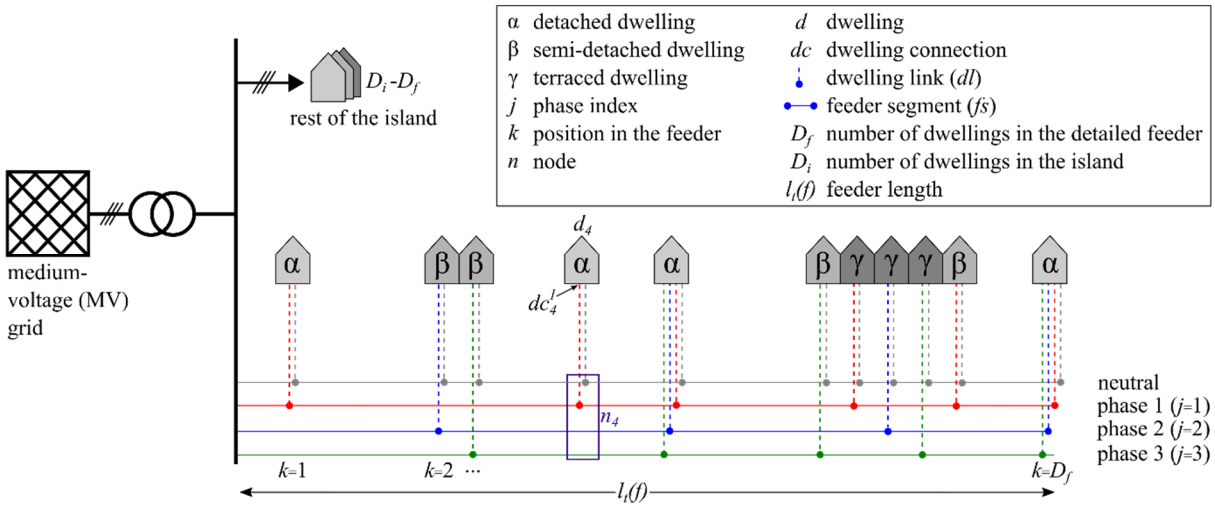

Figure 6 – Grid architecture

2.6.2 Model

2.6.2.1. Unbalanced power flow simulations

We implemented the grid model and quasi-stationary power flow analysis in Modelica and we used components of the IDEAS library (Van Roy, Salenbien, & Driesen, 2014). The model receives as input the active and reactive power profiles of each dwelling. These profiles are applied at each connection point in the detailed feeder, or aggregated and applied as a balanced load in a dummy feeder for the rest of the island. The power flow analysis is based on Joule's law for linear conductor and Kirchhoff's circuit laws (Van Roy et al., 2014). It computes for each simulation time step (10 minutes) the voltage and current at all nodes and branches. For this work, we specifically define the following outputs:

- The line-to-neutral voltage at each dwelling connection of the detailed feeder. We denote $v(dc_k^j)$ the line-to-neutral voltage at dwelling connection dc_k^j, which corresponds to the connection of the dwelling in position k to phase j (see Figure 6). If the dwelling is connected to three phases, we define three dwelling connections.
- The line-to-line voltages at each node of the detailed feeder. We denote $v(n_k^{j,j'})$ the line-to-line voltage at the node in position k between phases j and j'. In order to be able to calculate voltage unbalance (see Section 2.6.2.2), the line-to-line voltages between all 3 phases are defined for all positions k even for positions where the dwelling is connected to only 1 phase. For example, in Figure 6, $v(n_4^{1,2})$, $v(n_4^{2,3})$ and $v(n_4^{3,1})$ are defined for node 4, even though the dwelling is connected only to phase 1 at this position.
- The current in each feeder segment of the detailed feeder $i(fs)$.
- The current in each dwelling link connected to the detailed feeder $i(dl)$.
- The apparent power through the transformer $S(\tau)$.
- The current in each phase j of the transformer $i(\tau^j)$.

2.6.2.2. Grid stability indicators

We propose four grid stability indicators which are computed from the outputs of the LV grid model. We define these indicators not only to know when a grid stability constraint is violated, but also to be representative of the magnitude of this violation. Out of four grid stability indicators described in the next paragraphs, the feeder overloading, voltage unbalance and voltage deviation indicators are computed for the detailed feeder, and the transformer overloading is computed for the transformer serving the whole island (see Figure 6).

Voltage deviation indicator VD. The voltage at each dwelling connection $v(dc_k^j)$ is subject to the limitations set by the European Standard EN 50160 (Markiewicz & Klajn, 2004; Navarro-Espinosa & Ochoa, 2016). This standard requires the per unit voltage (expressed as fraction of the nominal voltage, 230 V in Europe) to remain always' between 0.85 and 1.1 pu and between 0.9 and 1.1 pu for at least 95 percent of the time each week (Markiewicz & Klajn, 2004; Navarro-Espinosa & Ochoa, 2016). The voltage levels are computed with a 10 minutes time step (Markiewicz & Klajn, 2004). In order to verify compliance with the Standard, we define the voltage deviation indicator for dwelling d_k: $VD(d_k)$. If the dwelling is connected to 1 phase, $VD(d_k)$ is equal to 1 if the Standard on voltage deviation is violated at least once during the whole simulation period for the phase to which the dwelling is connected, and equal to 0 otherwise. If the dwelling is connected to 3 phases, $VD(d_k)$ is equal to 1 if the Standard on voltage deviation is violated at least once during the whole simulation period for any of the 3 phases, and to 0 otherwise. The voltage deviation indicator for the whole feeder VD is equal

to the sum of the $VD(d_k)$ divided by the number of dwellings in the feeder D_f. The simulated case is considered as technically unsustainable if VD is higher than 0.

Voltage unbalance indicator VU. We define the voltage unbalance at the node n_k in position k at time t, using the equation proposed by (Chen, Yang, & Yang, 2013):

$$vu(n_k)(t) = \sqrt{\frac{1-\sqrt{3-6\cdot\beta(t)}}{1+\sqrt{3-6\cdot\beta(t)}}} \quad \text{where}$$

$$\beta(t) = \frac{\left(v\left(n_k^{1,2}\right)(t)\right)^4 + \left(v\left(n_k^{2,3}\right)(t)\right)^4 + \left(v\left(n_k^{3,1}\right)(t)\right)^4}{\left(\left(v\left(n_k^{1,2}\right)(t)\right)^2 + \left(v\left(n_k^{2,3}\right)(t)\right)^2 + \left(v\left(n_k^{3,1}\right)(t)\right)^2\right)^2} \tag{2}$$

The voltage unbalance is also computed with a 10 minutes time step (Markiewicz & Klajn, 2004). The European Standard EN 50160 subjects the voltage unbalance at each node to remain below 2% for at least 95% of the time each week (Baetens, 2015; Markiewicz & Klajn, 2004). We therefore define the voltage unbalance indicator at node n_k: $VU(n_k)$. It is equal to 1 if the Standard on voltage unbalance is violated at least once during the whole simulation period, and to 0 otherwise. The voltage unbalance indicator for the whole feeder VU is equal to the sum of the $VU(n_k)$ divided by the number of nodes in the feeder. The simulated case is considered as technically unsustainable if VU is higher than 0.

Feeder overloading indicator FL. We define the overloading of feeder segment fs at time t as (Navarro-Espinosa & Ochoa, 2016):

$$fl(fs)(t) = \max\left(\frac{|i_h(fs)(t)|}{i_{nom}(fs)} - 1, 0\right) \tag{3}$$

where $i_{nom}(fs)$ is the feeder segment ampacity and $i_h(fs)$ is the hourly average current in the feeder segment. $fl(fs)$ is thus computed with a 60 minutes time step (Navarro-Espinosa & Ochoa, 2016). We further define the feeder overloading indicator of the feeder segment: $FL(fs)$. It is equal to 1 if $fl(fs)$ is higher than 0, i.e. the segment is overloaded (Navarro-Espinosa & Ochoa, 2016), at least once during the whole simulation period, and to 0 otherwise. The feeder overloading indicator for the whole feeder FL is equal to the sum of the $FL(fs)$ divided by the number of feeder segments. The simulated case is considered as technically unsustainable if FL is higher than 0.

Transformer overloading TL. We define the overloading of the transformer τ at time t as (Navarro-Espinosa & Ochoa, 2016):

$$tl(\tau)(t) = \max\left(\frac{|S_h(\tau)(t)|}{S_{nom}(\tau)} - 1, 0\right) \tag{4}$$

where $S_{nom}(\tau)$ is the transformer nominal power and $S_h(\tau)$ is the hourly average apparent power that goes through the transformer τ. The transformer overloading $tl(\tau)$ is therefore computed with a 60 minutes time step. The transformer overloading indicator TL is equal to the maximum of the transformer overloading $tl(\tau)$ during the simulation period. If TL is higher than 0, the transformer is overloaded (Navarro-Espinosa & Ochoa, 2016), and the simulated case is considered technically unsustainable.

2.6.2.3. **Energy losses in transformer and cables**

The LV grid model also permits to evaluate the yearly energy losses in the detailed feeder $E_l(f)$ and in the transformer $E_l(\tau)$, which are inputs to the economic model (see Figure 3).

The energy losses in the detailed feeder $E_l(f)$ for year y are determined from the joule losses in each dwelling link dl and feeder section fs (Van Roy, 2015):

$$E_l(f)(y) = \int_y \left(\sum_{fs} R_l(fs) \cdot l(fs) \cdot |i(fs)(t)|^2 + \sum_{dl} R_l(dl) \cdot l(dl) \cdot |i(dl)(t)|^2 \right) dt \quad (5)$$

where $R_l(dl)$ and $R_l(fs)$ are the linear resistances (in Ω/m) of the dwelling link dl and the feeder segment fs respectively, and $l(dl)$ and $l(fs)$ are their lengths (in m).

The energy losses in the transformer $E_l(\tau)$ for year y are given by (Van Roy, 2015):

$$E_l(\tau)(y) = \int_y \left(P_0(\tau) + \sum_{j=1}^{3} R(\tau^j) \left| i(\tau^j)(t) \right|^2 \right) dt \quad (6)$$

where $R(\tau^j)$ is the phase resistance of the transformer (which is considered identical for the three phases (Van Roy, 2015)), $i(\tau^j)$ is the current through phase j of the transformer and $P_0(\tau)$ are the transformer no-load losses.

2.6.3 **Parameters**

2.6.3.1. **Identification**

In Table 3, we present the parameters that have to be known to define a LV grid, which are thus called “characteristic grid parameters”. They are either directly used as such in the grid model (e.g. nominal transformer capacity) or they allow to deduce the parameters used in the grid model through some assumptions, which are given in the ”Notes” column of Table 3. For example, the average length of dwelling links determines the length of each dwelling link $l(dl)$, which is used in the model (see equation (5)). Two parameters (transformer nominal power and feeder segments cross-section) are obtained through model initialisation (see section 2.4.2.2). The rest of the parameters are obtained from the literature on EU LV grids (see sections 2.6.3.2 and 2.6.3.3).

Table 3 – Description of characteristic grid parameters

Characteristic parameter	Notes	Possible values	Way of determination
Parameters related to the island configuration			
Number of dwellings per island D_i		Integer	Literature
Average number of dwellings per feeder	A feeder starts at the secondary of the transformer and ends at the final dwelling of the feeder. We consider that the number of dwellings D_f in the detailed feeder is equal to the average number of dwellings per feeder.	Integer	Literature
Percentage of dwellings connected to three phases	Dwellings can be connected to one (e.g. dwelling in position k = 1 in Figure 6) or three phases (e.g. dwelling in position k = 4 in Figure 6). This parameter represents the share of the dwellings of the island that are connected to three phases.	Continuous	Literature
Transformer nominal power $S_{nom}(\tau)$ (kVA)	The no-load losses P_0, the phase resistance $R(\tau^j)$ and reactance $X(\tau^j)$ of the transformer are deduced from the transformer nominal power $S_{nom}(\tau)$ (see Appendix B which is in Section 2.11.2).	150, 250, 400, 630, 800, 1000 kVA	Model initialisation
Parameters related to feeder segments			
Average length between two consecutive nodes (m)	In order to determine the length between each consecutive nodes (e.g. nodes in positions $k = 1$ and $k = 2$) from the average length between consecutive nodes, we consider that the nodes are equally spaced except for an exceptional random length, which is several times the usual length between nodes. This exceptional length is positioned at the beginning in urban feeders and in the middle in rural ones, to represent exceptional distances found in real feeders (Protopapadaki, 2018). The length of the feeder segments $l(fs)$ is then deduced from the length between consecutive nodes and the dwelling connections (1 or 3 phases, see Figure 6).	Continuous	Literature
Feeder cables cross-section $cr(f)$ (mm^2) and material	We consider that all the segments of the feeder have the same cross-section, equal to $cr(f)$, and material. The feeder segments cross-section and material determines their linear resistance $R_l(fs)$, linear reactance $X_l(fs)$ and ampacity $i_{nom}(fs)$ (see Appendix B which is in Section 2.11.2).	16, 25, 35, 50, 70, 95, 120, 150, 185, 240, 300, 400, 500 mm^2 (Usual values)*	Model initialisation for cross-section, literature for material
Parameters related to dwelling links			
Average length of dwelling links (m)	The length of each dwelling link $l(dl)$ is taken equal to the average length of dwelling links.	Continuous	Literature

Characteristic parameter	Notes	Possible values	Way of determination
Dwelling links cross-section (mm^2) and material	We consider that all dwelling links have the same material and cross-section. The dwelling links material and cross-section determines their linear resistance $R_l(dl)$, linear reactance $X_l(dl)$ and ampacity (see Appendix B which is in Section 2.11.2).	16, 25, 35, 50, 70, 95, 120 mm^2 (Usual values)*	Literature

Note. *: usual values are the ones that have been encountered 3 times or more in grids of the literature.

2.6.3.2. **Sources for data collection on grid parameters**

In order to collect data on the characteristic grid parameters, we used two sources that are complementary: open access grids and scientific articles/reports.

An open access grid corresponds to a grid that is provided for free by a university or an institution on a simulation software (e.g. Matlab, Python). Each open access grid provides a wide range of grid parameters and detailed values for these parameters, such as the resistance of each feeder segment.

Figure 7 shows the architecture corresponding to one of the open access grids studied. It is composed of a 630 kVA transformer, 9 feeders and 144 dwellings in total. The cross-section of feeder segments is 185 mm^2 and their length varies between 14 and 50 m. The cross-sections of dwelling links are 50 and 35 mm^2 and their length is 11 m.

Scientific articles and reports provide some information about grid parameters, but very rarely the values of all required characteristic parameters. However, they cover a wider range of EU countries than open access grids.

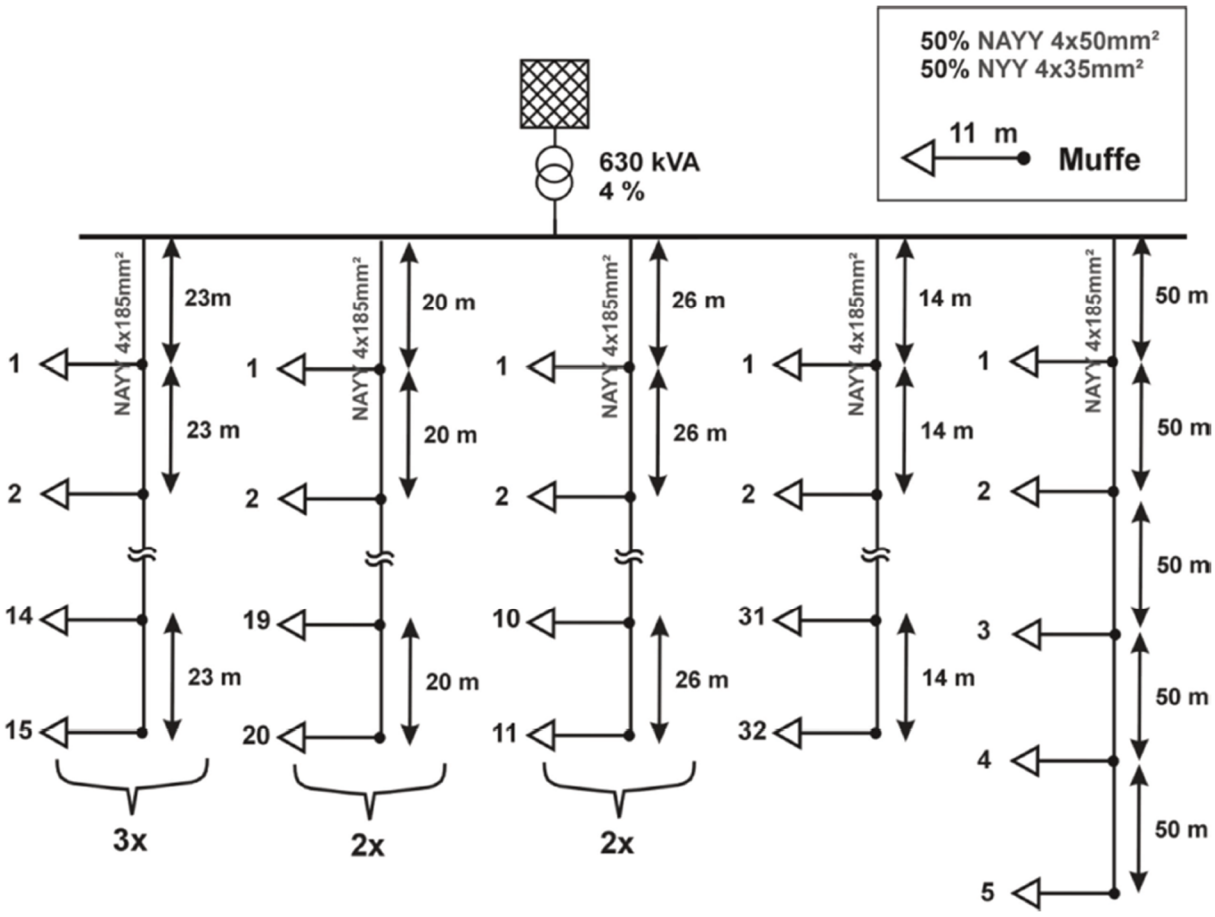

Figure 7 – Example of open access grid considered (Kerber, 2020)

2.6.3.3. **Collected data**

In Table 4, we present the values of the characteristic grid parameters collected through open access grids and scientific articles. Each line corresponds to a grid. We provide the reference in which this grid is found, such as (Rodriguez-Calvo, Cossent, & Frías, 2017), and if this reference is an open access grid repository (labelled 'OG') or a scientific article/report (labelled 'AR').

We split the grids per country and area (e.g. rural, urban). Some grids are designated as representing EU grids in general, so we label them 'EU' in the table. We introduced a new area, 'semi-urban', which corresponds to grids that were not designated as 'urban' or 'rural'. The denomination of this area varied between 'semi-rural', 'village', 'semi-urban', 'residential' and 'sub-urban' depending on the reference. These grids were gathered under the 'semi-urban' denomination for concision. Also note that some grids do not specify the country (labelled as 'Unknown country') or the area (labelled as 'Unknown area'). When there are more than one grid per country and area, we compute the average of the different parameters for this country and area.

Table 4 – Data collected on the values of characteristic grid parameters

Grid origin	Number of dwellings per island D_i	Average number of dwellings per feeder	Percentage of dwellings connected to three phases	Average length between two consecutive nodes (m)	Feeder cables material	Average length of dwelling links (m)	Dwelling links cross-sections (mm^2) and material
Notations. OG: open access grid, AR: scientific articles and reports // 50 (55%), 35 (45%) : the cross-section of 55% of dwelling links is 50 mm^2 and the one of 45% of dwelling links is 35 mm^2 // A (aluminium), C (Copper)							
			EU, Rural				
1 AR (Rodriguez-Calvo et al., 2017)	39	13	0	48			
2 AR (Rodriguez-Calvo et al., 2017)	24	6	0	190			
3 AR (Rodriguez-Calvo et al., 2017)	21	7	0	70			
4 AR (Rodriguez-Calvo et al., 2017)	27	9	0	21			
5 AR (Rodriguez-Calvo et al., 2017)	14	4.7	0	62			
6 AR (Mateo et al., 2018)†	51		0	27			
Average	**29**	**8**	**0**	**70**			
			EU, Semi-urban				
1 AR (Prettico et al., 2016)	108			11			
2 OG (CIGRE, 2014)	37	12.3		36			
3 AR (Rodriguez-Calvo et al., 2017)	233	46.6	0	7.5			
4 AR (Rodriguez-Calvo et al., 2017)	214	30.6	0	10			
5 AR (Mateo et al., 2018)†	87		0	8			
Average	**136**	**30**	**0**	**15**			
			EU, Urban				
1 AR (Prettico et al., 2016)	107	36					
2 AR (Mateo et al., 2018)†	101		0	4			
Average	**104**	**36**	**0**	**4**			
			EU, Unknown area				
1 OG (IEEE, 2020)		55	0	26			
			BE, Rural				
1 AR (Protopapadaki, 2018)	79	28	0	23	A	8	
2 AR (Protopapadaki & Saelens, 2017)	64	16	0	22.5	A		
3 AR (Baetens, 2015)	64	16		22.8	A		
Average	**69**	**20**	**0**	**23**	**A**	**8**	

Grid origin	Number of dwellings per island D_i	Average number of dwellings per feeder	Percentage of dwellings connected to three phases	Average length between two consecutive nodes (m)	Feeder cables material	Average length of dwelling links (m)	Dwelling links cross-sections (mm^2) and material
Notations. OG: open access grid, AR: scientific articles and reports // 50 (55%), 35 (45%) : the cross-section of 55% of dwelling links is 50 mm^2 and the one of 45% of dwelling links is 35 mm^2 // A (aluminium), C (Copper)							
			BE, Urban				
1 AR (Protopapadaki, 2018)	114	28	0	8	A	3	
2 AR (Baetens, 2015)	85	17		8.3	A		
Average	**100**	**23**	**0**	**8**	**A**	**3**	
			CH, Urban				
1 AR (Segundo Sevilla et al., 2018)	111						
			DE, Rural				
1 OG (Lindner et al., 2014)	47	11.8	83	46		21	50
2 OG (Lindner et al., 2014)	36	9	100	34		17	35
3 OG (Kerber, 2020)	13	13.0		21	A		
4 OG (Kerber, 2020)	8	4		49	A		
5 OG (Kerber, 2020)	8	4		105	A	26	50 A
6 OG (Kerber, 2020)	14	7		70	A	26	50 A
7 OG (Kerber, 2020)	26	26		12	A		
8 OG (Kerber, 2020)	27	27		13	A		
9 OG (Kerber, 2020)	26	13		26	A	26	50 A
10 OG (Kerber, 2020)	27	13.5		28	A	25	50 A
Average	**23**	**13**	**92**	**40**	**A**	**24**	**50 A***
			DE, Semi-urban				
1 OG (Lindner et al., 2014)	14	4.7	86	106		29	50
2 OG (Lindner et al., 2014)	11	2.8	73	67		4	35
3 OG (Kerber, 2020)	57	9.5		37	A	23	50 A
4 OG (Kerber, 2020)	58	11.6		31	A	23	50 A
5 OG (Kerber, 2020)	117	13		29	A	23	50 A
6 AR (Stetz, Marten, & Braun, 2013)	122	20.3					
Average	**63**	**10**	**80**	**54**	**A**	**20**	**50 A***

Grid origin	Number of dwellings per island D_i	Average number of dwellings per feeder	Percentage of dwellings connected to three phases	Average length between two consecutive nodes (m)	Feeder cables material	Average length of dwelling links (m)	Dwelling links cross-sections (mm^2) and material
Notations. OG: open access grid, AR: scientific articles and reports // 50 (55%), 35 (45%) : the cross-section of 55% of dwelling links is 50 mm^2 and the one of 45% of dwelling links is 35 mm^2 // A (aluminium), C (Copper)							
DE, Urban							
1 OG (Lindner et al., 2014)	109	9.9	93	30		18	35
2 OG (Kerber, 2020)	146	14.6		20	A	11	50 A
3 OG (Kerber, 2020)	144	16		22	A	11	50 A
4 OG (Kerber, 2020)	145	24.2		12	A	11	50 (55%) A, 35 (45%) C
5 OG (Kerber, 2020)	145	20.7		17	A	11	50 (52%) A, 35 (48%) C
6 OG (Kerber, 2020)	191	21.2		17	A	11	50 (57%) A, 35 (43%) C
7 OG (Kerber, 2020)	192	21.3		17	A	11	50 (49%) A, 35 (51%) C
Average	**153**	**18**	**93**	**19**	**A**	**12**	**50 A***
DE, Unknown area							
1 AR (Biener, Dallmer-Zerbe, Krug, Gust, & Wille-Haussmann, 2015)	80	40		30	A		
IT, Unknown area							
1 AR (Carpinelli, Mottola, Proto, & Varilone, 2017)	23	7.7		109	A, C		
UK, Unknown area							
1 AR (Vegunta, Twomey, & Randles, 2013)	265	66					
2 AR (Navarro-Espinosa & Ochoa, 2015)	351	58.5		26			
3 AR (Navarro-Espinosa & Ochoa, 2016)	636	90.9		29			
Average	**417**	**72**		**28**			
UK, Semi-urban							
1 AR (Navarro-Espinosa & Mancarella, 2014)	400	100		12	A		

Grid origin	Number of dwellings per island D_i	Average number of dwellings per feeder	Percentage of dwellings connected to three phases	Average length between two consecutive nodes (m)	Feeder cables material	Average length of dwelling links (m)	Dwelling links cross-sections (mm^2) and material
Notations. OG: open access grid, AR: scientific articles and reports // 50 (55%), 35 (45%) : the cross-section of 55% of dwelling links is 50 mm^2 and the one of 45% of dwelling links is 35 mm^2 // A (aluminium), C (Copper)							
Unknown country, Urban							
1 AR (van der Burgt, Vera, Wille-Haussmann, Andersen, & Tambjerg, 2015)	141	35.3					

Notes. †: results from this reference come from a survey filled by 79 EU DSOs.
*: For the cable cross-section and material, which takes discrete values, we considered the highest number of occurrences and not the average.
For some grids, it is not clear whether the dwelling links are considered and/or the difference is not made between the main feeder cables (which contribute to the 'length between two consecutive nodes') and the dwelling links. In such cases, as the length between two consecutive nodes is usually higher than the one of the dwelling links and in order to be on the conservative side in terms of grid reinforcements, we allocate the entire reported cables length to the main feeder cables. In the representative grids (see Table 5), the average length of dwelling links is obtained from the grids that explicitly consider dwelling links.

2.6.3.4. **Discussion and final values chosen for the grid parameters**

In Table 4, we observe that the only countries/regions for which there are more than one grid for both the rural and urban areas are Belgium, Germany and generic EU grids. We can also notice that German grids are by far the best documented. Throughout the review of open access grids and scientific articles, we also observed that all reviewed grids are three-phase four-wire radial grids. This confirms our choice of grid architecture (see section 2.6.1).

We also identify trends between rural and urban grids. We observe that the number of dwellings per island is in general higher in urban grids than in rural ones. The number of dwellings per feeder also appears to slightly increase with the population density. Finally, the average length between two consecutive nodes and the average length of dwelling links is usually higher in rural areas than in urban ones.

Given the available data, we propose to consider one rural and one urban grid for Belgium, one rural and one urban grid for Germany, as well as one rural and one urban grid for the rest of the EU, which will be used for the remaining EU countries. The parameters chosen for the grids are given in Table 5. These parameters were obtained from the average values given in Table 4, with the following modifications (which affect the numbers in green on Table 5):

- The average length of dwelling links is not known for the EU-rural and EU-urban grids. To determine its value for the EU-rural grid, we take the average between the value for the Belgian-rural grid (8 m) and for the German-rural one (24 m). We do the same for the EU-urban grid with the values from the Belgian-urban grid and the German-urban one.
- The feeder cables material is not known for the EU grids. We thus take the same material as for the German and Belgian grids.

- The dwelling links cross-sections are not known for EU and Belgian grids. We thus take the same values as for the German grids.
- The dwelling links material is not known for the EU and Belgian grids. We thus take the same material as for the German grids.

Table 5 – Final values chosen for the characteristic grid parameters

Number of dwellings per island D_i	Average number of dwellings per feeder	Percentage of dwellings connected to three phases	Average length between two consecutive nodes (m)	Feeder cables material	Average length of dwelling links (m)	Dwelling links cross-sections (mm^2) and material
			EU, Rural			
29	8	0	70	A	16	50 A
			EU, Urban			
107	36	0	7	A	8	50 A
			BE, Rural			
69	20	0	23	A	8	50 A
			BE, Urban			
100	23	0	8	A	3	50 A
			DE, Rural			
23	13	92	40	A	24	50 A
			DE, Urban			
153	18	93	19	A	12	50 A

Notation. A (Aluminium)

2.7 Economic

The economic model computes the cost corresponding to grid reinforcement options. In Section 2.7.1, we present the model. In Section 2.7.2, we summarize the economic parameters and present the values for these parameters in the EU.

2.7.1 Model

The model evaluates the life-cycle cost corresponding to reinforcements of the detailed feeder. It takes into account the investment costs IC and the operating costs OC during the considered lifetime L (i.e. the planning horizon for grid reinforcements). We then divide the cost for the detailed feeder by the number of dwellings in this feeder D_f in order to be able to compare costs between grids with different number of dwellings. The life-cycle cost per dwelling LCC_d is given by (Wu, Aye, Ngo, & Mendis, 2017; 3E, 2017):

$$LCC_d = \frac{IC + \sum_{y=1}^{L} \frac{OC(y)}{(1+\delta)^y}}{D_f} \tag{7}$$

where δ is the discount rate.

2.7.1.1. Investment costs

The investment cost IC for the detailed feeder is given by (Baetens, 2015; Fluvius, 2020):

$$\begin{aligned} IC = {} & b_\tau \cdot C(\tau) \cdot \frac{D_f}{D_i} + b_f\left(l_t(f) \cdot C_l(f) + D_f \cdot C_r\right) \\ & + \sum_{d=1}^{D_f} b_{3\phi}(d)\left(C_{3\phi,m} + l(dl) \cdot C_l(dl) + \bar{b_f} \cdot C_r\right) \end{aligned} \tag{8}$$

$b_\tau \cdot C(\tau) \cdot \frac{D_f}{D_i}$ is the cost associated to replacing the transformer by one with a higher nominal power. b_τ is a binary variable equal to 1 if the transformer is replaced, $C(\tau)$ is the cost of the newly installed transformer τ, D_i and D_f are the number of dwellings in the island and in the feeder respectively. The ratio D_f/D_i represents the share of the transformer replacement cost that is attributable to the detailed feeder.

$b_f\left(l_t(f) \cdot C_l(f) + D_f \cdot C_r\right)$ is the cost associated to replacing the main cables of the detailed feeder by cables of higher cross-section. b_f is a binary variable equal to 1 if the cables are replaced, $l_t(f)$ is the length of the detailed feeder (equal to the number of dwellings in the feeder D_f times the average length between two consecutive nodes), $C_l(f)$ is the linear cost of installing the new feeder cables and C_r is the cost of reconnecting a dwelling link to the feeder.

$\sum_{d=1}^{D_f} b_{3\phi}(d)\left(C_{3\phi,m} + l(dl) \cdot C_l(dl) + \bar{b_f} \cdot C_r\right)$ is the cost corresponding to connecting LCTs of dwellings of the detailed feeder to 3 phases. This applies to the case where the dwellings are initially connected to 1 phase. To connect LCTs to 3 phases, a new dwelling link is required. $b_{3\phi}(d)$ is a binary variable which is equal to 1 if at least one LCT of the dwelling d is being connected to three phases, $C_{3\phi,m}$ is the cost of a three-phase meter, $l(dl)$ is the dwelling link length, $C_l(dl)$ is the linear cost of replacing the current one-phase dwelling link by a three-phase cable. $\bar{b_f}$ is the negation of the b_f binary variable, used to include the cost of reconnecting dwelling links to the feeder, only if the main feeder

cables are themselves not replaced. In the latter case, this cost is already accounted for in the feeder replacement cost.

2.7.1.2. Operational costs

The operating costs are associated to energy losses in the feeder f and the transformer τ. The yearly operating cost OC at year y is given by (Baetens, 2015; Ćurčić, Strbac, & Zhang, 2001):

$$OC(y) = \left(E_l(\tau)(y) \cdot \frac{D_f}{D_i} + E_l(f)(y) \right) \cdot C(E_l) \quad (9)$$

where $C(E_l)$ is the cost per kWh of energy losses for the DSO.

After a large number of simulations on typical grids, we decided to neglect the cost of transformer ageing. Indeed, the share of the cost of transformer ageing on the total cost of technically viable reinforcement options was found to be lower than 1 %. In addition, considering transformer ageing requires 13 times longer simulation time, notably due to the non-linearity of the transformer ageing model and to the importance of transient states in this model.

2.7.2 Parameters

2.7.2.1. Identification

The economic parameters are:

- Transformer investment cost $C(\tau)$, in €
- Main feeder cables replacement linear cost $C_l(f)$, in €/m
- Dwelling link replacement linear cost $C_l(dl)$, in €/m
- Cost of reconnecting a dwelling link to the feeder C_r, in €
- Cost of a three-phase meter $C_{3\phi,m}$, in €
- Energy losses cost $C(E_l)$, in €/kWh
- Planning horizon L, in years
- Discount rate δ

Note that some grid parameters (see Section 2.6.3) are also used in the economic model.

2.7.2.2. Sources for data collection on economic parameters

Data on economic parameters were obtained from scientific articles and reports only. Unfortunately, no values are provided for economic parameters in open access grids.

2.7.2.3. Collected data

In Table 6, we present the values of the economic parameters collected through scientific articles and reports.

Table 6 - Data collected regarding the values of economic parameters

Parameter	Values from the literature
Transformer investment cost, i.e. cost of the newly installed transformer $C(\tau)$	• **150 kVA**: 6.7 k€ (Ma, Li, & Li, 2016)* • **250 kVA**: 7.6 k€ (Stetz et al., 2013), 18.6 k€ (Ma et al., 2016)*, 7.5 k€ (Baetens, 2015) • **400 kVA**: 8.9 k€ (Stetz et al., 2013), 8.5 k€ (Stetz et al., 2014), 30.5 k€ (Ma et al., 2016)*, 10.2 k€ (Baetens, 2015) • **630 kVA**: 10.9 k€ (Stetz et al., 2013), 11.7 k€ (Stetz et al., 2014), 21.6 k€ (Morvaj, Evins, & Carmeliet, 2017), 14.1 k€ (Baetens, 2015) • **800 kVA**: 14.3 k€ (Stetz et al., 2014) • **1000 kVA**: 28.3 k€ (Cossent, Olmos, Gómez, Mateo, & Frías, 2011)

Main feeder cables replacement linear cost $C_l(f)$†
 	
Dwelling link replacement linear cost $C_l(dl)$†
	Overall costs
	• UG & urban: 77 €/m, UG & semi-urban: 19 €/m, OH & rural: 18 €/m (Ma et al., 2016)*
	• UG & meadow ground: 24 €/m, UG & sidewalk ground: 48 €/m, UG & roadway ground: 72 €/m (Baetens, 2015)
	• OH & semi-urban: 11-15 €/m, UG & semi-urban: 71-78 €/m (Cossent et al., 2011)
	• Urban: 82 €/m (Morvaj et al., 2017)
	• Urban: 93-163 €/m (Navarro-Espinosa & Ochoa, 2015)*
	
	Cost breakdown
	• Cables
	  ○ 3×150 mm^2: 19 €/m (Stetz et al., 2013)
	  ○ 3×150 mm^2 & aluminium: 14 €/m (Stetz et al., 2014)
	  ○ 3×240 mm^2 & aluminium: 20 €/m (Stetz et al., 2014)
	• Laying cable: 27 €/m (Stetz et al., 2013)
	• Surface restoration: 58 €/m (Stetz et al., 2014)

Cost of reconnecting a dwelling link to the feeder C_r	453 € (Baetens, 2015)
Cost of a three-phase meter $C_{3\phi,m}$	149 € (Fluvius, 2020)
Energy losses cost $C(E_l)$	0.046 €/kWh (Elexys, 2020), 0.085 €/kWh (Stetz et al., 2013), 0.074 €/kWh (Stetz et al., 2014)
Planning horizon L	• Overall project planning horizon: 33 years (VREG, 2016) • Transformer lifetime: 40 years (Stetz et al., 2014) • Cables lifetime: 40 years (Stetz et al., 2014)
Discount rate δ	5% (3E, 2017), 8% (Stetz et al., 2014), 4% (Morvaj et al., 2017), 5% (Ma et al., 2016)
Countries considered in the references. EU: (Morvaj et al., 2017); BE: (3E, 2017; Baetens, 2015; Elexys, 2020; Fluvius, 2020; VREG, 2016); DE: (Stetz et al., 2013; Stetz et al., 2014); ES: (Cossent et al., 2011); UK: (Ma et al., 2016; Navarro-Espinosa & Ochoa, 2015)	

Note. UG: underground, OH: overhead.

†: Except for (Baetens, 2015) who explicitly specifies that the cable reconnection cost C_r is not included in the cable linear cost $C_l(f)/C_l(dl)$, the other references do not specify if they already include the reconnection cost in the cable linear cost value that they provide. In order to be on the conservative side, we suppose that they do not take it into account. Consequently, we always add the reconnection cost to the cable linear cost (see equation (8)) as done by (Baetens, 2015), who has provided the most detailed cost analysis.

Values from references with a star ('*') are converted from £ to € with the conversion rate of 1.11 €/£ from 3 August 2020 (XE, 2020).

We have corrected the costs that were obtained for years earlier than 2020 for inflation. We used an average EU yearly inflation rate of 1% (Statista, 2020) to transpose to 2020. The values given in the table for these costs are therefore "2020 equivalent" ones.

The majority of references does not mention value-added tax (VAT). The only reference that mentions it is (Baetens, 2015) and it does not include VAT for its grid reinforcement cost evaluation. As the other references conduct a similar study as (Baetens, 2015), we also suppose that they exclude VAT. Thus the costs of the table are assumed not to include VAT.

2.7.2.4. Discussion and final values chosen for the economic parameters

There is no country for which we have all the values for all the parameters. Thus, the final values chosen for the economic parameters, given in Table 7, are common to all EU countries. These final values are obtained based on the values given in Table 6 and using processing described in the following paragraphs.

Transformer investment cost. In Figure 8, we show the data of the transformer investment cost as a function of its nominal power for the different articles. We observe that, for a given nominal power, the transformer cost may strongly vary from one article to another. We tried several fits for the data and we retained the one presented in black: $C(\tau) = 7.13 \cdot \exp\left(0.0012 \cdot S_{nom}(\tau)\right), \mathrm{R}^2 = 0.33$). Despite its low R^2, we observe that the fit goes through the majority of the data points, except for the outliers from references (Ma et al., 2016), (Morvaj et al., 2017) and (Cossent et al., 2011). The cost values in Table 7, are obtained from the considered fit.

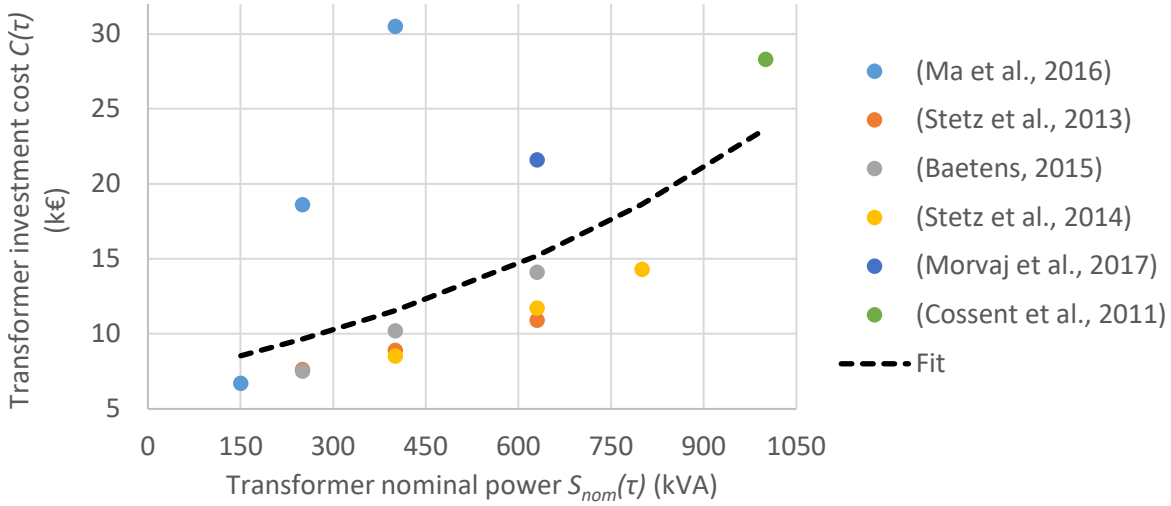

Figure 8 – Transformer investment cost as a function of its nominal power in the literature

Cable replacement cost. In Table 6, we observe through the cost breakdown that the majority of the cable replacement cost comes from the cable installation (laying the cable, surface restoration…) and not from the cable itself. In addition, the variation of the cable cost as a function of its cross-section has a small influence on the overall cable replacement cost. Consequently, we consider the same replacement cost for the main feeder cables and the dwelling links, i.e. $C_l(f) = C_l(dl)$.

We also see from the overall costs (see Table 6) that the cable replacement cost strongly varies depending on the area (urban/rural) and on the cable position (underground-UG/overhead-OH). In addition, despite certain local initiatives for the undergrounding of cables (Baetens, 2015), a clear trend towards cable undergrounding at the EU scale was not identified (Prettico et al., 2019) and we thus consider that UG cables are replaced by UG cables and OH cables by OH cables. We thus propose the following formula for the cable replacement cost:

$$C_l(f)(\text{area}) = C_l(dl)(\text{area}) = \%\text{UG}(\text{area}) \cdot C_l(\text{UG}, \text{area}) + \%\text{OH}(\text{area}) \cdot C_l(\text{OH}, \text{area}) \quad (10)$$

where:

- $\%\text{UG}(\text{area})$ and $\%\text{OH}(\text{area})$ are the percentages of the LV cable length which are underground and overhead in the considered area. We use the values considered by (Prettico et al., 2016), who gathered data from 79 EU DSOs. These percentages are reported in Table 7.
- $C_l(\text{UG}, \text{area})$ and $C_l(\text{OH}, \text{area})$ are the linear costs of underground and overhead cable replacement in the considered area. $C_l(\text{UG}, \text{area})$ strongly varies depending on the area as the work required to open and close a trench depends on the type of ground (Baetens, 2015). In urban areas, we take the average between the value from Ma et al. (2016) of 77 €/m and the value of sidewalk ground from Baetens (2015) of 48 €/m. This gives $C_l(\text{UG}, \text{urban})$ = 63 €/m. In rural areas, we take the average between the values for sidewalk and meadow grounds from Baetens (2015), which yields to 36 €/m. $C_l(\text{OH}, \text{area})$ is expected not to vary significantly depending on the area. For instance, the cost for rural areas, 18 €/m from Ma et al. (2016), is similar to the cost for semi-urban areas, 11-15 €/m from Cossent et al. (2011). Consequently, we consider the same cost for the rural and urban areas, equal to the average between 18 €/m and 11-15 €/m, which yields to 16 €/m.

For the **cost of reconnecting a dwelling link to the feeder** and the **cost of a three-phase meter**, we take the only available value each time.

For the **energy losses cost**, we take the average of the three available values.

For the **planning horizon**, we retain the value from VREG (2016) of 33 years. This value is coherent with the lifetime of 40 years considered by Stetz et al. (2014) for the main grid components (transformer and cables).

For the **discount rate**, we take the average of the four available values.

Table 7 – Final values chosen for the economic parameters

Parameter	Values chosen
Transformer investment cost $C(\tau)$	• 150 kVA: 8.5 k€ • 250 kVA: 9.6 k€ • 400 kVA: 11.5 k€ • 630 kVA: 15.2 k€ • 800 kVA: 18.6 k€ • 1000 kVA: 23.7 k€
Main feeder cables replacement linear cost $C_l(f)$ Dwelling link replacement linear cost $C_l(dl)$	$C_l(f)(\text{area}) = C_l(dl)(\text{area}) = \%\text{UG}(\text{area}) \cdot C_l(\text{UG}, \text{area}) + \%\text{OH}(\text{area}) \cdot C_l(\text{OH}, \text{area})$ where: • $\%\text{UG}(\text{urban})$ = 86%, $\%\text{OH}(\text{urban})$ = 14%; • $C_l(\text{UG}, \text{urban})$ = 63 €/m, $C_l(\text{OH}, \text{urban})$ = 16 €/m; • $\%\text{UG}(\text{rural})$ = 4%, $\%\text{OH}(\text{rural})$ = 96%; • $C_l(\text{UG}, \text{rural})$ = 36 €/m, $C_l(\text{OH}, \text{rural})$ = 16 €/m. we thus obtain: • $C_l(f)(\text{urban}) = C_l(dl)(\text{urban})$ = 56 €/m • $C_l(f)(\text{rural}) = C_l(dl)(\text{rural})$ = 17 €/m
Cost of reconnecting a dwelling link to the feeder C_r	453 €
Cost of a three-phase meter $C_{3\phi,m}$	149 €
Energy losses cost $C(E_l)$	0.068 €/kWh
Planning horizon L	33 years
Discount rate δ	5.5 %

2.8 Application of the methodology to Belgium and Italy

In this section, we assess the grid reinforcement cost for two case studies: Belgium and Italy. The objective of this section is to show concrete cases of application of the methodology. We chose Belgium and Italy because several input parameters vary between them:

- **The share of dwellings in rural and urban areas,** which influence the grid reinforcement cost in the country. For instance, as shown in Table 1, the percentage of household in rural areas is 4% in Belgium and 16% in Italy.
- **The dwelling parameters**, which influence the dwelling electricity profiles. For instance, according to WP1 data, wall U-values in Belgium are equal to 0.70 W/m²K while they are equal to 0.84 W/m²K in Italy (see Table 8).
- **The climate**, which influences the dwelling electricity demand. For instance, as winters are colder in Belgium than in Italy, when the heating demand is provided through HPs, the electricity demand for heating tends to be higher in Belgium.
- **The grid parameters**, which influence the grid stability and the reinforcement cost per dwelling. For Belgium, the specific grid parameters are known while for Italy we use the generic EU grid (see Table 5).

The objective of Section 2.8.1 is not only to provide the results for Belgium but also to detail the application of the methodology. In Section 2.8.2, we apply the same methodology to Italy. In Section 2.8.3, we compare the results of the Belgian and Italian case studies.

2.8.1 Belgium

In this section, we compute the LV grid reinforcement cost for Belgium $LCC^*(BE, LCT_\sigma)$ as a function of the LCT integration scenario LCT_σ. As presented in Section 2.4, $LCC^*(BE, LCT_\sigma)$ is given by:

$$LCC^*(BE, LCT_\sigma) = D_r(BE) \cdot LCC^*_{d,r}(BE, LCT_\sigma) + D_u(BE) \cdot LCC^*_{d,u}(BE, LCT_\sigma) \quad (11)$$

where:

- $D_r(BE)$ and $D_u(BE)$ are the number of dwellings in rural and urban areas of Belgium, equal to 1.86×10^5 dwellings and 4.95×10^6 dwellings respectively.
- $LCC^*_{d,r}(BE, LCT_\sigma)$ and $LCC^*_{d,u}(BE, LCT_\sigma)$ are the reinforcement costs per dwelling following LCT integration in rural and urban areas of the country respectively. They are computed from representative rural and urban grids.

In Section 2.8.1.1, we detail the computations for $LCC^*_{d,r}(BE, LCT_\sigma)$ and $LCC^*_{d,u}(BE, LCT_\sigma)$. In Section 2.8.1.2, we deduce $LCC^*(BE)$ from $LCC^*_{d,r}(BE, LCT_\sigma)$ and $LCC^*_{d,u}(BE, LCT_\sigma)$.

2.8.1.1. Computing the reinforcement costs per dwelling for representative grids

The reinforcement costs per dwelling, $LCC^*_{d,r}(BE, LCT_\sigma)$ and $LCC^*_{d,u}(BE, LCT_\sigma)$, are computed from the model presented in Section 2.4.2 (see Figure 3 which gives an overview of the model). In Section 2.8.1.1.1, we present the inputs that are required to compute the reinforcement costs per dwelling. In Section 2.8.1.1.2, we illustrate how the reinforcement costs per dwelling are computed as a function of the LCT integration scenario and we provide the results.

2.8.1.1.1. Inputs

Table 8 provides the inputs to compute the reinforcements costs per dwelling for Belgium and Italy (inputs for Italy are used in Section 2.8.2). These inputs come from the results of Sections 2.5 to 2.7. The inputs in Table 8 also integrate the following considerations (the parts concerned by the different considerations are identified by a green symbol in Table 8). Below, we detail the numerical application of these considerations for Belgium but the same considerations of course apply to Italy.

- **(C1) LCT integration scenario.** In this case study, we only integrate HPs and PV systems as low-carbon technologies. We want to be able to compute the reinforcement cost per dwelling for any combination of HP integration rate, varying between 0 and 100%, and PV system integration rate, also varying between 0 and 100%. An LCT integration scenario LCT_σ is thus denoted as "%HP & %PV".
- **(C2) Model initialisation for determining feeder cables cross-section and transformer nominal power in the initial grid.** The cross-section of the feeder cables $cr(f)$ and the nominal power of the transformer $S_{nom}(\tau)$ in the initial grid (without reinforcement) are obtained through model initialisation (see Section 2.4.2.2), for the rural and urban cases separately. For no LCT integration, we simulated the grid stability indicators and the cost LCC_d for each combination $cr(f)$ & $S_{nom}(\tau)$. Note that we considered only usual values of feeder cable cross-sections (see Table 3). We select the combination that satisfies the grid stability at the lowest cost. This yields 70 mm^2 for the feeder cable cross-section and 150 kVA for the transformer of the initial grid, for both the Belgian rural and urban cases.
- **(C3) Pre-selection of the reinforcement options.** The different modifications that can take place for reinforcing the grids are:
    - Replacing the distribution transformer by one of higher nominal power. The current transformer (150 kVA) may be replaced by one of 250, 400, 630, 800 or 1000 kVA.
    - Replacing the main feeder cables by cables of larger cross-section. The current feeder cables may be replaced by cables of cross-section 95, 120, 150 or 185 mm^2.
    - Connecting the HPs to three phases instead of one.
    - Connecting the PV systems to three phases instead of one.

When combining all these possibilities, we obtain 6 (transformers) × 5 (feeder cables) × 2 (HPs to one or three phases) × 2 (PV systems to one or three phases) = 120 reinforcement options. Simulating all these options corresponds to a very significant computing time.

To reduce the computing time we perform a pre-selection of the reinforcement options based on the following arguments. Firstly, we observed that the cable cross-section has a strong influence on the grid stability (e.g. voltage deviation, feeder overloading) and a negligible one on the feeder cable replacement cost (see Section 2.7.2.4). Consequently, we consider that the 70 mm^2 cable can be replaced by three sizes higher directly, i.e. 150 mm^2. This was for instance also considered in (Baetens, 2015).

Secondly, regarding the transformer nominal capacity, preliminary simulations inform us that, for the Belgian urban grid, the 400 kVA transformer is not overloaded in any LCT integration scenario. Additionally, increasing the transformer nominal capacity decreases voltage variation and thus improves voltage stability. Thus, to better explore the potential of increasing the transformer nominal power to improve voltage stability, we also consider the transformer size that is just above the size that is never overloaded. For the Belgian urban grid, we therefore consider 250 kVA,

400 kVA and 630 kVA as reinforcement options. For the Belgian rural grid, as the 250 kVA transformer is never overloaded in all integration scenarios, we thus consider 250 kVA and 400 kVA as reinforcement options.

Consequently, we obtain 4 (transformers) × 2 (feeder cables) × 2 (HPs to one or three phases) × 2 (PV systems to one or three phases) = 32 reinforcement options for the Belgian urban grid and 24 for the Belgian rural grid. Before running the final simulation (see Section 2.8.1.1.2), we make sure that no grid stability constraints are violated for the strongest reinforcement (400/630 kVA transformer, 150 mm^2 feeder cables, HPs connected to three phases and PV systems connected to three phases) in the following extreme LCT integration cases: 100% HP & 100% PV, 100% HP & 0% PV, 0% HP & 100% PV.

- **(C4) Number of random repetitions.** As presented in Section 2.4.2.2, for a given LCT integration scenario (e.g. 40% HP & 20% PV), we can simulate the results for several random repetitions, between which the occupancy profiles and the location of the LCTs vary. In Section 2.8.1.1.2 (step 2), we detail the concrete use of repetitions. We consider 5 random repetitions.

Table 8 – Inputs for Belgium and Italy

Parameter	Belgium	Italy
Dwelling parameters*		
Building type	Detached, terraced. Rural: 100 % detached Urban: 67% detached, 33% terraced	Detached, terraced. Rural: 100% detached Urban: 14% detached, 86% terraced.
Floor area (m^2)	Detached: 80 m^2, Terraced: 76 m^2	Detached: 95 m^2, Terraced: 71 m^2
Window-to-wall ratio	Detached: 0.3, Terraced: 0.17	
Orientation	North/South	
U-values of building elements (floor, walls, roof and windows) (W/m^2K)	Wall: 0.70 W/m^2K, Window: 1.93 W/m^2K, Roof: 0.74 W/m^2K, Basement: 0.66 W/m^2K	Wall: 0.84 W/m^2K, Window: 2.02 W/m^2K, Roof: 0.87 W/m^2K, Basement: 0.74 W/m^2K
Air change rate (h^{-1})	0.55 h^{-1}	
Type of heating/cooling system(s)	No cooling system (Heat roadmap europe, 2017) Heating systems: currently heating is for the largest majority provided by natural gas (44%), light fuel oil (38%), biomass solid (6%) and biogas (9%). Current heating systems may be replaced by a HP, depending on the LCT integration scenario.	20% of dwellings are currently equipped with cooling systems, powered by electricity (Heat roadmap europe, 2017) Heating systems: currently heating is for the largest majority provided by natural gas (49%), biomass solid (27%), biogas (15%) and light fuel oil (5%). Current heating systems may be replaced by a HP, depending on the LCT integration scenario.
Efficiency of electrical heating/cooling system(s)	Seasonal coefficient of performance of air-source HPs considered as LCT : 2.88	Seasonal coefficient of performance of cooling systems : 4.8 (Heat roadmap europe, 2017) Seasonal coefficient of performance of air-source HPs considered as LCT : 2.88
PV system rated capacity (W_p)	Detached: 3450 W_p, Terraced: 2990 W_p	Detached: 4140 W_p, Terraced: 2760 W_p
PV system inclination (°)	34° (Protopapadaki, 2018)	27° (Jacobson & Jadhav, 2018)
PV system orientation	South	
LCT integration scenario		
HP integration rates **(C1)**	0 to 100 %	
PV integration rates **(C1)**	0 to 100 %	
Weather data		
Location	Uccle (next to Brussels)	Rome
Grid parameters for the initial grid (no reinforcement)		
Number of dwellings per island D_i	Rural: 69 Urban: 100	Rural: 29 Urban: 107
Average number of dwellings per feeder	Rural: 20 Urban: 23	Rural: 8 Urban: 36
Percentage of dwellings connected to 3 phases	0	
Transformer nominal power $S_{nom}(\tau)$ (kVA) **(C2)**	150	

Parameter	Belgium	Italy
Average length between two consecutive nodes (m)	Rural: 23 m Urban: 8 m	Rural: 70 m Urban: 7 m
Feeder cables cross-section $cr(f)$ (mm^2) and material **(C2)**	70 mm^2 & aluminium	
Average length of dwelling links (m)	Rural: 8 m Urban: 3 m	Rural: 16 m Urban: 8 m
Dwelling links cross-section (mm^2) and material	50 mm^2 & aluminium	
Reinforcement options		
Transformer nominal power $S_{nom}(\tau)$ (kVA) **(C3)**	No reinforcement: 150 kVA Reinforcement, rural: 250, 400 kVA Reinforcement, urban: 250, 400, 630 kVA	No reinforcement: 150 kVA Reinforcement, rural: 250 kVA Reinforcement, urban: 250, 400 kVA
Cross-section of main feeder cables $cr(f)$ (mm^2) **(C3)**	No reinforcement: 70 mm^2 Reinforcement: 150 mm^2	
Number of phases to which HPs are connected **(C3)**	No reinforcement: 1 Reinforcement: 3	
Number of phases to which PV systems are connected **(C3)**	No reinforcement: 1 Reinforcement: 3	
Economic parameters		
Transformer investment cost $C(\tau)$	250 kVA: 9.6 k€ 400 kVA: 11.5 k€ 630 kVA: 15.2 k€	250 kVA: 9.6 k€ 400 kVA: 11.5 k€
Main feeder cables replacement linear cost $C_l(f)$ & Dwelling link replacement linear cost $C_l(dl)$	$C_l(f)(\text{urban}) = C_l(dl)(\text{urban}) = 56$ €/m $C_l(f)(\text{rural}) = C_l(dl)(\text{rural}) = 17$ €/m	
Cost of reconnecting a dwelling link to the feeder C_r	453 €	
Three-phase meter cost $C_{3\phi,m}$	149 €	
Cost of energy losses $C(E_l)$	0.068 €/kWh	
Planning horizon L	33 years	
Discount rate δ	5.5 %	
Simulation parameter		
Number of random repetitions **(C4)**	5	

Note. *: the dwelling parameters for which no reference is provided were obtained from work package 1 (WP1) (see deliverables of WP1 in the sEEnergies website, https://www.seenergies.eu/reports/)

2.8.1.1.2. Outputs

In order to illustrate how we compute the reinforcement cost per dwelling for the Belgian urban and rural representative grids $LCC^*_{d,r}(BE, LCT_\sigma)$ and $LCC^*_{d,u}(BE, LCT_\sigma)$ from the LCT integration scenario LCT_σ, we proceed as following:

- **Step 1.** For a given representative grid (rural in this case) and for a given integration scenario (80% HP & 40% PV), we detail how we compute the reinforcement cost per dwelling, $LCC^{*}_{d,r}(BE, 80\%\ \mathrm{HP}\ \&\ 40\%\ \mathrm{PV})$, with the model of Figure 3.
- **Step 2.** For the rural and urban grids, for selected LCT integration scenarios (all combinations between [0, 20, 40, 60, 80, 100] %HP and [0, 20, 40, 60, 80, 100] %PV), we compute the reinforcement cost per dwelling and present the results.
- **Step 3.** We show how we use the results of step 2 to build cost functions that allow determining the reinforcement cost per dwelling for any LCT integration rate (e.g. 29% HP & 57% PV) in a reduced computing time.

Step 1 – For a given grid and integration scenario, detail the computation of the reinforcement cost per dwelling

For the whole step 1, let us consider the representative rural grid where 80% HP and 40% PV are integrated. In addition, even though the results are computed for 5 random repetitions (see steps 2 and 3), in this step 1, we present the results for only 2 random repetitions for the sake of clarity.

For the 1st repetition, we perform a random choice of the LCT location and of the occupancy profiles. We obtain the situation in Figure 9.

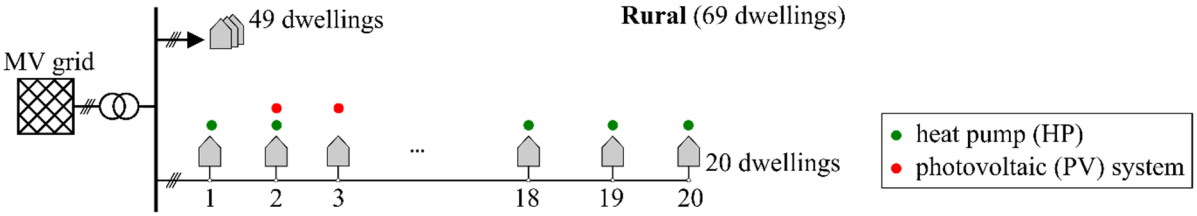

Figure 9 – Situation for the rural grid, 80% HP & 40% PV, 1st repetition

Thanks to the dwelling model, we determine the electrical demand and generation profiles of each dwelling during one year. For instance, in Figure 10, we plot the active power profiles for 2 days of the year for dwelling n°2, which is a detached building, and has both a HP and a PV system (see Figure 9).

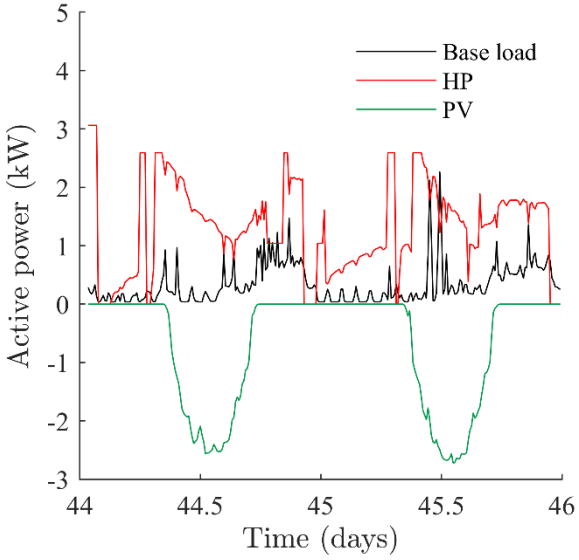

Figure 10 – Demand and generation profiles for dwelling n°2 in the case of the 1st repetition

Thanks to the LV grid and economic models, we compute the grid stability and economic indicators for each grid reinforcement option (see Figure 9). The results are given in Table 9 under "Repetition 1" (only non-zero values of the grid stability indicators are shown).

For the 2nd repetition, we perform a new random choice of occupancy profiles and LCT location and determine the new electrical dwelling profiles. For instance, for this 2nd repetition, dwelling n°2 has a HP and no PV system. For these new dwelling profiles, we compute, through the LV grid and economic models, the grid stability and economic indicators for each grid reinforcement option. The results are given in Table 9 under "Repetition 2".

Finally, for each indicator, we compute the average between the value for the 1st repetition and the value for the 2nd repetition. The results are given in Table 9 under "Average between repetitions". From these results, we observe that the reinforcement options may be split in two categories:

- The non-technically viable reinforcement options (red background in Table 9): reinforcement options for which at least one of the grid stability indicators is higher than 0. It means that there is at least one repetition for which the reinforcement option is not viable. For instance, the option (τ_2, f_1, hp_1, pv_1) (see notes of Table 9 for the correspondence of the symbols) is not viable because of voltage deviation problems for the first and second repetitions (VD > 0).
- The technically viable reinforcement options (green background in Table 9): reinforcement options for which all the grid stability indicators are equal to 0. For instance, (τ_2, f_2, hp_1, pv_1) is a viable reinforcement option.

We select the technically viable reinforcement option that has the lowest cost (in bold and dark green background in Table 9). In our case it is (τ_3, f_1, hp_1, pv_1), which corresponds to the 400 kVA transformer, the 70 mm^2 feeder cables and connecting HPs and PV systems to one phase. The cost of this reinforcement option thus corresponds to the reinforcement cost for the considered LCT scenario, denoted $LCC^*_{d,r}$ (a 'star' is added in superscript). In our case, we therefore obtain that $LCC^*_{d,r}(BE, 80\%\ \text{HP}\ \&\ 40\%\ \text{PV})$ = 378 €. The content of Table 9 is further analysed in the table notes.

Table 9 – Influence of the reinforcement options on the grid stability and economic indicators for a given LCT integration scenario (80%HP & 40%PV) and for the rural grid.

Reinforcement options	Repetition 1					Repetition 2					Average between repetitions				
	VD	*VU*	*FL*	*TL*	$LCC_{d,r}$ (€)	*VD*	*VU*	*FL*	*TL*	$LCC_{d,r}$ (€)	*VD*	*VU*	*FL*	*TL*	$LCC_{d,r}$ (€)
τ_1 f_1 hp_1 pv_1	0.3			0.1	246	0.15			0.08	207	0.23			0.09	227
τ_1 f_1 hp_1 pv_3	0.35			0.1	526	0.3			0.08	498	0.33			0.09	512
τ_1 f_1 hp_3 pv_1	0.3			0.1	816				0.08	782	0.15			0.09	799
τ_1 f_1 hp_3 pv_3	0.3			0.1	914				0.08	849	0.15			0.09	882
τ_1 f_2 hp_1 pv_1				0.09	1012				0.07	993				0.08	1003
τ_1 f_2 hp_1 pv_3				0.09	1119				0.07	1105				0.08	1112
τ_1 f_2 hp_3 pv_1				0.09	1230				0.07	1214				0.08	1222
τ_1 f_2 hp_3 pv_3				0.09	1267				0.07	1238				0.08	1253
τ_2 f_1 hp_1 pv_1	0.05				364	0.05				328	0.05				346
τ_2 f_1 hp_1 pv_3	0.05				644	0.15				619	0.10				632
τ_2 f_1 hp_3 pv_1					935					903					919
τ_2 f_1 hp_3 pv_3					1033					970					1002
τ_2 f_2 hp_1 pv_1					1132					1115					1124
τ_2 f_2 hp_1 pv_3					1239					1227					1233
τ_2 f_2 hp_3 pv_1					1351					1336					1344
τ_2 f_2 hp_3 pv_3					1387					1361					1374
τ_3 f_1 hp_1 pv_1					395					360					**378**
τ_3 f_1 hp_1 pv_3					676	0.05				651	0.03				664
τ_3 f_1 hp_3 pv_1					966					936					951
τ_3 f_1 hp_3 pv_3					1065					1003					1034
τ_3 f_2 hp_1 pv_1					1164					1148					1156
τ_3 f_2 hp_1 pv_3					1271					1260					1266
τ_3 f_2 hp_3 pv_1					1383					1369					1376
τ_3 f_2 hp_3 pv_3					1420					1394					1407

Notes. τ_1, τ_2, τ_3: 150, 250 and 400 kVA transformers respectively / f_1, f_2: 70 mm² and 150 mm² main feeder cables respectively / hp_1, hp_3: one and three phase connection of HPs / pv_1, pv_3: one and three phase connection of PV systems.

VD: voltage deviation indicator, *VU*: voltage unbalance indicator, *FL*: feeder overloading indicator, *TL*: transformer overloading indicator, $LCC_{d,r}$: reinforcement cost per dwelling.

Only non-zero values of the grid stability indicators are shown.

The background of technically non-viable reinforcement options is in red and the one of technically viable ones is in green (the background of the cheapest technically viable option is in dark green).

Observations and analysis of the main trends in the table:

- There are no voltage unbalance and feeder overloading problems.
- Increasing the nominal power of the transformer decreases transformer loading *TL* and reduces voltage deviation *VD*, as it decreases voltage variation.
- Increasing the cross-section of the main feeder cables decreases voltage deviation *VD* by reducing cable resistance.
- Transformer replacement is cheaper than PV connection to three phases which is cheaper than HP connection to three phases which is cheaper than main feeder cables replacement.

Step 2 – For the rural and urban grids, for selected LCT integration scenarios, compute the reinforcement cost per dwelling

For the rural grid, we repeat the procedure of step 1 for the following LCT integration scenarios: all combinations between [0, 20, 40, 60, 80, 100] %HP and [0, 20, 40, 60, 80, 100] %PV. Also, for each LCT integration scenario, we perform the calculations for 5 random repetitions. For each scenario, we obtain the reinforcement cost per dwelling $LCC^*_{d,r}$. The results are presented in Figure 11a.

We do the same for the urban grid. The results are presented on Figure 11b. Note that, even though the desired LCT integration rates are [0, 20, 40, 60, 80, 100] %, as the number of dwellings in feeders is finite, the actual rate of dwellings of the detailed feeder which receive an LCT may not exactly be equal to the desired one (e.g. rate of 21% instead of 20% for the urban grid, see Figure 11b). We also remind that the same LCT integration rate is applied to the detailed feeder as to the rest of the island (see Section 2.6.1).

In Figure 11, we also provide the mean of each row ('mean row') and of each column ('mean column') for both the rural and the urban grid. In addition, we analyse the results of Figure 11 in the comments below this figure.

Figure 11 – Grid reinforcement cost per dwelling for selected LCT integration scenarios for the rural and urban representative grids.

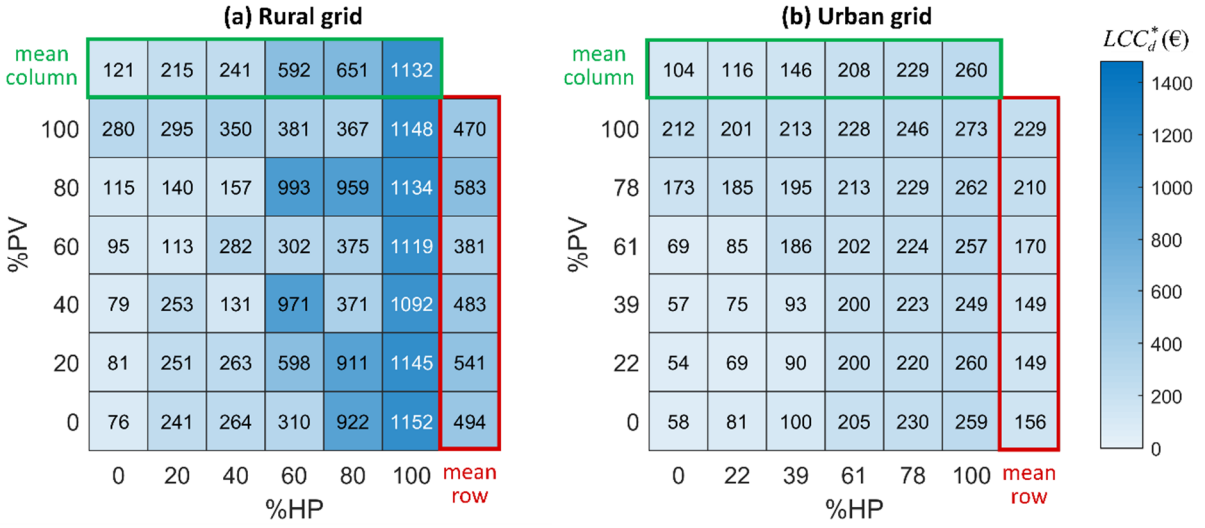

Note: *the grid reinforcement cost is the total cost for the whole considered lifespan of 33 years (see Section 2.7.1)*

Observations and analysis:

- For 0% HP and 0% PV, energy losses represent the only cost. It is equal to 76 € and 58 € in rural and urban grids respectively.
- An analysis of the cost breakdown (not shown here) reveals that grid reinforcements may trigger more significant costs (up to 983 €/dwelling) than energy losses (lower than 250 €/dwelling).
- For the rural grid, the large variation along 'mean column' shows that HP integration has the largest influence on the cost, while the small variation along 'mean row' highlights that PV integration has a low impact on the cost. This is notably due to the voltage deviation problems that add up to transformer overloading for HP integration, which thus trigger additional reinforcements (e.g. main feeder cables replacement). The higher influence of HPs than PV systems is notably related to the fact that PV generation is subtracted from the base load while HP power consumption adds up to it (see Figure 10).
- For the urban grid, for any percentage of integration of PV systems and HPs, the reinforcement cost is relatively low (<280 €), as transformer replacement is the only necessary reinforcement. The fact that HP integration requires fewer reinforcements for the urban grid than for the rural one is notably due to the smaller feeder length between two dwellings in the urban case. Indeed, this triggers smaller voltage drops, decreasing voltage deviation.

Step 3 – Building the cost functions for the rural and urban grids.

The cost function should relate the grid reinforcement cost per dwelling LCC_d^* to the LCT integration rates. For the rural grid, we fit the results of Figure 11a with a 3rd order polynomial. The choice of a 3rd order polynomial is justified in (Meunier, Protopapadaki, & Saelens, 2020). We obtain the polynomial given in equation (12).

$$LCC_{d,r}^*(BE, \%\text{HP} \,\&\, \%\text{PV}) = 79 + 6.3\times\%\text{HP} - 1.1\times\%\text{PV} - 0.024 \times (\%\text{HP})^2 - 0.022\times\%\text{HP}\times\%\text{PV} + 0.026\times(\%\text{PV})^2 + 0.00069\times(\%\text{HP})^3 + 0.00025\times\%(\text{HP})^2\times\%\text{PV} - 0.00028\times\%\text{HP}\times(\%\text{PV})^2 - 0.0000050\times(\%\text{PV})^3 \quad (12)$$

In Figure 12a, we plot the function of equation (12) and we also put the points of Figure 11a in red. We also indicate the R^2 and the root mean square (RMSE) associated to the fit. The RMSE of 182 € can be compared to the maximum $LCC_{d,r}^*$, equal to 1152 € (obtained for 100% HP & 0 %PV, see Figure 11a).

We apply the same procedure for the urban grid. We obtain the function in Figure 12b which has the following equation:

$$LCC^*_{d,u}(BE, \%\text{HP \& \%PV}) = 51 + 0.41\times\%\text{HP} - 1.6\times\%\text{PV} + 0.050\times(\%\text{HP})^2 + 0.0012\times\%\text{HP}\times\%\text{PV} + 0.051\times(\%\text{PV})^2 - 0.00033\times(\%\text{HP})^3 + 0.000034\times\%(\text{HP})^2\times\%\text{PV} + -0.00023\times\%\text{HP}\times(\%\text{PV})^2 - 0.00018\times(\%\text{PV})^3 \quad (13)$$

For the urban grid, the RMSE is equal to 17 €, while the maximum $LCC^*_{d,u}$ is equal to 273 € (obtained for 100% HP & 100% PV, see Figure 11b). We observe in Figure 12 that the accuracy of the fit is higher for the rural grid than for the urban one.

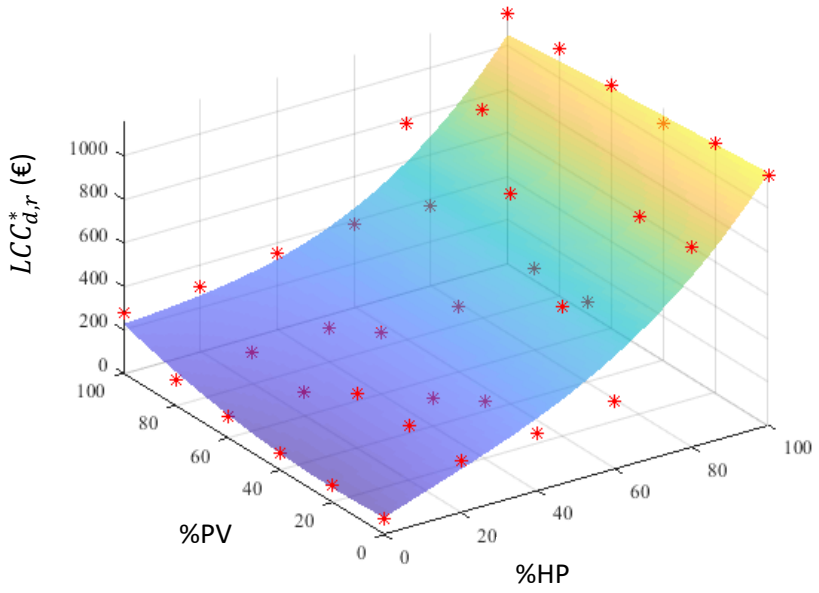

(a) Rural grid
(R^2 = 0.72, RMSE = 182 €)

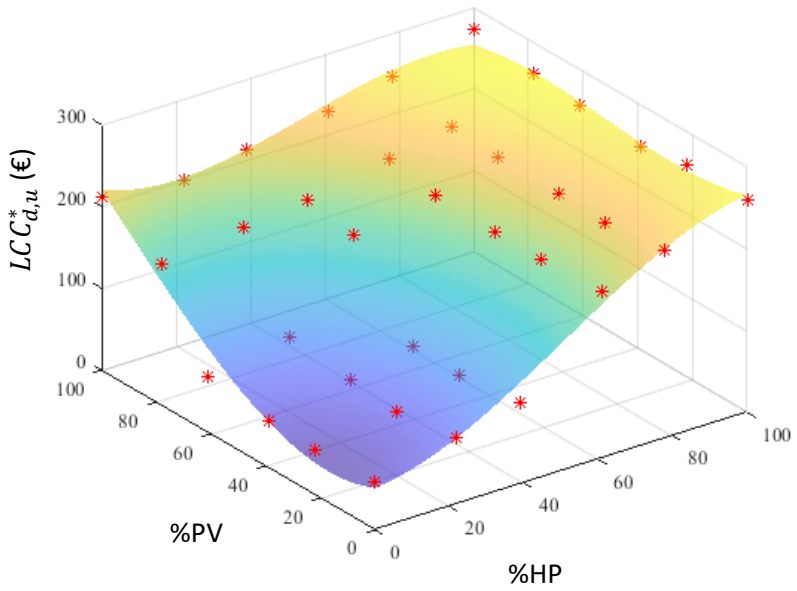

(b) Urban grid
(R^2 = 0.94, RMSE = 17 €)

Figure 12 – Cost functions for the representative rural and urban grids - Belgium
The points in red are the values from Figure 11. They are used as a training database to fit the polynomial functions.

Even though they are associated to an accuracy loss, the cost functions allow to estimate the reinforcement cost for any LCT integration scenario (e.g. 68% HP & 33% PV), only by using equations (12) or (13), and thus without having to go through the whole model (see Figure 3). For instance, the reinforcement cost per dwelling for 68% HP & 33% PV for the urban grid is equal to 195 € according to equation (13).

Another advantage of the cost functions is that they allow to significantly reduce computing time. Indeed, evaluating one LCT integration scenario for one grid with the whole model takes around 30 minutes per repetition[4], notably due to the non-linearity of the dwelling model and to the high number of equations in the grid model. On the other hand, with the cost function approach, once the cost for selected LCT integration scenarios ([0, 20, 40, 60, 80, 100] %HP×[0, 20, 40, 60, 80, 100] %PV) has been computed with the whole model, evaluating the cost of a new LCT integration scenario (e.g. 68% HP & 33% PV) through the cost function is instantaneous.

2.8.1.2. **Model results for the whole country**

By integrating equations (12) and (13) into equation (11), we obtain the following expression of the reinforcement cost for the whole Belgium:

$$LCC^*(BE, \%\text{HP} \,\&\, \%\text{PV}) = D_r(BE) \cdot LCC^*_{d,r}(BE, \%\text{HP} \,\&\, \%\text{PV}) + D_u(BE) \cdot LCC^*_{d,u}(BE, \%\text{HP} \,\&\, \%\text{PV})$$

where:

- $D_r(BE)$ = 1.86×10^5 dwellings
- $LCC^*_{d,r}(BE, \%\text{HP} \,\&\, \%\text{PV})$ = 79 + 6.3×%HP - 1.1×%PV - 0.024 × (%HP)^2 - 0.022×%HP×%PV + 0.026×(%PV)^2 + 0.00069×(%HP)^3 + 0.00025×%(HP)^2×%PV - 0.00028×%HP×(%PV)^2 - 0.0000050×(%PV)^3 (14)
- $D_u(BE)$ = 4.95×10^6 dwellings
- $LCC^*_{d,u}(BE, \%\text{HP} \,\&\, \%\text{PV})$ = 51 + 0.41×%HP - 1.6×%PV + 0.050×(%HP)^2 + 0.0012×%HP×%PV + 0.051×(%PV)^2 - 0.00033×(%HP)^3 + 0.000034×%(HP)^2×%PV + -0.00023×%HP×(%PV)^2 - 0.00018×(%PV)^3

Equation (14) can now be used to evaluate reinforcement costs for Belgium. For instance, for a LCT integration scenario of 68% HP & 33% PV we obtain a grid reinforcement cost for the whole Belgium of 1074 million € (i.e. in average 209 € per Belgian dwelling). Let us remind the reader that the computed reinforcement cost is the total cost for the whole considered lifespan of 33 years (see Section 2.7.1). Note that it is possible to simulate the cost for distinct LCT integration rates in rural and in urban areas. For example, if 43% HP & 52% PV are integrated in rural areas and 15% HP & 32% PV are integrated in urban areas, we obtain a reinforcement cost for the whole Belgium of 357 million €.

The cost functions do not require the detailed understanding of the models and softwares used. In the future, we will provide the costs functions for all the different EU countries directly to WP6.

[4] We use Intel Xeon E5-2640 v4 2.4 GHz processors and 128 GB RAM, running on Windows 10 Pro 64-bit

2.8.2 Italy

In this section, we apply the methodology to Italy. The input parameters for computing the reinforcement costs per dwelling in Italian rural and urban areas, $LCC^*_{d,r}(IT, \%\mathrm{HP}\ \&\ \%\mathrm{PV})$ and $LCC^*_{d,u}(IT, \%\mathrm{HP}\ \&\ \%\mathrm{PV})$, are given in Table 8. The application of the methodology provides the following equation for the reinforcement cost for the whole Italy $LCC^*(IT, \%\mathrm{HP}\ \&\ \%\mathrm{PV})$:

$$LCC^*(IT, \%\mathrm{HP}\ \&\ \%\mathrm{PV}) = D_r(IT) \cdot LCC^*_{d,r}(IT, \%\mathrm{HP}\ \&\ \%\mathrm{PV}) + D_u(IT) \cdot LCC^*_{d,u}(IT, \%\mathrm{HP}\ \&\ \%\mathrm{PV})$$

where:

- $D_r(IT)$ = 4.30×10^6 dwellings
- $LCC^*_{d,r}(IT, \%\mathrm{HP}\ \&\ \%\mathrm{PV})$ = 115 + 0.38×%HP + 0.25×%PV + 0.011×(%HP)^2 - 0.0041×%HP×%PV + 0.0069×(%PV)^2 - 0.000064×(%HP)^3 + 0.000019×%(HP)^2×%PV - 0.0000048×%HP×(%PV)^2 - 0.0000048×(%PV)^3 (15)
- $D_u(IT)$ = 2.28×10^7 dwellings
- $LCC^*_{d,u}(IT, \%\mathrm{HP}\ \&\ \%\mathrm{PV})$ = 82 - 0.73×%HP - 2.3×%PV + 0.034×(%HP)^2 + 0.018×%HP×%PV + 0.056×(%PV)^2 - 0.00010×(%HP)^3 - 0.000148×%(HP)^2×%PV - 0.00017×%HP×(%PV)^2 - 0.00018×(%PV)^3

The functions of the reinforcement costs per dwelling in rural and urban areas, $LCC^*_{d,r}(IT, \%\mathrm{HP}\ \&\ \%\mathrm{PV})$ and $LCC^*_{d,u}(IT, \%\mathrm{HP}\ \&\ \%\mathrm{PV})$, are plotted in Figure 13.

Equation (15) can now be used to evaluate reinforcement costs for the whole Italy. For instance, for a LCT integration scenario of 68% HP & 33% PV we obtain a grid reinforcement cost for the whole Italy of 3938 million € (i.e. in average of 145 € per Italian dwelling).

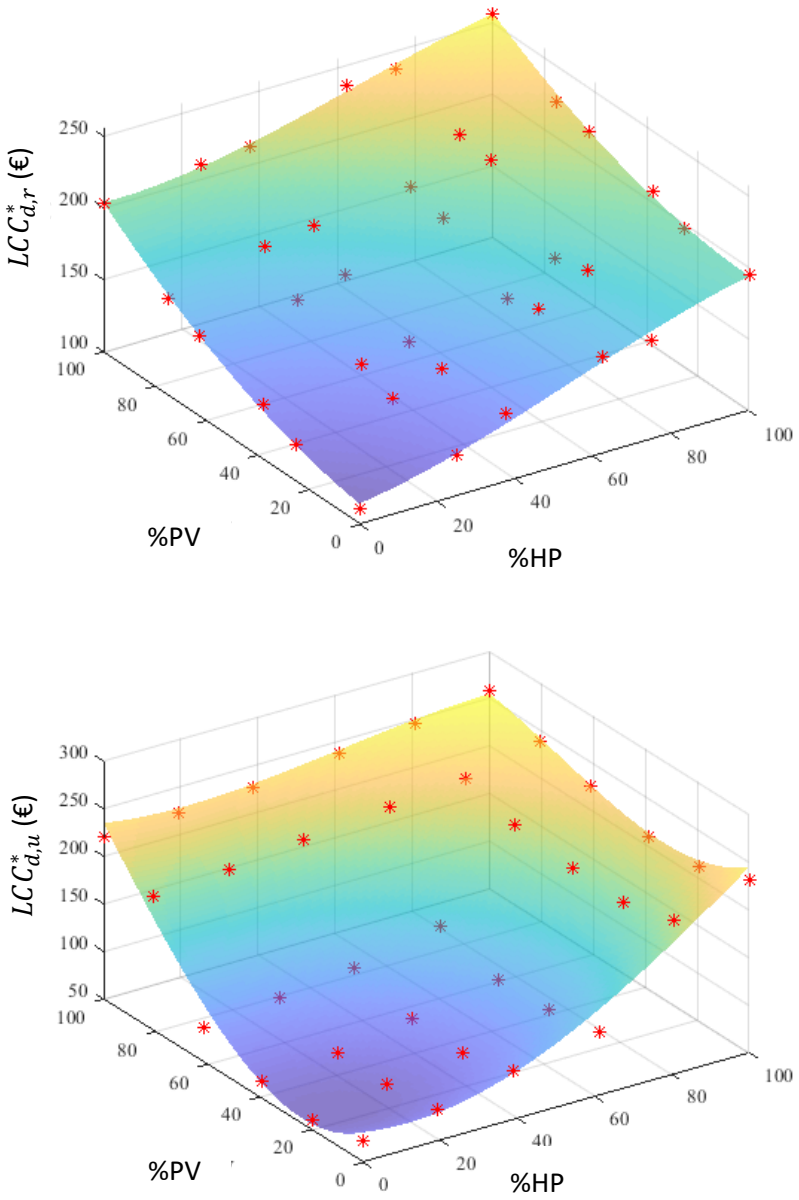

(a) Rural grid
(R^2 = 0.98, RMSE = 5 €)

(b) Urban grid
(R^2 = 0.93, RMSE = 17 €)

Figure 13 – Cost functions for the representative rural and urban grids – Italy

2.8.3 Comparison between Belgian and Italian results

We observe in Figure 12 and Figure 13 that, in the largest majority of cases, both the Belgian and Italian grids, the reinforcement cost per dwelling remains relatively low (< 350 €/dwelling). The only case where more significant reinforcement costs occur (> 350 €/dwelling and up to 1150 €/dwelling) is for the Belgian rural grid with HP integration rates larger than 40% (see Figure 12). This may be explained by the fact that the Belgian rural grid is the only one where the average length between nodes is high (23 m) and where there is a high number of dwellings along the detail feeder (20 dwellings). Additionally, as explained in Section 2.8.1.1.2, the higher influence of HPs than PV systems is notably due to the fact that PV generation is subtracted from the base load while HP power consumption adds up to it.

Nevertheless, as evidenced by Sections 2.8.1.2 and 2.8.2, the reinforcement costs per dwelling are weighted by the number of dwellings in rural and urban areas. For instance, for Belgium, if high HP integration rates (> 60%) are considered in rural areas, even though the reinforcement cost per dwelling may be high, as rural dwellings represent only 4% of all the dwellings, the overall cost for the whole of Belgium will remain moderate.

2.9 Discussion

As presented earlier, the objective of this study is to estimate the grid reinforcement cost as a function of the LCT integration scenarios for all EU countries. Given the complexity of this objective, several choices and assumptions had to be made. First, as discussed in 2.4.1, we chose a given definition to distinguish urban from rural areas amongst the possible definitions. Second, simplifying assumptions had to be made for the dwelling model notably to be able to integrate data from WP1. These assumptions are summarized in Section 2.5.3. Thirdly, regarding the low-voltage grid model, we always considered the same grid architecture which is in shown Figure 2 and Figure 6. Even though this architecture was encountered in most open access grids and articles that we consulted, some EU grids may of course differ from this architecture. Another difficulty regarding the grid model is the lack of data from reliable sources. For instance, even though some websites mention the increasing share of three phase connection of dwellings in the Netherlands, no reliable source regarding the current share of three phase connected dwellings was encountered for this country. Additionally, there is no guarantee that the grid parameters from the open access grids and articles are representative of the grids in the considered countries. In our view, these problems highlight the general lack of open access initiatives on electrical grids. If the distribution system operators were to provide more data, this would allow to consider specific trends in more countries and the representativeness of these trends would be increased. In the same way, the lack of accessible data regarding the cost of grid reinforcement options is also a problem for the economic model.

Given these simplifying assumptions, which are inherent to the wide scope of our study, our results thus have to be treated with caution. In the future, it is advised to continue working on the refinement of these assumptions. Additionally, the results are not the only outcome of this study. The data gathered and the methodology presented in this work on electricity grids are also relevant contributions.

In the future, it would also be relevant to take into account mitigation options other than grid reinforcements that may also favor the integration of LCTs at the low-voltage level, such as local storage, reactive power control, tap changing transformers and demand side management. Adding these new options to grid reinforcements in the pool of options that can be used to stabilize the grid may allow to further decrease the grid stabilization cost.

2.10 Conclusion

In this section on electricity grids, we develop a methodology for the quantification of EU LV grids reinforcement costs following LCT integration. This methodology uses urbanisation data to estimate the share of dwellings in urban and rural areas in the different EU28 countries. It is also based on a model that allows determining the grid reinforcement cost as a function of the LCT integration scenario for representative rural and urban grids.

The above-mentioned model is composed of three sub-models that we developed: the dwelling model, the grid model and the economic model. In addition to presenting each sub-model, we identified their key parameters. We also used data from 24 open access grids and 23 scientific articles to determine the values of the parameters of the grid and economic models for EU28 countries.

The developed dwelling model is based on a stochastic occupant behaviour model and building properties, and is implemented in the IDEAS Modelica library. It allows deriving realistic dwelling load and generation profiles depending on the integrated LCTs. It currently integrates HPs and PV systems as LCTs, but given its customizable components, it is also possible to integrate EVs. The parameters of the dwelling model were determined through interactions with WP1.

The grid model, based on unbalanced power flow simulations, evaluates the influence of the dwellings' load/generation profiles and of the reinforcement options on the grid stability (quantified with 4 indicators). We also implemented it in Modelica and we used components of the IDEAS library. In addition, for the grid simulations we use a dummy island approach, which reduces computing time. Using the data from open access grids and scientific articles/reports, we were able to define six sets of grid parameter values. These sets represent rural and urban grids of Belgium, Germany and the EU in general. The EU sets can be used for the remaining EU countries, for which sufficient data could not be retrieved.

The economic model evaluates the life-cycle cost associated to a grid reinforcement option. It includes both investment and operating costs of the LV grid. The literature review allowed us to define one set of economic parameter values that is common to all EU28 countries.

Finally, we illustrate the methodology by computing the grid reinforcement costs from LCT integration in Belgium and Italy.

2.11 Appendices

2.11.1 Appendix A : Share of dwellings in single and multi-family house per EU country

These share were obtained from the EU Building Stock Observatory (European Commission, 2021) with adjustments from WP1.

Country	Share of dwellings which are in a single-family house in 2020	Share of dwellings which are in a multi-family house in 2020
AT (Austria)	47%	53%
BE (Belgium)	68%	32%
BG (Bulgaria)	48%	52%
CY (Cyprus)	47%	53%
CZ (Czechia)	36%	64%
DE (Germany)	37%	63%
DK (Denmark)	48%	52%
EE (Estonia)	28%	72%
EL (Greece)	47%	53%
ES (Spain)	33%	67%
FI (Finland)	37%	63%
FR (France)	56%	44%
HR (Croatia)	73%	27%
HU (Hungary)	59%	41%
IE (Ireland)	90%	10%
IT (Italy)	27%	73%
LT (Lithuania)	38%	62%
LU (Luxembourg)	57%	43%
LV (Latvia)	30%	70%
MT (Malta)	42%	58%
NL (Netherlands)	65%	35%
PL (Poland)	39%	61%
PT (Portugal)	55%	45%
RO (Romania)	61%	39%
SE (Sweden)	48%	52%
SI (Slovenia)	60%	40%
SK (Slovakia)	50%	50%
UK (United Kingdom)	37%	63%

2.11.2 **Appendix B : Specifications of cables and transformer**

Cables: applies to feeder segments and dwelling links.

These specifications are based on the data from Bahra Cables Company (2015) on cables used in low-voltage grids. We consider four core cables with aluminium conductor, which are XLPE insulated and PVC sheathed. Indeed, through our literature review (see Sections 2.6.3.3 and 2.6.3.4) we observed that aluminium cables are the most common ones for feeder segments and dwelling links.

In addition, according to specifications of Bahra Cables Company (2015), the cable ampacity slightly depends on its position (overhead or underground), due to the variation of the thermal resistance of the medium in which the cable is (Meyers, 2003). Additionally, according to Prettico et al. (2016) who collected data from 79 EU DSOs, in rural areas 4% of the cables are underground and 96% overhead and in urban areas 86% of cables are underground and 14% overhead. We thus deduce the average ampacity in rural an urban areas from the data of Bahra Cables Company (2015) and Prettico et al. (2016).

Cross-section (mm^2)	Linear resistance $R_l(fs)$, $R_l(dl)$ (Ω/m)	Ampacity - rural $i_{nom}(fs)$, $i_{nom}(dl)$ (A)	Ampacity - urban $i_{nom}(fs)$, $i_{nom}(dl)$ (A)
16	2.45×10^{-3}	69	71
25	1.54×10^{-3}	93	93
35	1.11×10^{-3}	113	113
50	0.82×10^{-3}	138	136
70	0.57×10^{-3}	174	167
95	0.41×10^{-3}	214	201
120	0.33×10^{-3}	248	230
150	0.27×10^{-3}	284	258
185	0.21×10^{-3}	327	294
240	0.16×10^{-3}	387	339
300	0.13×10^{-3}	444	387
400	0.10×10^{-3}	519	444
500	0.082×10^{-3}	595	503

The linear reactance of feeder segments $X_l(fs)$ and dwelling links $X_l(dl)$ is considered constant equal to 0.084×10^{-3} Ω/m (Kerber, 2020, Lindner et al., 2014).

Transformer

The values provided in the following table are obtained from the data of the IDEAS library (Baetens et al., 2015).

Nominal power $S_{nom}(\tau)$ (kVA)	No load losses $P_0(\tau)$ (W)	Phase resistance $R(\tau^j)$ (Ω)	Phase reactance $X(\tau^j)$ (Ω)
150	251	0.022	0.072
250	355	0.012	0.045
400	511	0.007	0.029
630	750	0.004	0.019
800	927	0.003	0.016
1000	1135	0.003	0.013

3 Thermal grids

3.1 Summary of the section

The objective of the present section is to provide an introduction to the modelling of costs and capacities of current and future thermal grids for all of the EU28 as part of the sEEnergies project. A representative grid approach is being used, based on the experiences of the Heat Roadmap Europe series of projects. The explanations presented here focus on the current year situation, while the deliverable 4.5 (D4.5) focuses on the future years. Future results from the current project will include a documentation of the methods to perform mapping and spatial analytics in the pursuit to characterise future costs and potentials of thermal grids for the EU28.

The current year modelling relies on the findings and experiences from the Heat Roadmap Europe project, in which the original distribution capital cost model was first introduced and presented. Two key metrics constitute the vital mechanisms of this model, both of them rely on high-resolution spatial data. First, heat demand densities on the 100m resolution level facilitate the identification of “physical suitability” of heating grids. Secondly, the modelling of distribution capital cost based on spatial data and empirical cost and design data allow for a mapping of “economic suitability” of the deployment of district heating systems. This report presents the distribution capital cost model in overview and discusses some of its independent and intermediate input data parameters in more detail. Key results include district heating costs for the current year, and for all EU28 member states, presented in the form of tables, graphs, and map images.

The results provided by this section form the basis of the iterative development of representative models for the physical suitability and an economic assessment of district heat distribution grids in the EU28 for 2015, 2030 and 2050.

3.2 Introduction

3.2.1 Overall objective

The overall objective can be summarized as modelling and assessing investment costs for current (2015) and future (2030 and 2050) district heating systems in all EU28 member states. The chosen approach presupposes the spatial mapping of heat demand densities at 100 m grid size across the 28 Member States. The task will result in a geographic delineation of district heating areas and their share of heat demand. The work aims at providing enhanced insight into factors and circumstances that determine the potential for structural energy efficiency measures in future Europe.

The work is divided into three phases. The first of them is the objective of the present report. Here, the costs of heat distribution grids are being assessed for the current year. The subsequent phases, associated to deliverables 4.5 and 5.7 (D4.5 & D5.7), deal with future distribution of heat demand and efficiency, the costs of heat distribution infrastructure, the allocation of heat sources, and result in future data for the heat sector to be used in work package 6 (WP6).

The generation of representative thermal grids in EU28 initially includes a current year assessment based on the approaches developed during the Heat Roadmap Europe project (HRE, 2018), which included a first-time attempt to model the costs of district heating infrastructure at the 1-hectare level. Subsequently, the outputs from the work on future years mapping in the 2nd working phase, are subject of the D4.5 deliverable report, which will present several numerical and geographical datasets. Finally, the full account of the methods, approaches, and key assumptions developed and used within the project to produce the resulting future year datasets, will be documented in the final written output from WP5, that is in the public D5.7 deliverable report.

3.2.2 Specific objectives and scope

The specific objectives and the scope of the 1st working phase, which is presented in this deliverable, are the assessments of investment costs for conventional district heating systems (3rd generation), for the current year 2015 and for all Member States of EU28. In principal, and as far as approaches utilised to perform these assessments are considered, the methodological basis is identical to that which was developed in the Heat Roadmap Europe project. Two major metrics are being used: heat demand densities on the hectare level; and district heat distribution capital costs, derived from a distribution capital cost model, which also is prepared on the hectare level. This computational basis is going to be applied for all the work in the sEEnergies project to characterise representative thermal grids. For the mapping of future year heat demand densities and their corresponding district heating investment cost levels, new approaches are going to be developed whereby these two main metrics are established.

For the first metric, also labelled “physical suitability” (for district heating), as first introduced in (Persson, Wiechers, Möller, & Werner, 2019), such differences may consist in alternative combinations and use of various input data sources while also including, as a pioneering element, new approaches whereby to estimate the spatial distribution of future heat demand locations and concentrations. For the second metric, also recognised as “economic suitability” (ibid.), such differences may include improved empirical analysis of underlying input parameters (such as for example the concept of Effective Width (Persson & Werner, 2010) and as well updated and nation-specific construction cost levels, in particular with reference to so-called low-temperature systems (4th generation). However, the closer description of these differences is beyond the scope of this deliverable since the focus here is limited to the current year mapping and to conventional 3rd generation systems.

3.3 Distribution capital cost model

To provide a clearer understanding of the inherent structure and necessary parameters incorporated within the concept of the distribution capital cost model, Figure 14, which is used with permission from (Persson, 2015), provides a principal overview on the model developed and used within the Heat Roadmap Europe project.

As can be seen in Figure 14, the model consist of three categories of data: 1) Independent input data; 2) Intermediate input data, and 3) Final output data, where the resulting quantity of the "Distribution capital cost" may be expressed principally as the following quota (for further references, see also (Persson & Werner, 2011; Persson et al., 2019)):

$$Distribution\ capital\ cost\ [\frac{€}{GJ}] = \frac{Specific\ investment\ cost\ [\frac{€}{m}]}{Linear\ heat\ density\ [\frac{GJ}{m}]} \quad (16)$$

The numerator of this quota relates essentially to economic conditions such as construction costs (represented by the slope and intercept of a linear function on the basis of the empirical linear correlation between pipe diameters and construction costs) and an annuity representing the anticipated economic lifetime and real interest rate of the investment. The denominator on the other hand relates essentially to the spatial aspect of population numbers, settlement structures, the associated building heat demands, and the corresponding expectancy of pipe lengths by given land areas (as expressed in the independent input data parameter Effective Width).

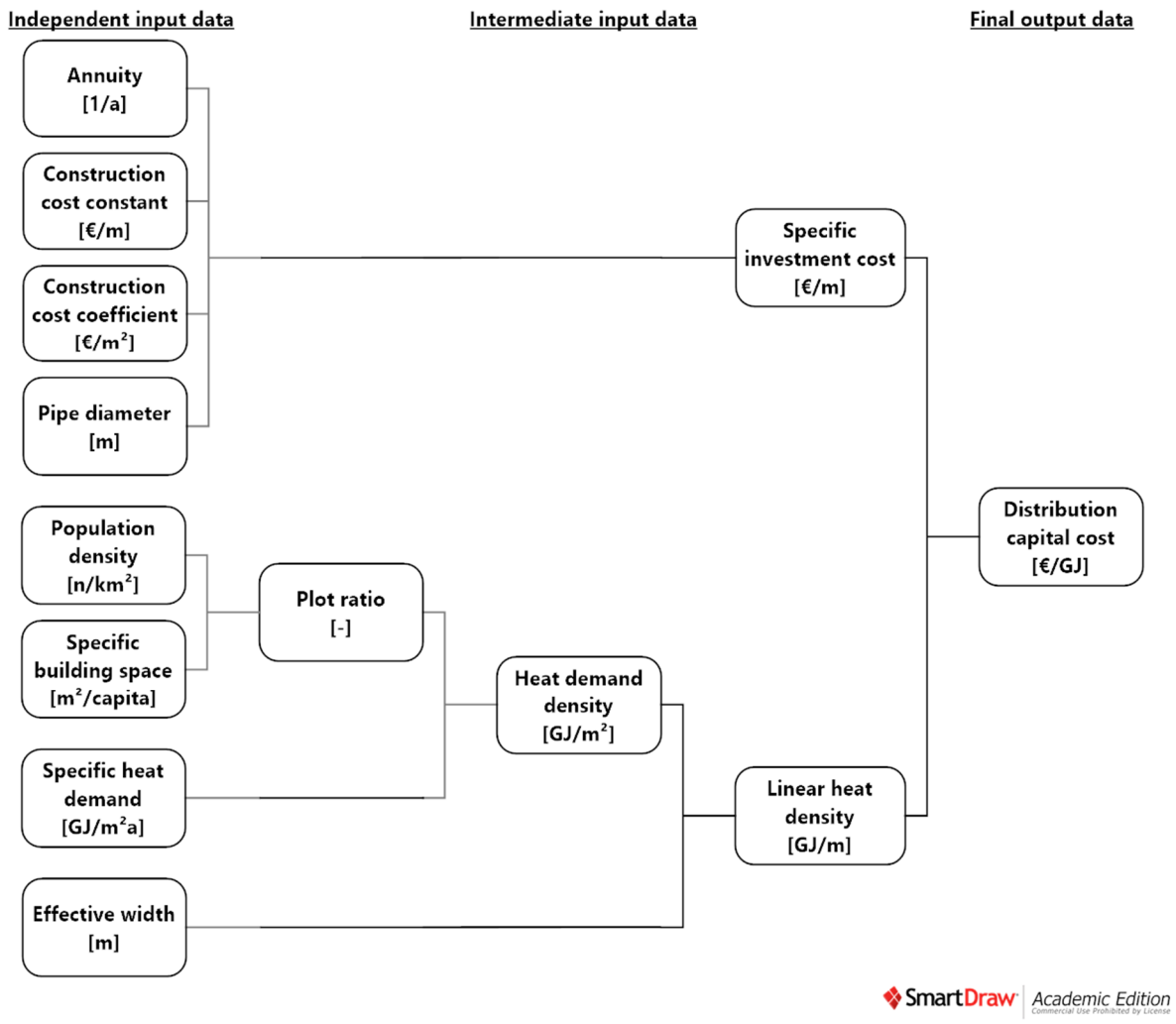

Figure 14 – Principal overview of the distribution capital cost model developed and used within the Heat Roadmap Europe project context.
Sources: Used with permission from (Persson, 2015).

Due to the largely interrelated nature of the denominator independent and intermediate input data parameters, where e.g. heat demand density may be expressed as the product of Plot ratio (or Building density (Grosse, Christopher, Stefan, Geyer, & Robbi, 2017)) and specific heat demand, the resulting quantity Linear heat density may be arrived at by several different routes. For the Linear heat densities developed within the Heat Roadmap Europe project, residential and service sector building heat demands (reference year 2015) were mapped at 100-meter geographical resolution in a hectare grid cell raster by means of combining top-down and bottom-up approaches to derive and distribute building floor areas by use of multi-linear regression models (this route is described further in (Möller, Wiechers, Persson, Grundahl, & Connolly, 2018; Persson, Möller, & Wiechers, 2017)).

Any route taken to assess Linear heat densities will need to incorporate the outlined independent input parameters in one way or another. However, since building heat demands for e.g. space heating and domestic hot water indirectly reflect other external conditions such as for example climatic, demographic, as well as socio-economic parameters, these may be established in various ways. Note also that Plot Ratio may be established as the product of Population density and Specific building space, but also as a quota of building floor areas and a given land area.

3.3.1 Characterisation of representative thermal grids

For the characterisation of representative thermal grids, both of the quota terms in equation (16) can be used since the independent input data parameters upon which they are founded can be made to reflect context-specific conditions (e.g. national, regional, local). The characterisation of thermal girds in the sEEnergies project is thus based on studies of existing district heating grids across Europe. Heat distribution technologies and costs around Europe may be characterised by these metrics, which, notably, does not represent dynamic operational conditions (as for electricity) but static overall conditions. Hereby, thermal grids are characterised in this context by representative heat demands (physical suitability) and representative cost curves (economic suitability).

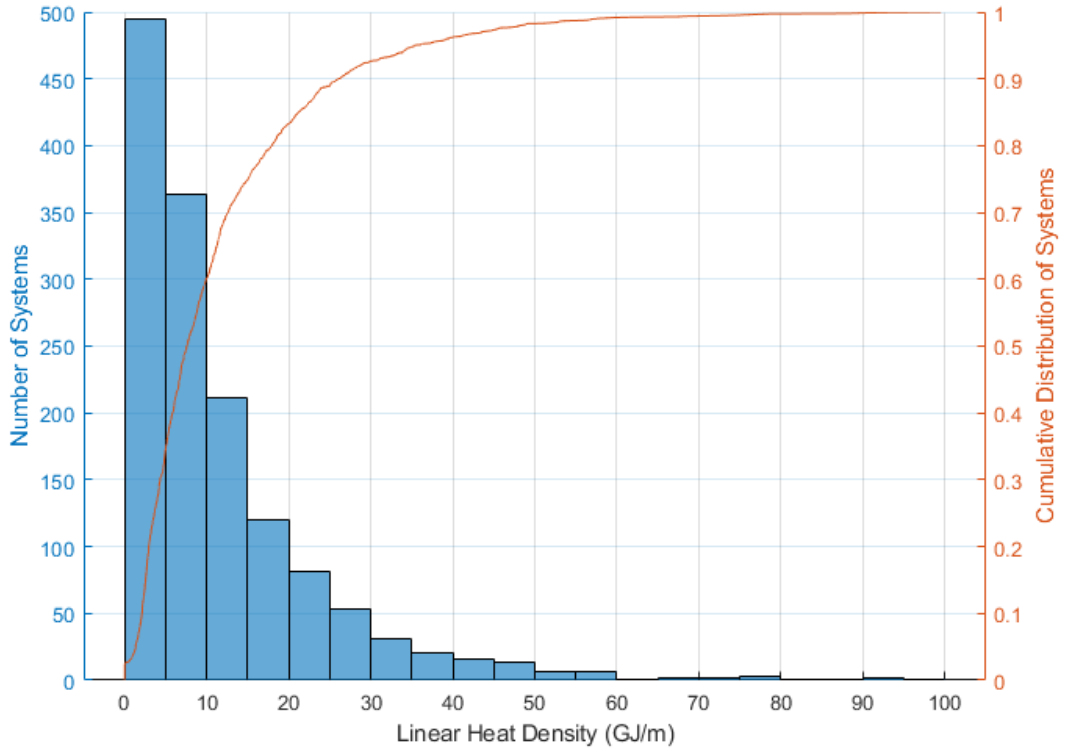

Figure 15 – Histogram depicting the distribution of Linear heat density values for 1434 out of 4732 European district heating systems for which data on annually sold heat and total trench length is available in version 5 of the Halmstad University District Heating and Cooling database.
Source: (HUDHC, 2019).

Figure 15 shows a histogram of the distribution of known Linear heat densities among 1,434 European district heating systems for which alternative input data (i.e. information on annually sold heat (Q_S) and total trench length (L)) for the calculation of Linear heat density is available in the Halmstad University District Heating and Cooling database (HUDHC, 2019). Representative district heat distribution costs are empirically derived by associating technical parameters like sold heat and total trench length of existing systems to other spatial characteristics, such as city or city district area, population, heat demands in the network area, connection rate etc..

Using highly detailed data from Danish district heating system, the concept of plot ratio and effective width is derived on the neighbourhood level. In Figure 16, the concept of Effective width as a function of Plot ratio is shown for the district heating system in Denmark's second to largest city Odense, located on the island of Fyn. A separate model for distribution pipes (left) and for service pipes (right)

has been prepared. The experimental analysis of these relationships, based on empirical geometric district heating network data in combination with cadastre-recorded building floor areas from the Danish Building Register, is a novel approach in the sEEnergies project. This effort facilitates a deeper understanding of the behaviour of these parameters, especially in low Plot ratio areas. Upon this basis, it allows to formulate more appropriate adapted functions (curve fits) to be used in the modelling of future year investment costs. Advantages of the approach are the inclusion of real design parameters on a very local urban level, for an entire city, and, compared to models of district heating network design, the inclusion of a series of urban characteristics by means of an empirical approach.

Figure 16 – Scatterplots depicting the correlation between Effective width values and Plot ratios for the case of distribution pipes (left) and for service pipes (right) in the district heating system of Odense, Denmark.

Depicted land areas (Individual data points) aggregated from hectare grid cells to 500 by 500-meter grid cells.

Other key quantities for which variations, particularly national variations, may be used for characterisation of thermal grids, are the construction costs parameters. For the sEEnergies cost assessments for future year networks especially (see deliverables D4.5 and D5.7), unlike previous studies mostly using EU averages (e.g. (Persson & Werner, 2011; Persson et al., 2019)), nation-specific cost conditions will be incorporated into the model where such data is available.

3.3.2 Physical suitability

Characterisation by general classifications is applied in the model also to physical suitability itself, where heat demand densities, established on highly detailed levels of resolution (e.g. hectare level) as indicated above, may be aggregated towards certain indicative threshold levels which correspond to typical conditions for different thermal supply and distribution systems. Figure 17 provides an example for the year 2015 from the Heat Roadmap Europe project (Persson et al., 2019), where differences in basic settlement structures among the Member States becomes visible. While mid-density settlement structures in the range between 50 and 120 Terajoules per square kilometre are predominant in some countries (such as e.g. the United Kingdom and the Netherlands), large shares of high-density settlement structures are present in some other countries (for example in Latvia, Luxembourg, and Italy).

By this kind of classification, which was partly based on previous Danish experience (Energistyrelsen, 2012), the characterisation of delimited geographically entities, such as towns, cities, and larger urban areas, allowed a conclusion that 48% of all residential and service sector building heat demands were located in dense (120-300 MJ/m^2) and very dense (>300 MJ/m^2) areas for EU28 on average during 2015. This finding became a solid foundation, the primary logic in fact, for the suggestion that district heating should be economically viable in most European urban areas – perhaps even up to an average EU28 50% heat market share.

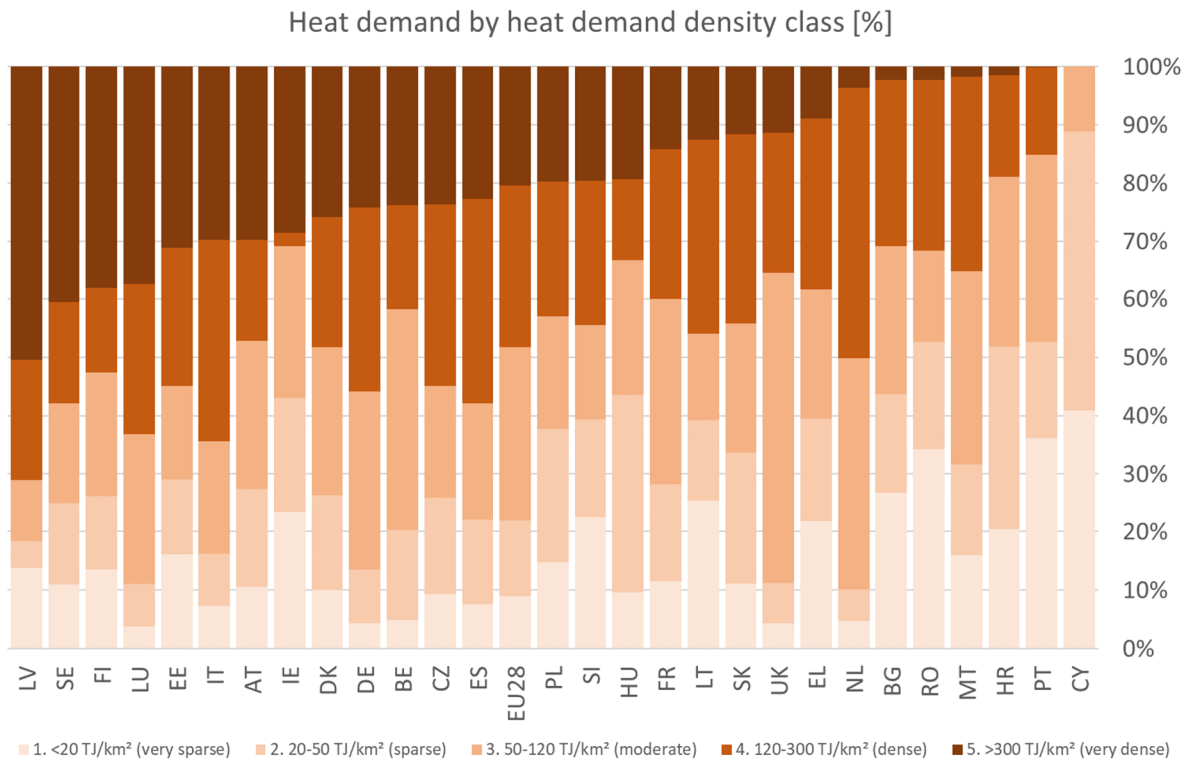

Figure 17 – Division of 2015 national residential and service sector heat demands by five heat demand density classes as modelled in the Heat Roadmap Europe project for EU28.
Elaborated based on (Persson et al., 2019).

The granularity and detail of the heat demand density data elaborated in the model is visualised in Figure 18 with a screenshot from the Pan-European Thermal Atlas Peta (version 5.1) for the example of Warsaw in Poland.

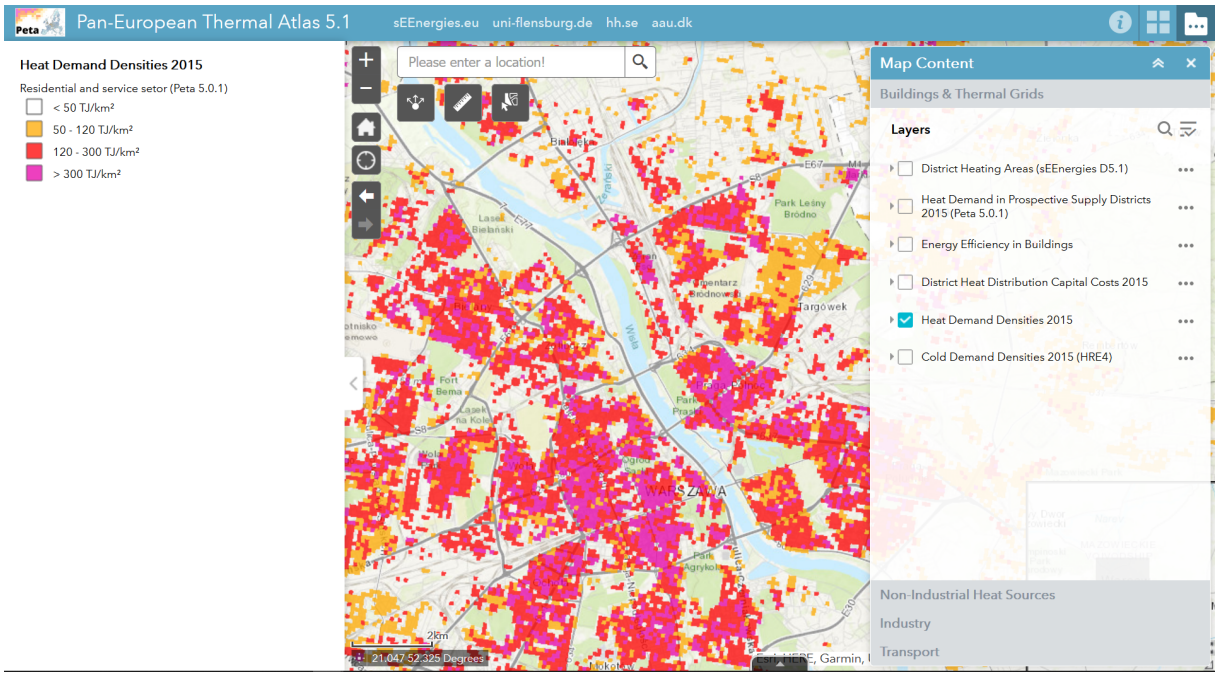

Figure 18 – Screenshot from the Pan-European Thermal Atlas (Peta 5.1) with activated layer "Heat Demand Densities 2015" for the Polish capital Warsaw and surrounding areas.
Source: (Peta5, 2021).

3.3.3 Economic suitability

As for the final output data of the distribution capital cost model, the Distribution capital cost represents the specific investment cost, i.e. the annuitized investment cost per energy unit to be distributed in the pipe network, and may be expressed in terms of marginal and average costs, as assessed in the Heat Roadmap Europe project and outlined for all of EU28 on average during the year 2015 in Figure 19.

By accumulating the sum of building heat demands that may be cost-effectively supplied with district heat distribution at every corresponding cost level and in any given area, and by relating this to the total heat demand, i.e. the total heat market, of that given area (all of EU28 in the case presented in Figure 19), cost supply curves may be drawn that expresses feasible levels of district heat deployment at corresponding investment cost levels. In the exemplified case, a 50% heat market share for district heating in EU28 on average was anticipated at an approximate marginal investment cost level of six euro per gigajoule (approximately three euro per gigajoule as the accumulated average investment cost). Given a current average EU28 deployment level of some 12% (see Table 10 for further references), marginal cost levels in the vicinity of two euro per gigajoule may be interpreted as a hypothetical past time feasibility level of this kind of investments.

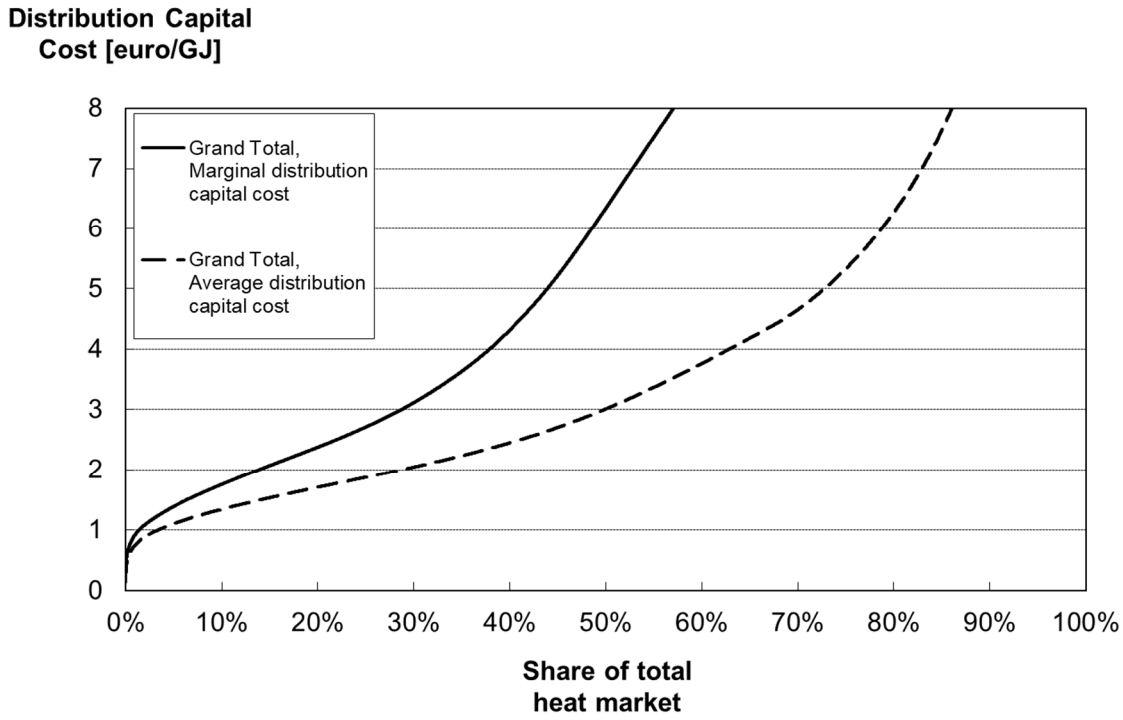

Figure 19 – Exemplification of national cost supply curves established on the basis of aggregated Distribution capital cost calculated at hectare level, expressed as accumulated relative shares of total heat markets by corresponding cost levels.
Source: (Persson et al., 2019).

This Distribution capital cost metric may further, when calculated in raster geometry on the basis of underlying hectare-level heat demand density layers, be established and summarized locally, regionally, and nationally. Hereby, economic suitability for district heating, as a key output parameter of the model, allows results to be extracted at several levels of analysis. Indirectly, moreover, the model also provides indications of those heat market shares – and locations – where heat supply technologies other than district heating, e.g. individual heat pumps, should be the most economically viable option.

For the current year modelling in the sEEnergies project, an indicative starting point for the upcoming analyses and results for the 2030 and 2050 heat demand density distributions, district heat investment cost levels, and feasible expansion level for various heat technologies and systems, may be found in the 28 Member State level outputs from the final exercise in the Heat Roadmap Europe project, as presented in Table 10.

Table 10 – Example of model output: Current and saturated deployment levels of district heating (DH) for residential and service sector buildings in the EU28 member states with corresponding average distribution capital costs and total investment costs (I).
Saturated deployment level corresponds to a common average EU28 market share of 50% at marginal distribution capital cost of 6.34 euro/GJ. Elaboration based on (Persson et al., 2019).

Member state	Current situation (2015)				Saturated (EU28, 50% average)				Expansion		
	DH [PJ/a]	DH [%]	Avg. Dist. Cost [€/GJ]	I [G€]	DH [PJ/a]	DH [%]	Avg. Dist. Cost [€/GJ]	I [G€]	DH [PJ/a]	Factor [-]	I [G€]
AT (Austria)	65	28%	1.5	1.9	109	47%	2.4	5.2	44	1.7	3.3
BE (Belgium)	5	2%	1.1	0.1	137	42%	2.6	7.1	132	26.9	7.0
BG (Bulgaria)	17	25%	3.3	1.1	31	45%	4.1	2.5	14	1.8	1.4
CY (Cyprus)	0	0%	..	0	0.02	0%	6.1	0.002	0.02	-	0.002
CZ (Czechia)	68	29%	1.9	2.6	133	56%	2.9	7.6	65	2.0	5.0
DE (Germany)	264	11%	1.5	7.6	1339	56%	2.9	76.9	1076	5.1	69.3
DK (Denmark)	95	58%	3.7	6.9	76	47%	2.7	4.0	-	0.8	-
EE (Estonia)	15	45%	2.1	0.6	19	55%	2.6	0.9	3	1.2	0.3
EL (Greece)	2	1%	1.6	0.1	55	47%	3.5	3.7	53	31.5	3.7
ES (Spain)	2	0.5%	1.0	0.04	328	67%	3.1	20.0	326	144.4	19.9
FI (Finland)	107	47%	1.8	3.9	111	49%	2.0	4.3	3	1.0	0.4
FR (France)	81	5%	1.2	2.0	669	43%	3.2	41.4	587	8.2	39.4
HR (Croatia)	7	10%	2.9	0.4	17	26%	4.0	1.3	11	2.5	1.0
HU (Hungary)	27	13%	1.7	0.9	71	34%	2.7	3.7	44	2.6	2.8
IE (Ireland)	1	1%	0.3	0.005	34	32%	1.7	1.1	33	41.3	1.1
IT (Italy)	51	4%	1.0	1.0	828	65%	2.9	46.9	777	16.2	45.9
LT (Lithuania)	24	52%	3.3	1.5	23	51%	3.2	1.5	-	1.0	-
LU (Luxembourg)	3	13%	1.0	0.1	14	53%	2.4	0.7	10	4.1	0.6
LV (Latvia)	23	50%	1.5	0.7	33	71%	2.2	1.4	10	1.4	0.7
MT (Malta)	0	0%	..	0.0002	2	55%	4.4	0.1	2	-	0.1
NL (Netherlands)	21	5%	2.3	0.9	230	54%	3.9	17.4	209	10.8	16.5
PL (Poland)	206	31%	2.2	8.9	304	46%	2.9	17.3	98	1.5	8.4
PT (Portugal)	1	2%	2.9	0.1	22	35%	4.7	2.0	21	17.5	2.0
RO (Romania)	42	23%	3.0	2.5	74	40%	3.8	5.5	32	1.8	3.0
SE (Sweden)	156	53%	2.1	6.3	165	56%	2.3	7.3	9	1.1	1.1
SI (Slovenia)	4	13%	1.6	0.1	16	45%	2.9	0.9	11	3.5	0.8
SK (Slovakia)	23	24%	2.4	1.1	47	49%	3.4	3.1	24	2.0	2.0
UK (United King.)	21	2%	1.0	0.4	503	37%	3.4	33.9	482	23.8	33.5
EU28	**1343**	**12%**	**2.0**	**51.5[a]**	**5398**	**50%**	**3.0**	**318**	**4076**	**4.0**	**269.3**

[a] A corrected sum of 48.5 billion euro was used in the paper since both DK (6.92 – 4.0 = 2.92 billion euro) and LT (1.54 – 1.5 = 0.04 billion euro) already at current conditions had expanded district heating beyond the stipulated saturation level.

In short, Table 10 presents the expansion potential for district heating on each national heat market up to an upper investment cost levels which corresponds to an average EU28 expansion of 50%, a situation which is here labelled “Saturated”. The indicated expansion factor for EU28 on average is found at four times current levels, but this factor ranges widely at the national level. A few Member States have already expanded district heating beyond this level (e.g. Denmark and Lithuania). In total, the expansion market for district heating in EU28 was assessed at 270 billion euros.

For comparison and reference, the corresponding granularity and detail of the Distribution capital cost data elaborated in the model is visualised in Figure 20 with a screenshot from Peta 5.1 for the example of Warsaw in Poland.

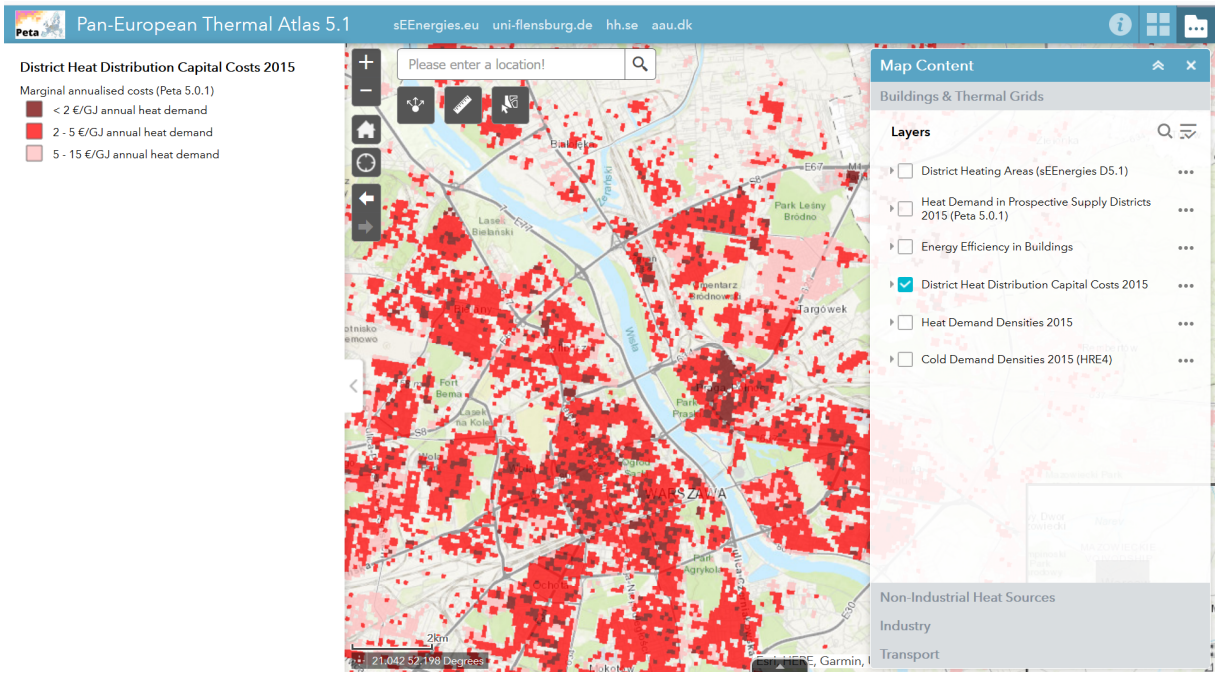

Figure 20 – Screenshot from the Pan-European Thermal Atlas (Peta 5.1) with activated layer “District Heat Distribution Capital Costs 2015” for the Polish capital Warsaw and surrounding areas.
Source: (Peta5, 2021).

3.3.4 Outlook

For the current year modelling, a complementary heat demand density layer is also being produced within the sEEnergies project based on new input data (from work package 1 (WP1)) to provide a coherent series of underlying data with reference to the future year mapping for 2030 and 2050, as well as to map the current year energy efficiency potential (part of deliverables D5.3 and D5.4). On this basis it is likely that a complementary new layer of the current year investment costs for district heating will be established as well. The full documentation of the development of these datasets will be part of the D5.7 report.

3.4 Conclusions

The analysis of costs and capacities for representative thermal grids in the sEEnergies project utilises two key metrics, Heat demand density and Distribution capital cost, to establish physical and economic suitability for district heating and alternative heat supply technologies. For the current year mapping (2015), the starting point for the analysis is the approach developed and conceived in the Heat Roadmap Europe project, the distribution capital cost model, which was applied to EU28 and the Member States by hectare level mapping of both metrics. In this report, the main findings from the current year analysis is presented with focus on independent and intermediate input model data parameters. The result of the present work is a cost-based assessment of district heating infrastructure investment costs for all of the EU, which is subsequently used to specify the potential for district heating based on increasing cost thresholds, in combination with efficiency measures in the built environment.

4 Gas grids

4.1 Summary of the section

The production of renewable gases from biomass or from renewable electricity (through electrolysis) and their use can significantly contribute to the reduction of greenhouse gas emissions. The existing natural gas infrastructure, which is well-developed and interconnected in Europe, can be retrofitted to transport and store these renewable gases, or new dedicated infrastructure can be developed.

With the objective of assessing the role of gas grids in future decarbonised energy systems, we present an overview of the technical and economic characteristics of the existing natural gas, biogas, biomethane, syngas and hydrogen grids and storages in European countries. We also discuss the collected data and their representativeness.

4.2 Introduction

Natural gas grids are well-developed and interconnected in Europe, making it a key infrastructure of the existing European energy system. However, the use of gas networks will evolve given the European ambitions of reducing greenhouse gas emissions (which requires a drastic reduction of natural gas consumption); the need for increased security of supply (almost all the gas consumed in Europe is imported); and increased electrification and district heating in the heating sector (heating is one of the main uses of gas).

Two main future trends can be identified when it comes to gas grids:

- The development and retrofit of the natural gas networks and related storages will be strongly linked to power-to-gas technologies that can integrate more renewable energy and use the grid as chemical storage.
- New types of gas grids will be developed such as biomethane, syngas and hydrogen grids.

Figure 21 provides an overview of the different components of this emerging gas infrastructure.

In this deliverable, we present the key technical and economic data on current European natural gas (section 4.3); biogas, biomethane, syngas (section 4.4); and hydrogen (section 4.5) grids and storages. We also discuss the representativeness of the data provided (more information on the data collection method are available in (Ridjan Skov & Schneider, 2021)).

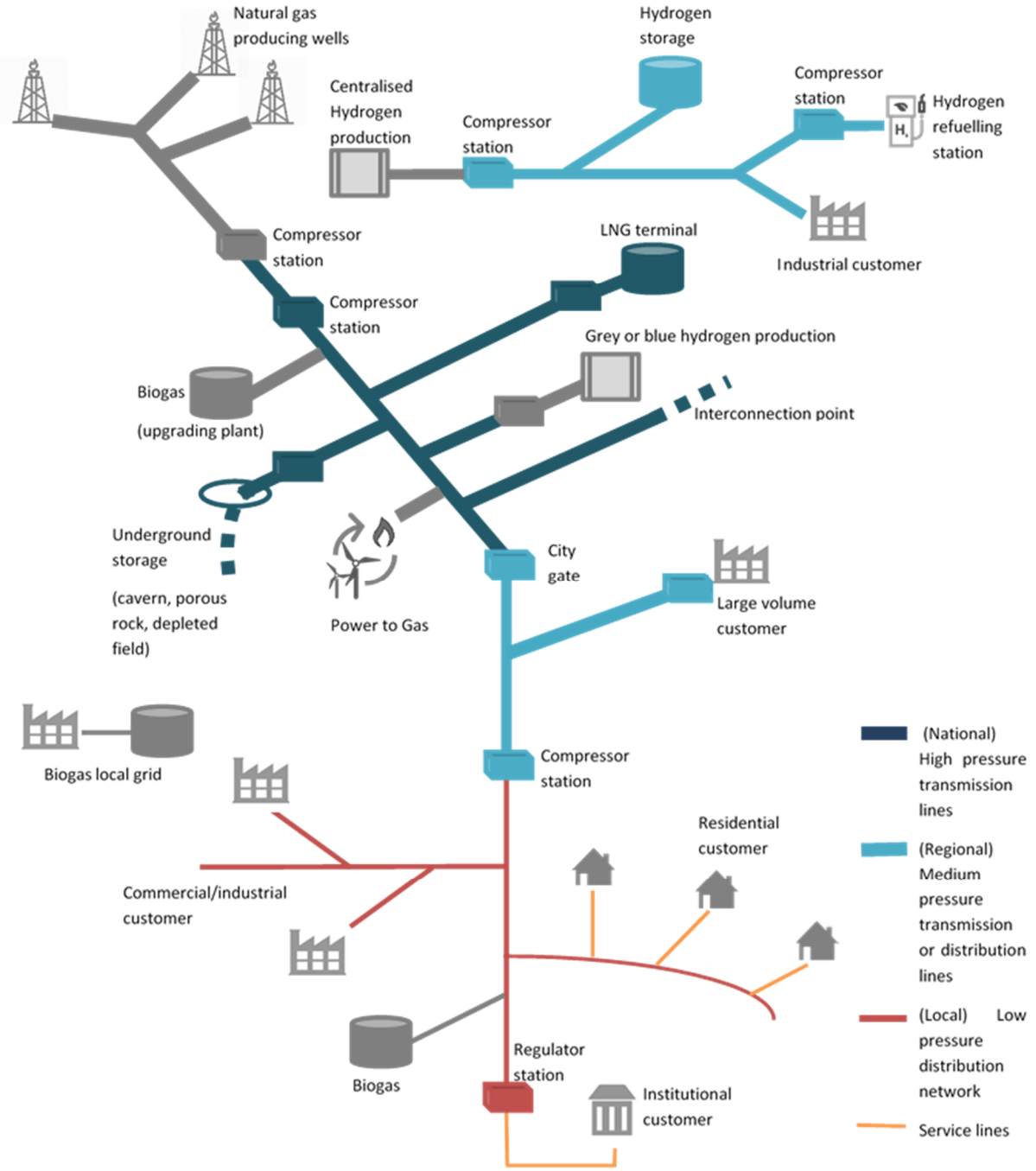

Figure 21 – Elements of the infrastructure for natural gas, biogas and biogas-derived fuels (biomethane and syngas), and hydrogen.
LNG: liquified natural gas

4.3 Natural gas

4.3.1 Technical description of the current capacities

The main components identified for natural gas grids and storages in Europe are:

- **transmission grids**: large diameter steel pipelines operating at high-pressure and compressor stations;
- **distribution grids**: medium to low-pressure natural gas transport system from transmission system to customer meters, including distribution pipelines, service lines and regulator stations;
- **gas storages**: underground storage facilities (depleted fields, aquifer, caverns) and liquefied natural gas (LNG) storage tanks.

Table 11 summarises the installed capacity for the natural gas transmission and distribution networks in each EU country. Table 12 presents the existing capacities of natural gas storage facilities in each EU country.

Table 11 – Installed capacity of natural gas grids components in EU28 countries

Country	Total length of transmission lines (km)	Total length of distribution lines (km)	Distribution pipelines material (%)			Number of service lines	Number of connected consumers
			Steel	Polyethylene	Other		
AT (Austria)	3.0×10^3	4.3×10^4	66%	26%	8%	7.3×10^5	1.3×10^6
BE (Belgium)	4.1×10^3	7.2×10^4	73%	24%	3%	2.7×10^6	3.2×10^6
BG (Bulgaria)	1.8×10^3	2.5×10^2	51%	39%	9%	N/A	7.4×10^4
CY (Cyprus)	0	0	0%	0%	0%	0	0
CZ (Czechia)	3.8×10^3	7.3×10^4	58%	42%	0%	1.6×10^6	2.8×10^6
DE (Germany)	6.3×10^4	5.0×10^5	51%	44%	5%	N/A	2.1×10^7
DK (Denmark)	8.3×10^2	1.8×10^4	86%	14%	0%	3.9×10^5	4.2×10^5
EE (Estonia)	8.9×10^2	2.2×10^3	51%	39%	10%	N/A	5.2×10^4
EL (Greece)	1.8×10^3	6.1×10^3	77%	21%	2%	6.8×10^4	3.3×10^5
ES (Spain)	1.3×10^4	7.0×10^4	85%	13%	2%	N/A	7.6×10^6
FI (Finland)	1.3×10^3	1.9×10^3	95%	4%	1%	N/A	3.1×10^4
FR (France)	3.7×10^4	2.0×10^5	70%	26%	3%	7.0×10^6	1.1×10^7
HR (Croatia)	2.0×10^3	1.8×10^4	51%	39%	10%	N/A	6.5×10^5
HU (Hungary)	5.8×10^3	8.4×10^4	51%	39%	10%	N/A	N/A
IE (Ireland)	2.4×10^3	1.1×10^4	99%	1%	0%	6.6×10^5	6.6×10^5
IT (Italy)	3.4×10^4	2.6×10^5	28%	70%	2%	1.2×10^7	2.3×10^7
LT (Lithuania)	2.1×10^3	8.3×10^3	51%	39%	10%	N/A	5.6×10^5
LU (Luxembourg)	2.0×10^3	2.0×10^3	51%	39%	10%	N/A	8.6×10^4
LV (Latvia)	1.2×10^3	5.5×10^3	51%	39%	10%	N/A	4.4×10^5
MT (Malta)	0	0	0%	0%	0%	0	0
NL (Netherlands)	1.2×10^4	1.3×10^5	17%	15%	68%	N/A	7.2×10^6
PL (Poland)	1.0×10^4	1.7×10^5	40%	60%	0%	N/A	6.9×10^6
PT (Portugal)	1.3×10^3	1.7×10^4	88%	12%	0%	N/A	1.4×10^6
RO (Romania)	1.3×10^4	1.7×10^4	52%	48%	0%	4.6×10^5	1.4×10^6
SE (Sweden)	6.0×10^2	2.7×10^3	51%	39%	10%	N/A	3.7×10^4
SI (Slovenia)	1.1×10^3	4.3×10^3	51%	39%	10%	N/A	1.4×10^5
SK (Slovakia)	8.5×10^3	3.3×10^4	44%	56%	0%	8.1×10^5	1.5×10^6
UK (United Kin.)	7.6×10^3	1.3×10^5	65%	6%	30%	N/A	2.3×10^7

Note. N/A: Not available.
Sources: (Marcogaz, 2018b, 2018a)

Table 12 – Installed natural gas storage capacity in EU28 countries

Country	Depleted field storage, technical working gas capacity (TWh)	Salt cavern storage, technical working gas capacity (TWh)	Aquifer storage, technical working gas capacity (TWh)	LNG tank storage capacity (m^3)
AT (Austria)	92	0	0	0
BE (Belgium)	0	0	9	3.9×10^5
BG (Bulgaria)	18	0	0	0
CY (Cyprus)	0	0	0	0
CZ (Czechia)	14	0	0	0
DE (Germany)	90	152	4	0
DK (Denmark)	0	0	10	0
EE (Estonia)	0	0	0	0
EL (Greece)	4	0	0	2.3×10^5
ES (Spain)	30	0	2	3.6×10^6
FI (Finland)	0	0	0	7.9×10^4
FR (France)	0	16	121	1.4×10^6
HR (Croatia)	6	0	0	0
HU (Hungary)	68	0	0	0
IE (Ireland)	0	0	0	0
IT (Italy)	269	0	0	4.9×10^5
LT (Lithuania)	0	0	0	1.7×10^5
LU (Luxembourg)	0	0	0	0
LV (Latvia)	0	0	24	0
MT (Malta)	0	0	0	1.3×10^5
NL (Netherlands)	127	4	0	5.4×10^5
PL (Poland)	29	17	0	3.2×10^5
PT (Portugal)	0	4	0	3.9×10^5
RO (Romania)	46	0	0	0
SE (Sweden)	0	0	0	5.0×10^4
SI (Slovenia)	0	0	0	0
SK (Slovakia)	39	0	0	0
UK (United Kingdom)	4	56	0	2.1×10^6

Sources: (GIE, 2018, 2019)

4.3.2 Economic data

Even though it is expected that the existing grid can cope with the future gas demands, new deployments, retrofitting or reinforcements may be required in some areas.

Therefore, we have estimated the average investment cost for the following components for EU28 countries:

- **Lines**
  - Transmission lines: 0.13 M€/bcma/km (bcma: billions cubic meters per annum)
  - Distribution main lines: 0.6 - 7 €/MW/m
  - Local distribution lines: 30 - 63 €/m
  - Service lines: 974 - 9128 €/unit
- **Stations:**
  - Compressor stations: ~2 M€/MW
  - Meter and regulator stations: ~24 k€/MW
- **Storage**
  - Depleted fields: 0.60 €/m^3
  - Salt caverns: 1.02 €/m^3
  - Aquifers: 0.90€/m^3
  - LNG tanks: 1.50 €/m^3

These economic data were obtained from the literature and for an important part from the Danish energy agency technology catalogues (Danish Energy Agency, 2017, 2018; Energinet & Danish Energy Agency, 2017; Ridjan Skov & Schneider, 2021). This may notably decrease the representativeness of the value for the service lines. Indeed, it is given in €/unit and the average length of service lines may vary from one country to another.

4.4 Biogas, biomethane and syngas

4.4.1 Technical description of current capacities

Biogas is a mixture of methane (CH_4), carbon dioxide (CO_2) and small quantities of other gases such as hydrogen sulphide (H_2S) and ammonia (NH_3). The complex composition of biogas as well as the presence of impurities cause problems such as corrosion, toxicity, and a reduced heating value (Danish Energy Agency, 2017; Nevzorova & Kutcherov, 2019). Therefore, biogas transportation over long distances has not been developed in Europe, and most of the biogas is used at the production site for generating heat and power (Scarlat, Dallemand, & Fahl, 2018).

Nevertheless, biogas can be upgraded to biomethane to improve its heating value and rid it of its impurities. Biomethane can then be injected into the natural gas grid or be used as a fuel for vehicles. Existing biomethane production plants are typically located in rural areas, where most of the feedstock for biogas production is available. Additionally, as collection from the different production plants and transportation to the urban gas grids is costly, biomethane production units are usually located close to the natural gas grid or fitted with fuelling stations for vehicles on site.

We have registered 663 biomethane production units in the main EU28 biomethane producing countries at the end of 2019. These installations have a total biogas upgrading capacity of 656,000 Nm^3/h, i.e. up to 30 TWh of biomethane can be produced per year (de Lorgeril, 2020). Table 13 presents the existing biomethane production capacities and the injected volume into natural gas grids in the main EU28 producing countries in 2019. We observe that Germany is the clear leader in biomethane production in Europe. France experiences the fastest growth with the quantity of biomethane injected into French distribution networks having reached 1235 GWh in 2019, which is 73% more than it was in 2018.

Synthetic methane (syngas) production via gasification or power-to-methane plants remains at the pilot stage.

Table 13 – Data on biomethane production and injection into the natural gas grid in the main EU28 biomethane producing countries in 2019.

Country	Number of biogas upgrading plants	Biomethane production capacity (thousands of Nm^3/h)	Injected quantity of biomethane into the natural gas grids (TWh)
AT (Austria)	15	6	0.2
BE (Belgium)	4	2	0.01
DE (Germany)	232	262	10.6
DK (Denmark)	46	65	2
FI (Finland)	17	11	0.2
FR (France)	124	50	1.2
IT (Italy)	13	22	0.6
NL (Netherlands)	53	49	2.5
SE (Sweden)	71	85	0.5
UK (United Kingdom)	88	104	4.2

Source: (de Lorgeril, 2020)

4.4.2 Economic data

We have estimated the average investment cost in the EU28 for:

- biogas to biomethane upgrading plants to 0.30 M€/MW;
- grid connection plants (which allow to input biomethane into the natural gas grid) to 0.12 M€/MW.

In some cases, additional costs may be required to install equipment to treat the methane slip and compressor units.

4.5 Hydrogen

4.5.1 Technical description of current capacities

Pipeline transport of hydrogen can either take the form of (1) blending hydrogen with methane and using the existing natural gas infrastructure or (2) dedicated hydrogen transport.

Hydrogen injection into the natural gas grid is not allowed yet in a large number of EU countries such as Belgium, Croatia, Denmark, Estonia, Hungary, Poland, Portugal, Romania (ACER, 2020). In countries where it is allowed such as Austria, Germany, Latvia, the Netherlands, Spain, and Sweden (ACER, 2020), hydrogen injection remains at the demonstration scale and the permitted concentration of hydrogen in the natural gas grid varies significantly depending on the country. The Netherlands has the highest legal concentration of hydrogen in the transmission network with 12% while in Latvia the legal limit is 0.1% (ACER, 2020; Hydrogen Europe, 2020).

If implemented with relatively low concentrations, storing and delivering hydrogen through the natural gas grid appears to be viable without significantly increasing risks associated with the utilisation of the gas blend in end-use devices (such as household appliances), the overall public safety, or the durability and integrity of the existing natural gas grid (Melaina, Antonia, & Penev, 2013). However, the appropriate blend concentration between hydrogen and natural gas depends on the pipeline network and gas compositions and must therefore be assessed on a case-by-case basis.

The transportation of larger volumes of hydrogen into the existing gas grid can be challenging in view of the material durability. The durability of some metal pipes can degrade when they are exposed to hydrogen over long periods, particularly with hydrogen in high concentrations and at high pressures (Melaina et al., 2013). This is particularly critical for high pressure steel transmission lines. However, there is no major concern regarding the hydrogen aging effect on polyethylene (PE) pipe materials, which are the most used in EU28 distribution systems. Another challenge is that hydrogen is more mobile than methane in many polymer materials, including polyethylene (Melaina et al., 2013). This leads to more leakage, which into confined spaces may pose a safety risk. Therefore, delivering hydrogen will increase the operation and maintenance costs for distribution systems as these systems will need to be inspected more frequently and will require additional leak detection devices (Melaina et al., 2013). Currently, both the injection of larger volumes of hydrogen into natural gas networks and the use of underground storage facilities for hydrogen are at the pilot stage, and only in a few EU countries.

Regarding dedicated hydrogen transport, existing infrastructures in the EU28 are located in industrial clusters, mostly in Northern Europe (Belgium, North of France, the Netherlands and Germany). In 2016, around 1600 km of hydrogen pipelines were installed in EU countries and they were distributed as follows (Pacific Northwest National Laboratory, 2016):

- BE (Belgium): 613 km
- FR (France): 303 km
- DE (Germany): 390 km
- IT (Italy): 8 km
- NL (Netherlands): 237 km
- SE (Sweden): 18 km
- UK (United Kingdom): 40 km

Renewable hydrogen production is still at the pilot and demonstration stage in the EU28. However, according to the EU's hydrogen strategy (European Commission, 2020), at least 6 GW of electrolysers powered by renewable energy should be installed between 2020 and 2024 (which could produce up to 30 TWh of renewable hydrogen per year). The installed capacity should then increase to 40 GW by 2030.

4.5.2 Economic data

We have estimated the average investment costs for retrofitting existing natural gas grids to allow the transportation of large volumes hydrogen in the EU28 to:

- 0.26 M€/km for transmission lines;
- 0.19 M€/km for distribution lines;
- ~1 M€/MW for compressor stations.

We could not find reliable data on dedicated hydrogen infrastructures in the EU28 as they are not yet developed at a significant scale and as the few existing grids are privately owned. However, based on literature, the investment cost for new 100% hydrogen pipelines have been estimated to 1.77 M€/km for transmission lines and to 0.25 M€/km for distribution lines (Cihlar et al., 2020).

4.6 Conclusion

In this section on gas grids, we provided and discussed key technical and economic data on natural gas, biogas, biomethane, syngas and hydrogen grids and storages in EU28 countries. This techno-economic review provides key information to evaluate the cost of retrofitting and developing gas grids as a function of decarbonisation scenarios.

5 General conclusion

Throughout the deliverable we have analysed several potential transformations of the energy grids.

Regarding **electricity** grids, the developed techno-economic methodology allows to estimate the low-voltage grids reinforcement cost for each EU country as a function of the residential low-carbon technologies integration scenario. We illustrated the methodology by computing the grid reinforcement costs from heat pump and photovoltaic systems integration in Belgium and Italy. We observed that, in the largest majority of cases, both for the Belgian and Italian case studies, the reinforcement cost per dwelling is lower than 350 € per dwelling (total cost for the whole lifespan of 33 years). The only case where more significant reinforcement costs occurred (> 350 €/dwelling and up to 1150 €/dwelling) is for the Belgian rural case with heat pump integration rates larger than 40%.

In the section on **thermal** grids, we investigated the cost of thermal grids deployment per heat demand unit in the EU. More specifically, our analysis of costs and capacities for representative thermal grids uses two key metrics, heat demand density and distribution capital cost, to establish physical and economic suitability for district heating. For the current year mapping (2015), the starting point for the analysis is the approach conceived in the Heat Roadmap Europe project, the distribution capital cost model, which was applied to all EU28 countries by hectare level mapping of both metrics. We presented the main findings from the current year analysis with focus on independent and intermediate input model data parameters.

In the section on **gas** grids, we presented and discussed the key techno-economic data on existing European natural gas grids and storages, as well as on biogas, biomethane, syngas and hydrogen infrastructures. We also analysed the potential to use the existing natural gas grids for biogas, biomethane, syngas and hydrogen.

References

3E. (2017). *Aansluiting met flexibele toegang in Vlaanderen - FINAAL RAPPORT SIMULATIESTUDIE*. Retrieved from: https://www.vreg.be/sites/default/files/simulatiestudie_aansluiting_met_flexibele_toegang_externe_publicatie.pdf

ACER. (2020). *NRA Survey on Hydrogen, Biomethane, and Related Network Adaptations. Evaluation of Responses Report.* Retrieved from https://www.acer.europa.eu/Official_documents/Acts_of_the_Agency/Publication/ACER%20Report%20on%20NRAs%20Survey.%20Hydrogen%2C%20Biomethane%2C%20and%20Related%20Network%20Adaptations.docx.pdf

Andoni, M., Robu, V., Früh, W.-G., & Flynn, D. (2017). Game-theoretic modeling of curtailment rules and network investments with distributed generation. *Applied Energy*, 201, 174–187. Retrieved from https://doi.org/10.1016/j.apenergy.2017.05.035

Baetens, R. (2015). *On externalities of heat pump-based low-energy dwellings at the low-voltage distribution grid*. PhD thesis, KU Leuven. Retrieved from https://bwk.kuleuven.be/bwf/PhDs/PhDRuben

Baetens, R., De Coninck, R., Jorissen, F., Picard, D., Helsen, L., & Saelens, D. (2015). *Openideas-an open framework for integrated district energy simulations*. 14th Conference of the International Building Performance Simulation Association, Hyderabad, India. Retrieved from https://www.iea-annex60.org/downloads/p2243.pdf

Baetens, R., & Saelens, D. (2016). Modelling uncertainty in district energy simulations by stochastic residential occupant behaviour. *Journal of Building Performance Simulation*, 9(4), 431–447. Retrieved from https://doi.org/10.1080/19401493.2015.1070203

Bahra Cables Company. (2015). *Low voltage power cables*. Retrieved from http://www.bahra-cables.com/downloads.aspx

Biener, W., Dallmer-Zerbe, K., Krug, B., Gust, G., & Wille-Haussmann, B. (2015*). Automated distribution grid planning considering Smart Grid and conventional grid reinforcement technologies*. International ETG Congress, Bonn, Germany. Retrieved from https://ieeexplore.ieee.org/document/7388519

Carpinelli, G., Mottola, F., Proto, D., & Varilone, P. (2017). Minimizing unbalances in low-voltage microgrids: Optimal scheduling of distributed resources. *Applied Energy*, 191, 170–182. Retrieved from https://doi.org/10.1016/j.apenergy.2017.01.057

Chen, T.-H., Yang, C.-H., & Yang, N.-C. (2013). Examination of the definitions of voltage unbalance. *International Journal of Electrical Power & Energy Systems*, 49, 380–385. Retrieved from https://doi.org/10.1016/j.ijepes.2013.02.006

CIGRE. (2014). *CIGRE Networks of Task Force C6.04.02*. Retrieved from https://pandapower.readthedocs.io/en/v2.1.0/networks/cigre.html

Cihlar, J., Lejarreta, A. V., Wang, A., Melgar, F., Jens, J., & Rio, P. (2020). *Hydrogen generation in Europe: Overview of costs and key benefits.* Retrieved from https://op.europa.eu/en/publication-detail/-/publication/7e4afa7d-d077-11ea-adf7-01aa75ed71a1/language-en?WT.mc_id=Searchresult&WT.ria_c=37085&WT.ria_f=3608&WT.ria_ev=search

Ciric, R. M., & Markovic, M. L. J. (2017). Power Factor Analysis in Distribution Network with Roof Photovoltaic Units. *Journal of Electrical Engineering and Electronic Technology*, 6(4), 1–8. Retrieved from https://doi.org/10.4172/2325-9833.1000148

Cossent, R., Olmos, L., Gómez, T., Mateo, C., & Frías, P. (2011). Distribution network costs under different penetration levels of distributed generation. *European Transactions on Electrical Power*, 21(6), 1869–1888. Retrieved from https://doi.org/10.1002/etep.503

Ćurčić, S., Strbac, G., & Zhang, X.-P. (2001). Effect of losses in design of distribution circuits. *IEE Proceedings-Generation, Transmission and Distribution*, 148(4), 343–349. Retrieved from https://ieeexplore.ieee.org/document/941378

Danish Energy Agency. (2017). *Technology Data for Renewable Fuels. Updated February 2021*. Retrieved from https://ens.dk/en/our-services/projections-and-models/technology-data/technology-data-renewable-fuels

Danish Energy Agency. (2018). *Technology Data. Energy Storage. Updated January 2020*. Retrieved from https://ens.dk/en/our-services/projections-and-models/technology-data/technology-data-energy-storage

de Lorgeril, C. (2020). *European biomethane benchmark*. Retrieved from https://www.sia-partners.com/system/files/document_download/file/2020-12/Sia Partners_Benchmark_Europe_Biomethane_2020_EN_0.pdf

De Soto, W., Klein, S. A., & Beckman, W. A. (2006). Improvement and validation of a model for photovoltaic array performance. *Solar Energy*, 80, 78-88. Retrieved from https://doi.org/10.1016/j.solener.2005.06.010

eia. (2018). *Use of energy explained - Energy use in commercial buildings*. Retrieved from https://www.eia.gov/energyexplained/use-of-energy/commercial-buildings-in-depth.php

Elexys. (2020). *IceEndexPowerBE*. Retrieved from https://my.elexys.be/MarketInformation/IceEndexPowerBE.aspx

Energinet & Danish Energy Agency. (2017). *Technology Data for Energy Transport*. Retrieved from https://ens.dk/sites/ens.dk/files/Analyser/technology_data_for_energy_transport.pdf

Energistyrelsen. (2012). *Individual Heating Plants and Energy Transport: Technology Data for Energy Plants, May 2012*. Retrieved from Energistyrelsen (Danish Energy Agency). :

Energy Sector Management Assistance Program. (2020). *What is Power Factor?* Retrieved from https://esmap.org/sites/default/files/esmap-files/47.%20Fact_Sheet_-_Power_Factor.pdf

European Commission. (2021). *EU Building Stock Observatory*. Retrieved from https://ec.europa.eu/energy/topics/energy-efficiency/energy-efficient-buildings/eu-bso_en

European Commission. (2020). *Communication from the Commission to the European Parliament, the Council, the European Economic and Social Committee and the Committee of the Regions: A hydrogen strategy for a climate-neutral Europe*. Retrieved from https://op.europa.eu/en/publication-detail/-/publication/5602f358-c136-11ea-b3a4-01aa75ed71a1/language-en

Eurostat (2011). *2011 Census*. Retrieved from https://ec.europa.eu/eurostat/web/population-and-housing-census/census-data/2011-census

F2 Energy. (2018). *Electrical Power Systems in Buildings*. Retrieved from http://f2energy.com/electrical-power-systems-in-buildings/

Few, S., Djapic, P., Strbac, G., Nelson, J., Candelise, C. (2020). Assessing local costs and impacts of distributed solar PV using high resolution data from across Great Britain. *Renewable Energy*, 162, 1140–1150. Retrieved from https://doi.org/10.1016/j.renene.2020.08.025

Fluvius. (2020). *Elektriciteit tariefbladen finaal*. Retrieved from https://www.fluvius.be/sites/fluvius/files/2019-12/fluvius-aansluittarieven-elektriciteit-2020.pdf

GIE. (2018). *Storage Database*. Retrieved from https://www.gie.eu/index.php/gie-publications/databases/storage-database

GIE. (2019). *LNG Database*. Retrieved from https://www.gie.eu/index.php/gie-publications/databases/lng-database

Good, N., Ceseña, E. A. M., Zhang, L., & Mancarella, P. (2016). Techno-economic and business case assessment of low carbon technologies in distributed multi-energy systems. *Applied Energy*, 167, 158–172. Retrieved from https://doi.org/10.1016/j.apenergy.2015.09.089

Grosse, R., Christopher, B., Stefan, W., Geyer, R., & Robbi, S. (2017). *Long term (2050) projections of techno-economic performance of large-scale heating and cooling in the EU*. Retrieved from Publications Office of the European Union, Luxembourg: https://op.europa.eu/en/publication-detail/-/publication/312f0f62-dfbd-11e7-9749-01aa75ed71a1/language-en:

HRE. (2018). *Heat Roadmap Europe - A low-carbon heating and cooling strategy for Europe*. Retrieved from: https://heatroadmap.eu/

Heat roadmap europe. (2017). *Heating and cooling, facts and figures*. Retrieved from https://www.euroheat.org/wp-content/uploads/2017/07/29882_Brochure_Heating-and-Cooling_web-1.pdf

HUDHC. (2019). *Halmstad University District Heating and Cooling Database_version 5 (2016 update by date 2019-09-30)*. Halmstad University, Sweden.

Hydrogen Europe. (2020). *Clean Hydrogen Monitor 2020*. Retrieved from https://hydrogeneurope.eu/sites/default/files/2020-10/Clean%20Hydrogen%20Monitor%202020_0.pdf

IEEE. (2020). *PES Test feeders*. Retrieved from https://site.ieee.org/pes-testfeeders/resources/

Jacobson, M. Z., & Jadhav, V. (2018). World estimates of PV optimal tilt angles and ratios of sunlight incident upon tilted and tracked PV panels relative to horizontal panels. *Solar Energy*, 169, 55–66. Retrieved from https://doi.org/10.1016/j.solener.2018.04.030

Jonard, F., Lambotte, M., Ramos, F., Terres, J.-M., & Bamps, C. (2009). *Delimitations of rural areas in Europe using criteria of population density, remoteness and land cover*. JRC Scientific Report. Retrieved from https://publications.jrc.ec.europa.eu/repository/bitstream/JRC49927/reqno_jrc49927_rural_typologies_final_report[1].pdf

Jorissen, F., Reynders, G., Baetens, R., Picard, D., Saelens, D., Helsen, L. (2018). Implementation and Verification of the IDEAS Building Energy Simulation Library. *Journal of Building Performance Simulation*, 11(6), 669-688. Retrieved from https://doi.org/10.1080/19401493.2018.1428361

Kakoulaki, G., Kougias, I., Taylor, N., Dolci, F., Moya, J., & Jäger-Waldau, A. (2021). Green hydrogen in Europe – A regional assessment: Substituting existing production with electrolysis powered by renewables. *Energy Conversion and Management,* 228. Retrieved from https://doi.org/10.1016/j.enconman.2020.113649

Kerber, G. (2020). *Kerber networks*. Retrieved from https://pandapower.readthedocs.io/en/v2.3.1/networks/kerber.html

Lampe, L., Tonello, A. M., & Swart, T. G. (2016). *Power Line Communications: Principles, Standards and Applications from Multimedia to Smart Grid* (2nd ed.). Hoboken, United States (NJ): Wiley.

Lindner, M., Aigner, C., Witzmann, R., Wirtz, F., Berber, I., Gödde, M., & Frings, R. (2014). *Synthetic Voltage Control LV Networks*. Retrieved from https://pandapower.readthedocs.io/en/v2.0.1/networks/synthetic_voltage_control_lv_networks.html

Ma, K., Li, R., & Li, F. (2016). Quantification of Additional Asset Reinforcement Cost From 3-Phase Imbalance. *IEEE Transactions on Power Systems*, 31(4), 2885–2891. Retrieved from https://doi.org/10.1109/TPWRS.2015.2481078

Marcogaz. (2018a). *Survey methane emissions for gas distribution in Europe*. Retrieved from https://www.marcogaz.org/app/download/7926774363/WG-ME-17-25.pdf?t=1541592032

Marcogaz. (2018b). *Survey methane emissions for gas transmission in Europe*. Retrieved from https://www.marcogaz.org/app/download/7926773063/WG-ME-17-09.pdf?t=1541674874

Markiewicz, H., & Klajn, A. (2004). *Voltage Disturbances – Standard EN, 50160*. Retrieved from http://copperalliance.org.uk/uploads/2018/03/542-standard-en-50160-voltage-characteristics-in.pdf

Mateo, C., Prettico, G., Gómez, T., Cossent, R., Gangale, F., Frías, P., & Fulli, G. (2018). European representative electricity distribution networks. *International Journal of Electrical Power & Energy Systems*, 99, 273–280. Retrieved from https://doi.org/10.1016/j.ijepes.2018.01.027

McKenna, R., Djapic, P., Weinand, J., Fichtner, W., & Strbac, G. (2018). Assessing the implications of socioeconomic diversity for low carbon technology uptake in electrical distribution networks. *Applied Energy,* 210, 856–869. Retrieved from https://doi.org/10.1016/j.apenergy.2017.07.089

Melaina, M., Antonia, O., & Penev, M. (2013). *Blending Hydrogen into Natural Gas Pipeline Networks: A Review of Key Issues*. Retrieved from https://doi.org/10.2172/1068610

Meteotest. (2009). *Meteonorm Version 6.1 - Edition 2009*. Retrieved from https://meteonorm.com/

Meunier, S., Protopapadaki, C., & Saelens, D. (2020). Towards mapping grid reinforcement costs from residential low-carbon technologies penetration in Europe. 6th International Conference on Smart Energy Systems, Aalborg, Denmark. Retrieved from https://smartenergysystems.eu/

Meyers, R. A. (2003). *Encyclopedia of Physical Science and Technology* (3rd Edition). Academic press.

Möller, B., Wiechers, E., Persson, U., Grundahl, L., & Connolly, D. (2018). Heat Roadmap Europe: Identifying local heat demand and supply areas with a European thermal atlas. *Energy, 158*, 281-292.Retrieved from https://doi.org/10.1016/j.energy.2018.06.025

Morvaj, B., Evins, R., & Carmeliet, J. (2017). Decarbonizing the electricity grid: The impact on urban energy systems, distribution grids and district heating potential. *Applied Energy*, 191, 125–140. Retrieved from https://doi.org/10.1016/j.apenergy.2017.01.058

Navarro-Espinosa, A., & Mancarella, P. (2014). Probabilistic modeling and assessment of the impact of electric heat pumps on low voltage distribution networks. *Applied Energy*, 127, 249–266. Retrieved from https://doi.org/10.1016/j.apenergy.2014.04.026

Navarro-Espinosa, A., & Ochoa, L. F. (2015). *Increasing the PV hosting capacity of LV networks: OLTC-fitted transformers vs. reinforcements*. 2015 IEEE Power & Energy Society Innovative Smart Grid Technologies Conference (ISGT), Washington (WA), USA. Retrieved from https://doi.org/10.1109/ISGT.2015.7131856

Navarro-Espinosa, A., & Ochoa, L. F. (2016). Probabilistic Impact Assessment of Low Carbon Technologies in LV Distribution Systems. *IEEE Transactions on Power Systems*, 31(3), 2192–2203. Retrieved from https://doi.org/10.1109/TPWRS.2015.2448663

Nevzorova, T., & Kutcherov, V. (2019). Barriers to the wider implementation of biogas as a source of energy: A state-of-the-art review. *Energy Strategy Reviews*, 26. Retrieved from https://doi.org/10.1016/j.esr.2019.100414

Pacific Northwest National Laboratory. (2016). *Hydrogen Pipelines*. Retrieved from https://h2tools.org/hyarc/hydrogen-data/hydrogen-pipelines

Persson, U. (2015). *District heating in future Europe: Modelling expansion potentials and mapping heat synergy regions.* Energy and Environment, Chalmers University of Technology, Dissertation Thesis. Series Nr: 3769. Göteborg.

Persson, U., Möller, B., & Wiechers, E. (2017). *Methodologies and assumptions used in the mapping. Deliverable 2.3: A final report outlining the methodology and assumptions used in the mapping. August 2017*. Retrieved from Heat Roadmap Europe 2050, A low-carbon heating and cooling strategy: https://heatroadmap.eu/wp-content/uploads/2018/11/D2.3_Revised-version_180928.pdf

Persson, U., & Werner, S. (2010). *Effective Width - The Relative Demand for District Heating Pipe Lengths in City Areas*. 12th International Symposium on District Heating and Cooling, Tallinn, Estonia.

Persson, U., & Werner, S. (2011). Heat distribution and the future competitiveness of district heating. *Applied Energy,* 88(3), 568-576. Retrieved from: https://doi.org/10.1016/j.apenergy.2010.09.020

Persson, U., Wiechers, E., Möller, B., & Werner, S. (2019). Heat Roadmap Europe: Heat distribution costs. *Energy,* 176, 604-622. Retrieved from: https://doi.org/10.1016/j.energy.2019.03.189

Peta5. (2021). *Pan-European Thermal Atlas 5.0.1 (Peta 5.0.1).* Europa-Universität Flensburg, ArcGIS Online. sEEnergies: Quantification of synergies between Energy Efficiency first principle and renewable energy systems. Retrieved from: https://euf.maps.arcgis.com/apps/webappviewer/index.html?id=8d51f3708ea54fb9b732ba0c94409133.

Prettico, G., Gangale, F., Mengolini, A., Lucas, A., Fulli, G. (2016). *Distribution system operators observatory: from European electricity distribution systems to reference network*. Retrieved from https://publications.jrc.ec.europa.eu/repository/bitstream/JRC101680/ldna27927enn.pdf

Protopapadaki, C. (2018). *A probabilistic framework towards metamodeling the impact of residential heat pumps and PV on low-voltage grids*. PhD thesis, KU Leuven. Retrieved from https://lirias.kuleuven.be/2328633?limo=0

Protopapadaki, C., & Saelens, D. (2017). *Sensitivity of Low-Voltage Grid Impact Indicators to Modeling Assumptions and Boundary Conditions in Residential District Energy Modeling*. 15th Conference of the International Building Performance Simulation Association, San Francisco (CA), USA. Retrieved from https://www.ashrae.com/File%20Library/Conferences/Specialty%20Conferences/2018%20Building%20Performance%20Analysis%20Conference%20and%20SimBuild/Papers/C108.pdf

Protopapadaki, C., & Saelens, D. (2019). Towards metamodeling the neighborhood-level grid impact of low-carbon technologies. *Energy and Buildings*, 194, 273–288. Retrieved from https://doi.org/10.1016/j.enbuild.2019.04.031

Ridjan Skov, I., & Schneider, N. C. A. (2021). *Technology data and costs for gas grids in the context of a Smart Energy System.* Report in the frame of the H2020 EU project sEEnergies.

Rodriguez-Calvo, A., Cossent, R., & Frías, P. (2017). Integration of PV and EVs in unbalanced residential LV networks and implications for the smart grid and advanced metering infrastructure deployment. *International Journal of Electrical Power & Energy Systems*, 91, 121–134. Retrieved from https://doi.org/10.1016/j.ijepes.2017.03.008

Scarlat, N., Dallemand, J.-F., & Fahl, F. (2018). Biogas: Developments and perspectives in Europe. *Renewable Energy*, 129, 457–472. Retrieved from https://doi.org/10.1016/J.RENENE.2018.03.006

sEEnergies. (2020). sEEnergies Open Data. In. Europa-Universität Flensburg. Retrieved from: https://tinyurl.com/sEEnergies-Hub

Segundo Sevilla, F. R., Parra, D., Wyrsch, N., Patel, M. K., Kienzle, F., & Korba, P. (2018). Techno-economic analysis of battery storage and curtailment in a distribution grid with high PV penetration. *Journal of Energy Storage*, 17, 73–83. Retrieved from https://doi.org/10.1016/j.est.2018.02.001

Statista. (2020). *Inflation rate in the European Union and the Euro area from 2009 to 2021*. Retrieved from https://www.statista.com/statistics/267908/inflation-rate-in-eu-and-euro-area/

Stetz, T., Diwold, K., Kraiczy, M., Geibel, D., Schmidt, S., & Braun, M. (2014). Techno-Economic Assessment of Voltage Control Strategies in Low Voltage Grids. *IEEE Transactions on Smart Grid*, 5(4), 2125–2132. Retrieved from https://doi.org/10.1109/TSG.2014.2320813

Stetz, T., Marten, F., & Braun, M. (2013). Improved Low Voltage Grid-Integration of Photovoltaic Systems in Germany. *IEEE Transactions on Sustainable Energy,* 4(2), 534-542. Retrieved from https://ieeexplore.ieee.org/document/6213176

Synergrid. (2019). *Prescriptions techniques spécifiques de raccordement d'installations de production décentralisée fonctionnant en parallèle sur le réseau de distribution - edition 2.1*. Retrieved from https://www.sibelga.be/uploads/assets/58/fr/20191104142219000000-Synergrid_Technical_prescription_C10-11_FR.pdf

Tsemekidi-Tzeiranaki, S., Bertoldi, P., Labanca, N., Castellazzi, L., Serrenho, T., Economidou, M., & Zangheri, P. (2018). *Energy Consumption and Energy Efficiency Trends in the EU-28 for the Period 2000–2016*. Retrieved from https://op.europa.eu/en/publication-detail/-/publication/89937a89-fcf9-11e8-a96d-01aa75ed71a1/language-en

United Nations Statistics Division. (2017). *Population density and urbanization*. Retrieved from https://unstats.un.org/unsd/demographic/sconcerns/densurb/densurbmethods.htm

U.S. department of energy. (2020). Heat pump systems. Retrieved from: https://www.energy.gov/energysaver/heat-and-cool/heat-pump-systems

van der Burgt, J., Vera, S. P., Wille-Haussmann, B., Andersen, A. N., & Tambjerg, L. H. (2015). *Grid impact of charging electric vehicles; study cases in Denmark, Germany and The Netherlands*. 2015 IEEE PowerTech, Eindhoven, Netherlands. Retrieved from https://ieeexplore.ieee.org/document/7232234

Van Roy, J. (2015). *Electric Vehicle Charging Integration in Buildings: Local Charging Coordination and DC Grids*. PhD thesis, KU Leuven. Retrieved from https://limo.libis.be/primo-explore/fulldisplay?docid=LIRIAS1731293&context=L&vid=Lirias&search_scope=Lirias&tab=default_tab&lang=en_US&fromSitemap=1

Van Roy, J., Salenbien, R., & Driesen, J. (2014). *Modelica library for building and low-voltage electrical AC and DC grid modeling*. 10th International Modelica Conference, Lund, Sweden. Retrieved from https://ep.liu.se/ecp/096/031/ecp14096031.pdf

Vegunta, S. C., Twomey, P., & Randles, D. (2013). *Impact of PV and load penetration on LV network voltages and unbalance and potential solutions*. 22nd International Conference and Exhibition on Electricity Distribution (CIRED), Stockholm, Sweden. Retrieved from https://ieeexplore.ieee.org/document/6683859

Vito. (2016). *Steunpunt energie: Nota potentieel 2030 -warmtepompen*. Retrieved from https://www.energiesparen.be/groene-energie-en-wkk/cijfers-en-studies

VREG. (2016). *Tariefmethodologie voor distributie elektriciteit en aardgas gedurende de reguleringsperiode 2017-2020*. Retrieved from https://www.vreg.be/sites/default/files/document/tariefmethodologie_reguleringsperiode_2017-2020_2.pdf

Wu, D., Aye, L., Ngo, T., & Mendis, P. (2017). Optimisation and financial analysis of an organic Rankine cycle cooling system driven by facade integrated solar collectors. *Applied Energy, 185*, 172–182. Retrieved from https://doi.org/10.1016/j.apenergy.2016.10.071

XE. (2020). *GBP to EUR Chart*. Retrieved from https://www.xe.com/currencyconverter/convert/?Amount=1&From=GBP&To=EUR